Modelos numérico y analítico para el diseño de laminados compuestos híbridos con capacidad de falla gradual bajo cargas de flexión

Juan Manuel Macías López

Numerical and analytical models for the design of hybrid composite laminates with gradual failure behaviour under bending loads

Juan Manuel Macías López

Tesis de grado presentada como requisito parcial para optar al título de:
Magister en Ingeniería de materiales y procesos

Director(a):
Ph.D. Juan Manuel Meza Meza
Co-director(a):
Ph.D. Meisam Jalalvand

Línea de Investigación:
Modelamiento de falla en materiales compuestos híbridos
Grupo de Investigación:
Design of Advanced Composite Materials Research Group
DADCOMP

Universidad Nacional de Colombia
Facultad de minas, Departamento de Materiales y Minerales
Medellín, Colombia
2020

Dedicatoria

A mi compañía en arduos días y noches de trabajo, gracias por enseñarme que el amor no requiere palabras.

Agradecimientos/Acknowledgments

Resumen

El presente trabajo describe el estudio reciente de los laminados de materiales compuestos híbridos sujetos a cargas de flexión, para luego usar este conocimiento en la creación de herramientas analíticas y numéricas que asisten el diseño de laminados híbridos con capacidad de falla gradual en un ensayo de flexión a cuatro puntos. Estas herramientas son inicialmente verificadas usando datos experimentales de laminados en los cuales se logró obtener falla gradual, pero la naturaleza de la falla y los mecanismos por los cuales se da, requieren un mayor entendimiento. El modelo en el cual se basa la herramienta analítica consiste en una adaptación de la solución analítica para ensayos de flexión a cuatro puntos en el cual el material es sometido a grandes deformaciones en combinación con la teoría clásica de laminados y mecánica de la fractura. Por otra parte, el modelo numérico utiliza elementos cohesivos para modelar tanto el daño intralaminar como el interlaminar, usando las propiedades de la resina para definir el comportamiento cohesivo interlaminar y usando una distribución de resistencias intralaminares según el modelo estadístico de Weibull. Una vez verificados los modelos, estos son usados para diseñar nuevos laminados híbridos optimizados, que reducen la cantidad de láminas ultradelgadas y por lo tanto, el número total de láminas requeridas para un mismo espesor, esto a su vez implica una posible reducción en el costo de fabricación y el tiempo de manufactura. Además, un laminado estándar (laminado no hibridado) es fabricado con fines comparativos; los ensayos en estos nuevos laminados validan la capacidad predictiva de ambas herramientas en casos falla gradual y falla repentina, tanto en laminados híbridos como estándar; y demuestran que es posible conseguir laminados híbridos con capacidad de falla gradual a un menor costo.

Palabras clave: Materiales compuestos híbridos, ensayo de flexión, herramientas analíticas y numéricas, validación experimental..

Abstract

The present work describes the recent studies on hybrid composite laminates under bending loads; then, this knowledge is used to create analytical and numerical tools that assist the design of hybrid layups which can fail gradually in a four-point bending test. These tools are initially verified using experimental data from layups where such a gradual failure was achieved, but the nature of the failure process and failure mechanisms need additional study. The analytical tool is based on modifications from the analytical solution of large deflections of a beam in a four-point bending test together with the classical laminate and fracture mechanics theories. On the other hand, the numerical model is set using cohesive elements to model intralaminar as well as interlaminar damage, where the interlaminar strength is based on resin properties and the intralaminar strength is set based on Weibull statistical distribution. Once the models were verified, they are used to design new optimised hybrid layups that reduce the number of thin-plies required and therefore, the total amount of plies required for the same layup thickness; these imply a potential decrease in the cost of the layup and the time to be manufactured. One non-hybrid layup was also manufactured for baseline comparison, testing results on all these new layups exhibited the expected failure sequence and failure mechanisms; validating the accuracy of the tools to predict brittle and gradual failure in hybrid and standard composites; besides, it shows that it is possible to obtain hybrid layups with gradual failure capabilities using other configurations.

Keywords: Hybrid composite materials, bending test, numerical and analytical tools, experimental validation.

Content

List of Figures

List of Tables

Symbols and abbreviations

Symbol	Definition	Units SI	Location
$u(x,y,z)$	Displacement in the x direction	$[mm]$	$Equation : 2-1$
$v(x,y,z)$	Displacement in the y direction	$[mm]$	$Equation : 2-1$
$u_0(x,y,z)$	Middle surface displacement in the x direction	$[mm]$	$Equation : 2-1$
$v_0(x,y,z)$	Middle surface displacement in the y direction	$[mm]$	$Equation : 2-1$
φ_x	Middle surface rotation around the x direction	$[mm]$	$Equation : 2-1$
φ_y	Middle surface rotation around the y direction	$[mm]$	$Equation : 2-1$
ϵ_x^0	Normal strain in the x direction	$[mm/mm]$	$Equation : 2-3$
ϵ_y^0	Normal strain in the y direction	$[mm/mm]$	$Equation : 2-3$
γ_{xy}^0	Shear strain in the $x.y$ plane	$[mm/mm]$	$Equation : 2-3$
κ_x	Curvature in the x direction	$[mm^{-1}]$	$Equation : 2-3$
κ_y	Curvature in the y direction	$[mm^{-1}]$	$Equation : 2-3$
κ_{xy}	Twisting in the $x.y$ plane	$[mm^{-1}]$	$Equation : 2-2$
σ_x	Normal stress in the x direction	$[MPa]$	$Equation : 2-4$
σ_y	Normal stress in the y direction	$[MPa]$	$Equation : 2-4$
σ_{xy}	Shear stress in the $x.y$ plane	$[MPa]$	$Equation : 2-4$
$[T]$	Rotation matrix, local to global coordinates	$[-]$	$Equation : 2-4$
$[Q]$	Plane-stress stiffness matrix, local coordinates	$[MPa]$	$Equation : 2-4$
$[R]$	Reuter matrix	$[-]$	$Equation : 2-4$

Symbol	Definition	Units SI	Location
$[\bar{Q}]$	Plane-stress stiffness matrix, global coordinates	$[MPa]$	$Equation : 2-5$
E_1	Young's modulus in the fibre direction	$[MPa]$	$Equation : 2-7$
E_2	Young's modulus in the transverse direction	$[MPa]$	$Equation : 2-7$
v_{12}	Poisson's ratio in the 1,2 plane	$[-]$	$Equation : 2-7$
G_{12}	Shear modulus in the 1,2 direction	$[MPa]$	$Equation : 2-7$
N_x	Tensile force per unit length in the x direction	$[N/mm]$	$Equation : 2-8$
N_y	Tensile force per unit length in the y direction	$[N/mm]$	$Equation : 2-8$
N_{xy}	Shear force per unit length in the $y.x$ plane	$[N/mm]$	$Equation : 2-8$
M_x	Bending moment per unit length in the x direction	$[N.mm/mm]$	$Equation : 2-8$
M_y	Bending moment per unit length in the y direction	$[N.mm/mm]$	$Equation : 2-8$
M_{xy}	Twisting moment per unit length in the xy plane	$[N.mm/mm]$	$Equation : 2-8$
t	Laminate thickness	$[mm]$	$Equation : 2-8$
z_k	Thickness coordinate of lamina k	$[mm]$	$Equation : 2-8$
z_{k-1}	Thickness coordinate of lamina $k-1$	$[mm]$	$Equation : 2-8$
$[A]$	In-plane stiffness matrix	$[MPa.mm^2]$	$Equation : 2-9$
$[B]$	Bending-extension coupling stiffness matrix	$[MPa.mm^2]$	$Equation : 2-9$
$[D]$	Bending stiffness matrix	$[MPa.mm^2]$	$Equation : 2-9$
T	Strength for one particular cohesive section	$[MPa]$	$Equation : 2-13$
T^0	Strength scale factor	$[MPa]$	$Equation : 2-13$

Symbol	Definition	Units SI	Location
m	Weibull modulus	$[-]$	$Equation : 2-13$
n	Random variable between 0 and 1	$[-]$	$Equation : 2-13$
σ_{eq}	Equivalent stress in the glass ply	$[MPa]$	$Equation : 2-14$
V	Volume of the glass layers	mm^3	$Equation : 2-14$
M_i	Failure bending moment of lamina i	$[N.mm/mm]$	$Equation : 3-1$
$(\epsilon_i)_{max}$	Failure strain of lamina i	$[mm/mm]$	$Equation : 3-1$
E_i	Young modulus in the fibre direction of lamina i	$[MPa]$	$Equation : 3-1$
I_i	Moment of inertia of lamina i	$[mm^4]$	$Equation : 3-1$
c_i	Centroid distance to lamina i	$[mm]$	$Equation : 3-1$
N_i	Change area factor for lamina i	$[-]$	$Equation : 3-1$
R	Support reaction	$[N]$	$Equation : 5-1$
EI	Equivalent beam stiffness	$[MPa.mm^4]$	$Equation : 5-1$
a	Distance support - upper noses	$[mm]$	$Equation : 5-1$
α	Angle at point 0 in **5-1**	$[radians]$	$Equation : 5-1$
β	Angle at point A in **5-1**	$[radians]$	$Equation : 5-1$
Y_a	Vertical displacement of the upper noses	$[mm]$	$Equation : 5-2$
ϕ	Dummy integration variable	$[radians]$	$Equation : 5-3$
$1/r$	Beam curvature	$[mm^{-1}]$	$Equation : 5-4$
M	Bending moment due to force reactions	$[N*mm]$	$Equation : 5-5$
L	Support spam	$[mm]$	$Equation : 5-6$
F	Upper noses reaction load	$[N]$	$Equation : 5-8$
L_n	Current support spam	$[mm]$	$Equation : 5-9$
L_0	Initial support spam	$[mm]$	$Equation : 5-9$
r_p	Upper noses and support radius	$[mm]$	$Equation : 5-9$
a_n	Current value of a	$[mm]$	$Equation : 5-10$
a_0	Initial value of a	$[mm]$	$Equation : 5-10$
Y_n	Real vertical displacement	$[mm]$	$Equation : 5-11$
Y_a	Apparent vertical displacement	$[mm]$	$Equation : 5-11$
F_{hyb}	Load taken by the hybrid specimen	$[N]$	$Equation : 5-12$

Symbol	Definition	Units SI	Location
F_{M55}	Load taken by the M55 plies	$[N]$	$Equation : 5 - 12$
F_T	Load taken by the T1000 plies	$[N]$	$Equation : 5 - 12$
σ_{hyb}	Average stress of the hybrid layup	$[MPa]$	$Equation : 5 - 13$
A_{hyb}	Transversal area of the hybrid	$[mm^2]$	$Equation : 5 - 13$
σ_{M55}	Average stress of the M55 layers	$[MPa]$	$Equation : 5 - 13$
A_{M55}	Transversal area of the M55 layers	$[mm^2]$	$Equation : 5 - 13$
σ_T	Average stress of the T1000 layers	$[MPa]$	$Equation : 5 - 13$
A_T	Transversal area of the T1000 layers	$[mm^2]$	$Equation : 5 - 13$
E_{hyb}	Longitudinal modulus of the hybrid specimen	$[MPa]$	$Equation : 5 - 14$
ε	Longitudinal normal strain	$[mm/mm]$	$Equation : 5 - 14$
E_{M55}	Longitudinal modulus of the M55 layers	$[MPa]$	$Equation : 5 - 15$
E_T	Longitudinal modulus of the T1000 layers	$[MPa]$	$Equation : 5 - 16$
G_{II}	Mode II energy release rate	$[J/mm^2]$	$Equation : 5 - 19$
$\bar{u}_{before}$	Internal energy after delamination	$[J/mm^3]$	$Equation : 5 - 20$
$\bar{u}_{after}$	Internal energy before delamination	$[J/mm^3]$	$Equation : 5 - 21$

1. Chapter 1: Introduction

1.1. Introduction

Composite materials in structural applications offer many advantages over traditional single constituent materials like plastics, ceramics, or metals; this is because composites provide higher strength and stiffness to weight ratio, besides, they offer combined increased corrosion resistance and improved fatigue behaviour [William et al., 2007]. However, composite materials usually fail suddenly, showing no sign of damage prior to failure; this creates limitations for their applicability because it demands more testing in the design process and requires higher safety factors, reducing its weight saving capability [Swolfs, 2019]. Hybrid composite materials that can fail gradually have been recently proved to be a possible solution to these limitations [Idárraga, 2019, Jalalvand et al., 2014, Swolfs, 2019], but their study is still immature.

The investigation on hybrid composite materials with pseudo-plasticity or gradual failure behaviour has been focused mainly on tensile tests, using both unidirectional and quasi-isotropic laminates, here the main contributions come from Jalalvand and Wisnom [Jalalvand et al., 2014, Jalalvand et al., 2015, Czél et al., 2017]; they have developed numerical modelling methodologies and analytical tools which allow to accurately design such hybrid laminates. On the other hand, for a bending load scenario much work has been done in hybrid materials [Lim et al., 2014, Jesthi et al., 2018, Kalantari et al., 2016a, Kalantari et al., 2016b, Kalantari et al., 2016c, Sudarisman et al., 2009, Dong, 2016, Dong and Davies, 2014, Reis et al., 2007, Dong and Davies, 2013, Dong et al., 2012, Dong and Davies, 2015, Fiore et al., 2011, Zhang et al., 2012, Velmurugan and Manikandan, 2007], but only few author have been found to even mention gradual failure [Idárraga, 2019, Cusack, 2018]. The most important contribution is the one done by Idárraga [Idárraga, 2019], as he was able to design hybrid configurations that can lead to a gradual failure in bending.

This work is a continuation of [Idárraga, 2019], taking his results as reference, the main purpose is the development of analytical and numerical tools for the design of hybrid composite layups that can exhibit gradual failure, these tools are able to capture all possible failure mechanisms and are further validated with new experimentation using different materials and configurations. The process followed for the development of such tools and their experimental validation is explained in this document.

1.2.   Problem Statement

Nowadays environmental pollution is one of the biggest challenges this generation has to overcome. One of the main contributors to this issue is energy and fuel consumption for transport applications. This is why, there is a strong tendency towards making transportations system more efficient and environmentally friendly [Albaigés, 2013].

The efficiency of any kind of transportation system is primarily affected by the quality of its design and the performance of its materials; considering that the last one has the greatest impact and implies the biggest limitations [Barbero, 2018]. For this reason, the transportation industry has been going from traditional materials like basic metallic alloys and wood to high performance materials like super alloys and plastic reinforced materials also called composite materials; a clear example of this can be drawn from the commercial aeronautic industry, where by the year of 1999 about 15 % of the structural weight of the commercial aircrafts were built using advanced fibre-reinforced polymer composites [Mangalgiri, 1999], but by the year of 2009 they have reached 50 % [William et al., 2007], and it has been increasing even more in the last few years.

Composite materials have been of particular interest for structural applications, but due to their inherent brittle behaviour and their large amount of failure modes; their applicability is still limited [Barbero, 2018]. These materials need large scale and expensive testing at every stage of design; besides, their structures are always built using higher safety factors, which means more budget and weight [William et al., 2007].

Although during the last few years huge advances in the understanding of pseudo-plastic hybrid composites when they are submitted to tension have been done [Jalalvand et al., 2014, Jalalvand et al., 2015]; there is almost nothing regarding flexure behaviour [Idárraga, 2019]; despite this loading condition appearing in many structural applications. Just at the time of writing this work pseudo-ductility of hybrid composites under flexion has been experimentally demonstrated but both analytical and numerical models are still immature.

To overcome this problem, the present work is mean to answer the question: Is it possible to understand the failure mechanism of pseudo-ductility hybrid composites in flexion and thus to propose both analytical and numerical models as tools to design them?

1.3.   Justification

During the last few decades there has been an increased use of composite materials in structural applications such as electric vehicles, ships and aircrafts; this is due to the excellent mechanical properties these materials provide, such as high stiffness, strength, and fracture toughness combined with a low density and high corrosion resistance [Swolfs et al., 2014]. With the advent of the plastic reinforced materials it has been possible to create lighter and stronger structures, and when it comes to mobile structures such as vehicles, light means less energy consumption, less maintenance spends and more efficiency [William et al., 2007].

Even though composite materials can show higher performance in comparison with traditional materials like steel and aluminium; the way composites fail is usually catastrophic, they display little or no sign of damage or plasticity when compared to regular metallic materials [Swolfs et al., 2014]. As a consequence of this, composite material structures require higher safety factors and oversizing, which limits their weight-saving potential [Swolfs et al., 2014]. It has been proved by several authors that hybridizing can help overcome composites inherent brittle limitations; there are experimental evidence of pseudo-plastic response of hybrid composite materials under pure tensile loading [Jalalvand et al., 2014, Jalalvand et al., 2015, Swolfs et al., 2014]; besides, there are already analytical and numerical tools able to accurately explain and predict the damage progression of hybrid materials in pure tension [Jalalvand et al., 2014, Jalalvand et al., 2015]; so, right now it is possible to design and manufacture hybrid composite materials laminates that can fail gradually if they are subjected to pure tensile or compressive loads. The major limitation for pseudo-ductile hybrid composites is the cost; as these kinds of hybrids require a lower percentage of defects, expensive materials as thin pre-pregs and complicated manufacture process as autoclave curing are usually needed [Jalalvand et al., 2015].

On the other hand, when it comes to more complex loads states; even thought, it has recently been experimentally proved that it is possible to get gradual failure using hybrid composite materials under bending loads [Idárraga, 2019]; the numerical and analytical methods cannot predict the full damage response, they are mainly limited to first ply failure [Dong, 2016, Dong and Davies, 2012, Ary Subagia et al., 2014]. Therefore, there is still the scientific need for understanding all the failure mechanisms and the way they interact in the process of gradual failure in a hybrid composite laminate in bending [Idárraga, 2019]; and beyond this, there is a technological need of developing a tool that allows to accurately design these kinds of laminates.

1.4.   Objectives

General objectives

Develop and validate numerical and analytical models as design tools for hybrid composite laminates that can fail in a gradual fashion under bending loads.

Specific objectives

- To study and analyse the damage mechanisms and failure sequence that take place in hybrid composite laminates under bending loads.

- To develop a numerical model capable of predicting the failure mechanisms in a hybrid composite laminate under bending loads.

- To develop an analytical model capable of predicting the failure mechanisms in a hybrid composite laminate under bending loads.

- To perform experimental bending tests on hybrid composite materials that can fail both gradually and catastrophically in order to validate the numerical and analytical models.

1.5.   Methodology

To understand the way hybrid composite materials fail in bending; an extensive review of the literature and the background is done. The literature review starts from setting a clear concept of composite materials and hybrid composite materials; besides, it explains the analytical (Classical Laminate Theory, Ply discount and non-linear beam theories) and numerical tools (cohesive, 2D and 3D elements) available and best suited for modelling this kind of materials. Here, not only the theory from basic textbooks is studied, but also the approaches that several authors have been following to tackle this problem; so, the most relevant work done for modelling failure in hybrid composites materials is reviewed. As the problem at hand is bending, some of the studies in hybrid composites in tension can be useful, and indeed some of the most relevant publications are mentioned. However, a deeper search was done about research on hybrid composites in bending; the recent trends and extends have to be understood in order to progress further on.

The background review goes deeper; here, the actual previous results are analysed and double-checked using the knowledge acquired in the literature review. In this work, the numerical and analytical tools developed are verified using the experimental results of Idárraga et al [Idárraga, 2019] and Cusack et al [Cusack, 2018]; but before going into that, the background review also asses the quality of the analysis prior to that experimentation, namely the design tools used by Idárraga and Cusack. Regarding the development of the analytical tool capable of modelling the behaviour of the hybrid composite materials in bending, it will also be gradually constructed and debugged to account for the different failure mechanisms and sources of non-linearities, at each step every piece of theory implement is explained in detail, besides, verified by comparing it with the experimental available data.

Finally, for the experimental validation of the numerical and analytical models, some hybrid composite layups (designed with the aid of the tools developed here) are tested. Two new hybrid configurations, as well as a single carbon fibre composite with one of the base materials of the hybrids is also tested as a base-line for comparison. The test procedure is carried following the methodology of Idárraga [Idárraga, 2019], as it has proven to avoid shear failure and yield sound results. The materials are selected mainly according to the availability of the stock in the University of Strathclyde (main collaborator) but taking into account the desired behaviour.

1.6. Scope

In this project, one numerical and one analytical model will be developed, these models are gradually verified by comparison with experimental results, the models as design tools are able to capture the influence of gradual failure, large displacements, and contact. The validation of the models is done experimentally. Three new hybrid layups are designed using the proposed tools, and then tested for validation.

2. Chapter 2: State of the art

In this section, the concepts involved and needed to model numerically (using the finite element method) and analytically the quasi-static failure of hybrid composite materials in a four-point bending test will be briefly explained. The review works as follows:

A general concept of traditional composite materials and hybrid composite materials are introduced; then a brief description of the most traditional continuum mechanic approaches for modelling stiffness and first ply failure in composite layups (The Classical Laminate Theory) is also presented. The ply discount method is also explained, as it is one the first approximations for dealing with progressive failure in composite laminates, the section ends with a review of the analytical methods for modelling non-linear deformations in a four-point bending test.

The next section deals with numerical tools available for modelling stiffness and failure of composite materials using finite element analysis. Here, different kinds of 2D and 3D elements are described; continuum and discrete damage models are explained as well.

The final section shows the work that has been done in hybrid composite materials, the experimental results; numerical, and analytical approaches for modelling these kind of materials. This section explains how many of the tools available for modelling traditional composites were used to understand the behaviour of hybrid composites.

2.1. Composite materials

The general definition of a composite material is a material created by the combination of two or more different materials which possess different microstructures and have boundaries that separate the different constituents. A composite material is formed by a filler or reinforce material, which is in charge of providing stiffness and strength to the composite, such filler could be in the form of either whiskers, particles, short or long fibres; there is also a bulk material called matrix, which binds the fillers and make them act as a whole [Askeland, 2018], see Figure **2-1**.
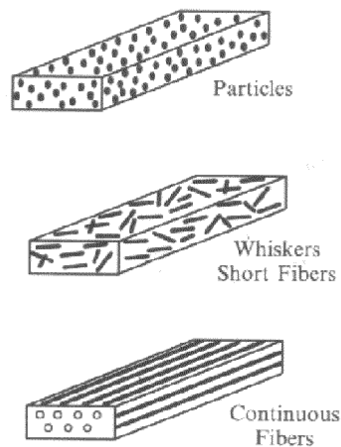
Figure 2-1.: Different types of composite reinforcements [kansu.tripod.com,].

The idea is combining different materials in order to obtain a new material with improved characteristics or properties that could not be obtained with single constituents [Vasiliev and Morozov, 2007]. In the particular case of fibre-reinforced polymer composites, the desired characteristics are the high stiffness and high strength combined with a low density; an additional advantage is that they can be stacked and oriented for the specific load scenario at hand; it means, they can be tailored to be stiff and withstand high loads only in the required directions [Swolfs, 2019].

Through this work, the term composite material will refer mainly (when is not explicitly stated) to a material created by a polymer matrix (usually epoxy resin) reinforced by unidirectional long fibres (usually carbon or glass) with diameters in the order of micrometres.

2.2.   Hybrid composite materials

When a polymer matrix is reinforced using more than one type of fibre, the material is called fibre-hybrid composite material [Swolfs et al., 2014]. The process of adding more than one type of fibre to a polymer matrix is called hybridization, and it can be done at various scales:

- The minimum scale at which hybridization can be done is at the intra-yarn scale, also called fibre-by-fibre hybridization; this method, even though gives the greatest dispersion, where the term "dispersion" refers to how well the fibres are mixed, is also the most expensive and complicated kind of hybrid composite [Swolfs, 2019], see Figure **2-1** (a).

- Hybridization can be done at the yarn level, when the yarns of different types of fibre are woven into a single fabric; it is called yarn-by-yarn hybridization. This method gi-

ves a lower dispersion, but is less complicated and expensive [Swolfs, 2019], see Figure
2-1 (b).

- The last scale at which hybridization is done is at the ply level, also called ply-by-ply
  hybridization; the way it is done is by laying up laminas of different fibre types to
  create a single laminate. This is the cheapest method and gives the lowest dispersion
  [Swolfs, 2019], see Figure **2-1** (c).
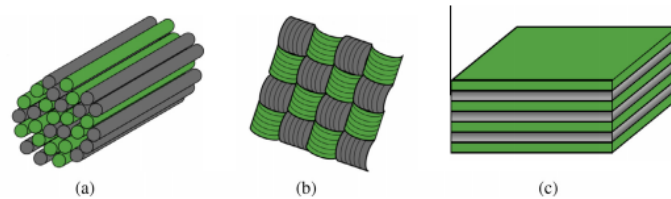
Figure 2-2.: Different hybrid configurations; (a) fibre-by-fibre, (b) yarn-by-yarn, and (c)
layer-by-layer [Swolfs et al., 2014].

Different kinds of hybrid configurations can be used in the same layup (for ex: hybrid fabrics
can be stacked with single fabrics); this is done to achieve different properties in different
directions and load scenarios [Swolfs et al., 2014].

Hybridization opens a new range of versatility to the design of composite laminates, because
it can bring additional advantages to traditional single reinforcement composites; these ad-
vantages can be broadly characterized as hybrid effect and pseudo-plasticity [Swolfs et al.,
2014].

2.3. Hybrid effect

The study of the hybrid effect is restricted to the mixture of only two types of fibre; where
usually the first type has a low modulus and a high failure strain (HE) and the other one
it's the opposite, a high modulus and a low failure strain (LE). The hybrid effect is defined
as "a deviation from the simple rule of mixtures" [Swolfs et al., 2014]; and it accounts for an
improvement or deterioration on any specific property, see Figure **2-3**. The hybrid effect can
be both positive and negative depending on the property that is being considered; sometimes
it is possible to achieve a layup with a positive hybrid effect in some properties and negative
or neutral in some others [Swolfs et al., 2014].

The rule of mixtures requires a compositional parameter, which is usually the volumetric
fraction; this variable can create a lineal rule of mixture in properties like stiffness or strength
in tension; but when different kinds of properties are considered, like fracture properties,

damage tolerance, or bending strength, the rule of mixtures can get a non-lineal form [Swolfs et al., 2014]. Besides, the rule of mixtures does not consider the staking sequence as a parameter; but, as it is shown later, it can play a huge role in the strength and failure modes of almost any hybrid configuration.
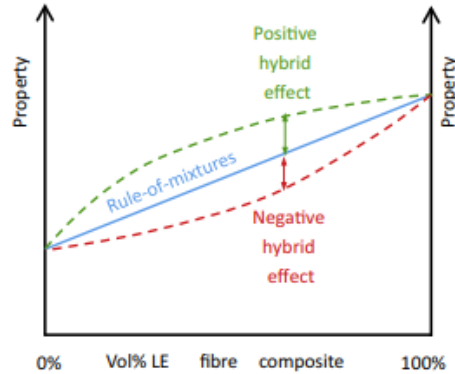
Figure 2-3.: Graphical definition of hybrid effect [Swolfs et al., 2014].

The hybrid effect accounts for relationships between specific properties before and after hybridization, but it does not consider either the mechanisms that make possible the increase or decrease of specific properties nor the nature or the type of failure; taking the glass-carbon hybrid as an example, the addition of glass fibre to a composite material initially reinforced with carbon can create a positive hybrid effect when it comes to the increase in the maximum strain before failure; but a negative hybrid effect on the decrease in the laminate stiffness.

2.4. Pseudo-plasticity

On the other hand, pseudo-plasticity does not concern much for the values of specific properties but rather stands in the nature of the failure initiation and progression, it means, hybridization can be desired if it changes the nature of failure, even if it bring down some specific properties like stiffness or strength. Therefore, hybridization can be a mean to achieve gradual failure or pseudo-plasticity in a composite material; this has been done in unidirectional tension and compression tests [Jalalvand et al., 2014, Jalalvand et al., 2015, Czél et al., 2017]; as well as four point bending [Idárraga, 2019]; the way it is achieved is by carefully controlling the specific failure mechanisms presented and the order in which they do [Jalalvand et al., 2015].

2.4.1. Pseudo-plasticity in tension

Gradual failure in tension is usually obtained by using sandwich layups in which the central layer is a thin low strain material (usually carbon fibre/epoxy) and the top and bottom layers are standard thickness high strain materials (usually glass fibre/epoxy) [Swolfs, 2019]; it has been widely studied the way the relative and absolute thickness, and the relation between the Young's modulus in the fibre direction plays an important role in the failure progression of a hybrid laminate [Idárraga, 2019, Jalalvand et al., 2014, Jalalvand et al., 2015]. The major contribution to this topic is the work done by [Jalalvand et al., 2015], where he identifies all the possible failure modes and progression of carbon/epoxy and glass/epoxy hybrid layups based on their thicknesses and mechanical properties (see Figure **2-4**).
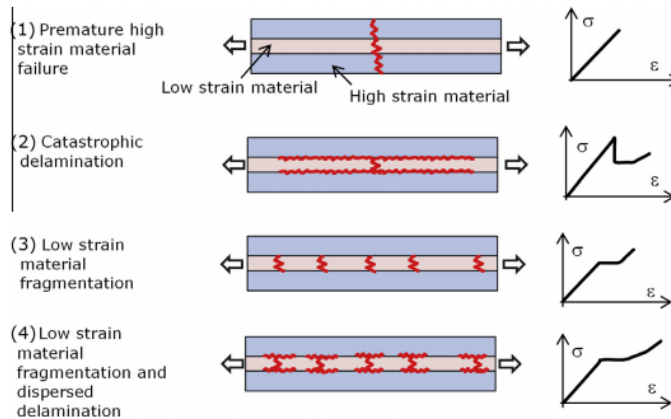
Figure 2-4.: Damage scenarios for Unidirectional hybrid composites [Jalalvand et al., 2015].

2.4.2. Pseudo-plasticity in bending

Although there are some papers dealing with hybrid composites under flexure loads, reported failure is almost exclusively brittle. The only study that has been found on the topic of gradual failure of hybrid composites in bending is the work done by [Idárraga, 2019], he showed that gradual failure in bending can be achieved by using three different materials stacked in the form of non-symmetric laminates. The contribution of his work is mainly experimental, because as it is shown in later sections, even though he could probe that it is possible to obtain gradual failure in bending, the numerical and analytical results, where he was based on, can be further improved; and his analysis previous to experimentation needs to account for more details, such as the large non-linear behaviour and fragmentation.

2.5. Classical laminate theory

The Classical Laminate Theory defines the "relationships between the structural properties of the final laminate and those of the laminas and their orientations" [Barbero, 2018]; This theory shows these associations in the form of "a simple relationship between the forces and moments applied to a laminate and the strains and curvatures induced" [Barbero, 2018]. This method is one of the most widely used for modelling behaviour and failure of thin layered materials loaded as panels or membranes [Barbero, 2018].

2.5.1. Conventions

The laminate is modelled as a plate or shell under plane stress, its coordinates are defined as (x, y, z) coordinates, the x and y correspond to the length and width of the plate which are much larger than the thickness defined in the z coordinate, see Figure **2-5**. The ply coordinates are defined as $(1, 2, 3)$, where 1 and 2 correspond to the fibre and transversal direction of the ply, and 3 is the thickness; the orientation of each lamina is defined as the angle between the 1 local axis and the x axis, see Figure **2-6**.
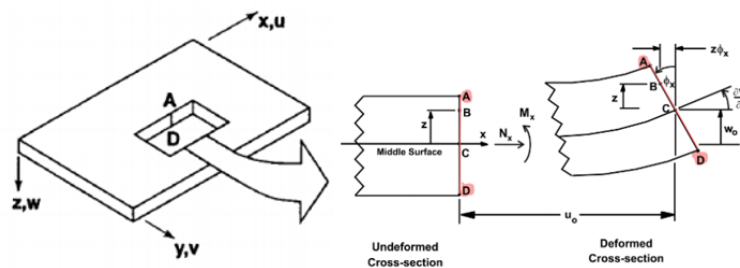
Figure 2-5.: Laminate axis orientation, laminate section before and after deformation [Barbero, 2018, Philpot et al., 2002].
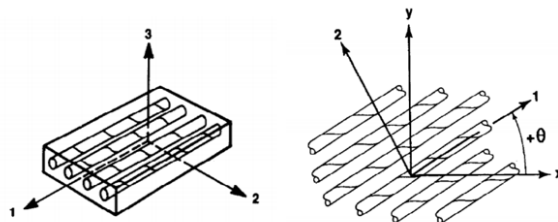
Figure 2-6.: lamina axis orientation [Philpot et al., 2002].

Stress and strains are defined in the laminate coordinates system according to **2-7**; the strains in the laminate coordinates follow the same convention. In the ply coordinate system, sub-index x is replaced by 1, y by 2, and z by 3.
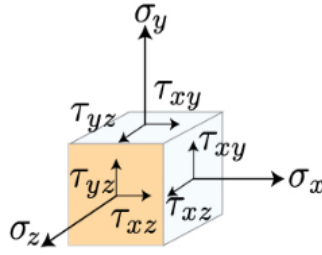
Figure 2-7.: Stress convention [Philpot et al., 2002].

2.5.2. Assumptions

- The thickness of the laminate is much smaller than the other dimensions.

- The transverse stress σ_z and normal strain ϵ_z are small enough to be considered equal to zero.

- "A line originally straight and perpendicular to the middle surface remains straight after the plate is deformed" [Barbero, 2018] (line A–D in Figure **2-5**); it means, the shear strains γ_{xz} and γ_{yz} are constant through the thickness.

- Infinitesimal strain state is assumed.

2.5.3. Displacements

The deformation of a laminate is described in **2-5**, from here, it can be shown that the displacement at every point is described by Equation 2-1.

$$u(x, y, z) = u_0(x, y) - z\varphi_x(x, y)$$
$$v(x, y, z) = v_0(x, y) - z\varphi_y(x, y)$$

$$(2\text{-}1)$$

Where $u(x, y, z)$ is the displacement in the x-direction at each point (x, y, z) and $v(x, y, z)$ is the displacement in the y-direction. The variables $u_0(x, y)$ and $v_0(x, y)$ stand for the displacements of every point (x, y) of the middle surface of the laminate. The functions φ_x and φ_y are the rotations of a line perpendicular to the middle surface (line A–D of Figure **2-5**).

2.5.4. Strain

From the definition of infinitesimal strain tensor [Megahed, 2019], the strain displacement relationship can be written as Equation 2-2 shows.

$$
\begin{aligned}
\epsilon_x(x,y,z) &= \frac{\partial u_0}{\partial x} - z\frac{\partial \varphi_x}{\partial x} \\
\epsilon_y(x,y,z) &= \frac{\partial v_0}{\partial y} - z\frac{\partial \varphi_y}{\partial y} \\
\gamma_{xy}(x,y,z) &= \frac{\partial u_0}{\partial y} + \frac{\partial v_0}{\partial x} - z\left(\frac{\partial \varphi_x}{\partial y} + \frac{\partial \varphi_y}{\partial y}\right)
\end{aligned}
\tag{2-2}
$$

For notation convenience Equation 2-2 is usually written in matrix form as Equation 2-3.

$$
\begin{Bmatrix} \epsilon_x \\ \epsilon_y \\ \gamma_{xy} \end{Bmatrix} = \begin{Bmatrix} \epsilon_x^0 \\ \epsilon_y^0 \\ \gamma_{xy}^0 \end{Bmatrix} - z \begin{Bmatrix} \kappa_x \\ \kappa_y \\ \kappa_{xy} \end{Bmatrix}
\tag{2-3}
$$

Where ϵ_x^0, ϵ_y^0, and γ_{xy}^0 are the middle surface strains; κ_x and κ_y are the bending curvatures; and κ_{xy} is the twisting curvature.

2.5.5. Stress

The stress in the laminate direction inside each lamina can be expressed as Equation 2-4, simplified according to Equation 2-5, and presented for better understanding as Equation 2-6.

$$
\begin{Bmatrix} \sigma_x \\ \sigma_y \\ \sigma_{xy} \end{Bmatrix} = [T]^{-1}[Q][R][T][R]^{-1} \begin{Bmatrix} \sigma_x \\ \sigma_y \\ \sigma_{xy} \end{Bmatrix}
\tag{2-4}
$$

$$
[\bar{Q}] = [T]^{-1}[Q][R][T][R]^{-1}
\tag{2-5}
$$

$$
\begin{Bmatrix} \sigma_x \\ \sigma_y \\ \sigma_{xy} \end{Bmatrix} = [\bar{Q}] \begin{Bmatrix} \sigma_x \\ \sigma_y \\ \sigma_{xy} \end{Bmatrix}
\tag{2-6}
$$

Where $[T]$ is the rotation matrix from the local $(1,2,3)$ coordinate system to the laminate coordinate system (x,y,z), $[Q]$ is the plane stress stiffness matrix for a lamina in the local directions, $[\bar{Q}]$ is the plane stress stiffness matrix for a lamina in the global (laminate) directions, and $[R]$ is the Reuter matrix. For a detailed explanation of single ply mechanics

check chapter five of [Barbero, 2018]. Matrix $[Q]$ can be calculated from the in-plane material properties according to Equation 2-7.

$$[Q] = \begin{bmatrix} E_1/\Delta & \nu_{12}E_2/\Delta & 0 \\ \nu_{12}E_2/\Delta & E_2/\Delta & 0 \\ 0 & 0 & G_{12} \end{bmatrix} \qquad\qquad \Delta = 1 - \nu_{12}^2 E_2/E_1 \qquad\qquad (2\text{-}7)$$

Where E_1 is the Young modulus in the fibre direction, E_2 is the Young modulus in the transverse direction, G_{12} is the shear modulus, and ν_{12} is the Poisson ratio measured in the fibre direction.

The strain distribution is assumed uniform through the whole laminate, but as every lamina has a different stiffness, the resultant stress distribution is only piece-wise continuous as shown in Figure **2-8**.
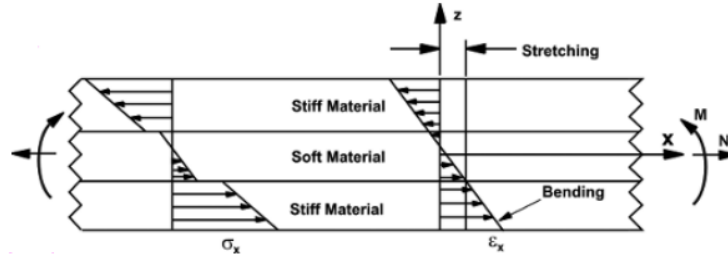
Figure 2-8.: Strain and stress distribution inside a general laminate [Barbero, 2018].

2.5.6. Stiffness

The force and moments per unit length along the boundary of the laminate can be found using the expression in Equation 2-8, which is integrated according to Figure **2-9**, to obtain the algebraic form shown in Equation 2-9.

$$\begin{Bmatrix} N_x \\ N_y \\ N_{xy} \end{Bmatrix} = \int_{-t/2}^{t/2} \begin{Bmatrix} \sigma_x \\ \sigma_y \\ \sigma_{xy} \end{Bmatrix} dz = \sum_{k=1}^{N} \int_{z_{k-1}}^{z_k} \begin{Bmatrix} \sigma_x \\ \sigma_y \\ \sigma_{xy} \end{Bmatrix}^k dz$$

$$\begin{Bmatrix} M_x \\ M_y \\ M_{xy} \end{Bmatrix} = -\int_{-t/2}^{t/2} \begin{Bmatrix} \sigma_x \\ \sigma_y \\ \sigma_{xy} \end{Bmatrix} z\,dz = -\sum_{k=1}^{N} \int_{z_{k-1}}^{z_k} \begin{Bmatrix} \sigma_x \\ \sigma_y \\ \sigma_{xy} \end{Bmatrix}^k z\,dz \qquad (2\text{-}8)$$
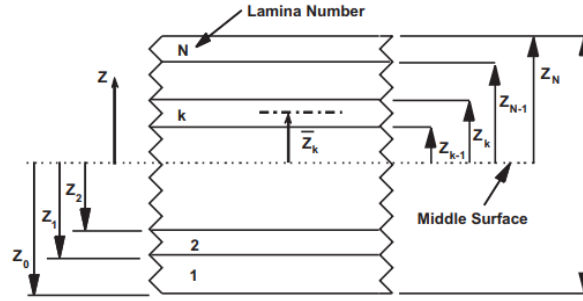
Figure 2-9.: Integrations limits for laminate stiffness [Barbero, 2018].

$$
\begin{Bmatrix}
N_x \\
N_y \\
N_{xy} \\
M_x \\
M_y \\
M_{xy}
\end{Bmatrix}
=
\begin{bmatrix}
[A] & [B] \\
[B] & [D]
\end{bmatrix}
\begin{Bmatrix}
\epsilon_x^0 \\
\epsilon_y^0 \\
\gamma_{xy}^0 \\
\kappa_x \\
\kappa_y \\
\kappa_{xy}
\end{Bmatrix}
\tag{2-9}
$$

Where:

- N_x, N_y, and N_{xy} are the tensile and shear forces per unit length along the side of the laminate [Barbero, 2018].

- M_x, and M_y are the bending moments, and M_{xy} is the twisting moment per unit length along the side of the laminate [Barbero, 2018].

- ϵ_x^0, ϵ_y^0, and γ_{xy}^0 are the middle surface strains; κ_x and κ_y are the bending curvatures; and κ_{xy} is the twisting curvature [Barbero, 2018].

- z_k and z_{k-1} are the coordinates of the bottom and top faces of lamina k [Barbero, 2018].

- $[A]$ is called in-plane stiffness matrix or extensional stiffness matrix. It directly relates in-plane strains (ϵ_x^0, ϵ_y^0, and γ_{xy}^0) to in-plane forces (N_x, N_y, and N_{xy}) [Barbero, 2018], it can be calculated according to Equation 2-10.

- $[B]$ is called bending-extension coupling stiffness matrix. It relates in-plane strains to bending moments and curvatures to in-plane forces [Barbero, 2018], it can be calculated according to Equation 2-11.

- [D] is called bending stiffness matrix. It relates curvatures (κ_x, κ_y and κ_{xy}) to bending moments (M_x, M_y and M_{xy}) [Barbero, 2018], it can be calculated according to Equation 2-12.

$$A_{ij} = \sum_{k=1}^{N} (\bar{Q}_{ij})_k (z_k - z_{k-1}) \tag{2-10}$$

$$B_{ij} = {}^{-1}\!/\!{}_2 \sum_{k=1}^{N} (\bar{Q}_{ij})_k (z_k^2 - z_{k-1}^2) \tag{2-11}$$

$$D_{ij} = {}^{-1}\!/\!{}_3 \sum_{k=1}^{N} (\bar{Q}_{ij})_k (z_k^3 - z_{k-1}^3) \tag{2-12}$$

The Classical Laminate Theory works as follows: once the laminate is completely defined, the A, B, D matrix can be calculated; these matrices represent the stiffness of a unit length and unit width shell. According to Equation 2-9, there are six independent variables and six dependent variables; so, usually either three force components and three bending moments can be applied and the resultant deformation can be found; or three in-plane strains and three bending curvatures can be applied and the resultant force and moment reactions can be found. In practice, as long as six independent values are set, the remaining six can be found; it does not matter if some of the values correspond to strains and curvatures, or forces and moments, or a combination of all of them; as long as the variables chosen are mutually exclusive, the algebraic system can be solved. For instance, if κ_x is chosen to be one of the six independent variables, the only condition to choose the remaining five is that M_x must be a dependent variable.

2.6. Non-linear beam theory

Analytic solution for the four-point bending test of a rectangular beam is usually found using the Classic Beam Theory, which deals with the small deformations assumption. This kind of solution may capture the essential features when modelling thick rigid beams under relatively small deformations [Recupero et al., 2005], but when it comes to composite sheets, as it is the problem at hand, thin composite laminates can undergo large deformations under relatively small loads, while keeping sub-critical stresses and strains.
S. I. Paolinelis and R. M. Ogorkiewicz at [Paolinelis and Ogorkiewicz, 1976] found an analytic solution for the problem of the four point bending beam depicted in Figure **2-10** (all variables are explained in detail in section 5.1). Their assumptions were the following:

- The beam undergoes large deformations while keeping small strains.

- The beam is made of a homogeneous linear elastic material.

- The points where the upper noses loads and support reactions are applied do not change with deformation.

Even though their assumptions may look limited, as it is shown later, with a few modifications this solution can be applied to the bending of a hybrid composite sheet where the upper noses and support radios are considered. The mathematical foundation of this solution is explained in the implementation of the analytical solution for the hybrid composite beam.
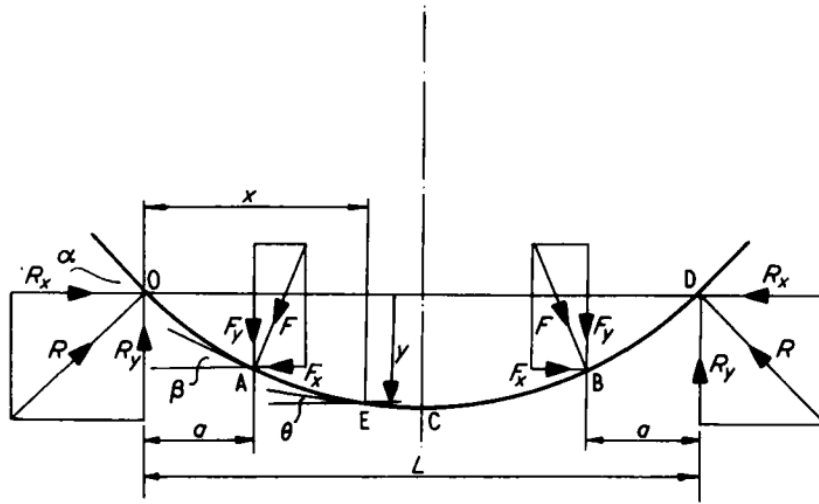
Figure 2-10.: Free body diagram of a four point bending beam under large deformations [Barbero, 2008].

2.6.1.   First ply failure and ply discount method

Given a load or deformation imposed, the Classical Laminate Theory allows to calculate the stresses and strains in the local coordinates for each ply in the laminate; this way, different failure criteria can be assessed to determine the ply where failure is expected. Usually this theory is used to predict only the first ply that is expected to fail, beyond that depending on the nature of the laminate and its fracture mechanics properties, either global collapse can be determined to follow or gradual failure methods like the Ply Discount can be used [Whitney, 2005].

The ply discount works as follows [Whitney, 2005]:

1. Compute or update the ABD matrix for the current layup configuration.

2. Apply or increase the load or deformation to the laminate.

3. Calculate stresses and strains for each ply.

4. Apply failure criteria to determine the plies where failure is expected.

5. If a lamina meets a failure criteria, set the stiffness coefficients of that lamina equal to zero.

6. Go to step 1.

The process progress until all the laminas in the laminate have failed [Whitney, 2005].

2.7. Finite element analysis of composite materials

2.7.1. Modelling scale

Modelling composite materials using the finite element method can be done at multiple scales: from the micromechanics scale (Figure **2-11** (a)) in which the fibres and matrix are meshed as separate entities with boundaries between them. Also at the lamina level (Figure **2-11** (b)), when even though a single lamina is considered to be a homogeneous material with orthotropic properties, the laminate by itself is analysed by the interaction of all the laminas inside it. Finally, the largest scale and simplest modelling approach is the laminate level (Figure **2-11** (c)), in which the full layup is modelled as a single equivalent orthotropic material.
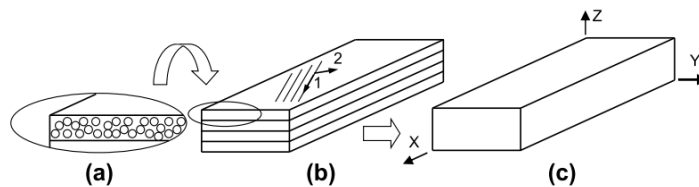
Figure 2-11.: Finite element modelling scale for composite materials. a) Micromechanics, b) Lamina level, c) Laminate level [Barbero, 2008].

In this work, the main purpose is to identify failure onset and progression in hybrid composite laminates; that is why, numerical modelling is performed at the lamina scale, this way, the interaction between the laminas and individual failure mechanisms inside the laminate can be analysed. This kind of approach allows to identify the exact location and nature of failure as it progress, because it differentiates between intralaminar failure modes such as fibre fracture, buckling and matrix fracture; and interlaminar failure modes such as delamination due to mode I or mode II loading [Barbero, 2008]. The development of the numerical tool is done using the software Abaqus and following the recommendations of Barbero [Barbero, 2008].

2.7.2. Conventional element types

There are four different element types that can be used to model elastic behaviour of composite materials at the lamina scale and they are described next:

- **Conventional shell elements**

  The geometry of a conventional shell element is based on a surface that has no thickness; the stiffness matrix of this type of element is defined according to the Classical Laminate Theory [Barbero, 2008], therefore, using a mesh of this elements implies working with the assumptions described in 2.5.2. This type of element in Abaqus has a linear and quadratic formulation when using an implicit analysis, but only linear when the analysis is explicit [Simulia, 2014].

- **3D solid elements**

  The geometry of a 3D solid element is based on a 3D volume. They use no assumptions related to shell theory, so their aspect ratio should not be greater than 10. These elements provide the more accurate analysis as no assumptions on stress fields has to be made; they provide detailed results of stress variation, and they can capture through thickness shear stress variations (this cannot be captured by elements based on shell theories) [Barbero, 2008]. In Abaqus they can have a linear or quadratic formulation in implicit analysis, but only linear in explicit [Simulia, 2014].

- **Continuum shell elements**

  The geometry of a continuum shell element is based on a 3D volume, these elements "are basically 3D solid elements where the classical laminate theory is enforced by special interpolation functions"; therefore, their side-to-thickness ratio can be higher than in 3D solid elements. In Abaqus continuum shell elements can only be linear either for explicit or implicit analysis; so, when using them to model bending, dense meshes are needed [Simulia, 2014].

- **2D plane-strain or plane-strain elements**

  The geometry of a 2D plane elements is based on a 2D plate. These are basically 3D solid elements where the in plane-stress/strain is enforced; thus, they can only be used to model in plane-stress or in plane-strain central sections of unidirectional or cross ply laminates (no normal-shear coupling is presented) [Grupo, 2008]. These type of element in Abaqus can have a linear and quadratic formulation when using an implicit analysis, but only linear when the analysis is explicit [Simulia, 2014].

Composite laminate structures usually have very small thickness when compared to the width and length dimensions (side dimensions), this impose no restrictions or limitations when using continuum or conventional shell elements, as they can be meshed with large side-to-thickness ratios; but 3D solids and 2D plane elements are limited to ratios lower than 10 (for accurate results); therefore, when using 3D solids and 2D plane elements the mesh is expected to be more dense; thus, more computationally expensive [Barbero, 2008, Simulia, 2014].

All the aforementioned element types can be used to model elastic behaviour, besides, continuum damage mechanic theories can be added to increase the capabilities of the analysis, but if discrete damage analysis (fracture mechanics) needs to be performed either Extended Finite Element Method (XFEM) or Cohesive Damage Models have to be used [Barbero, 2008].

2.8. Cohesive elements

Cohesive damage models can be used in conjunction with any of the previously mentioned element types in order to model fracture and delamination. The fracture properties are captured by the cohesive behaviour while the properties of the elastic or continuum damage are captured by the continuum or "conventional" elements described in section 2.7.2 [Turon Travesa, 2007].

Cohesive modelling assumes that "the stress transfer capacity between the two separating faces is not lost completely at damage initiation, but rather is a progressive event governed by progressive stiffness reduction of the interface between the two separating faces" [Barbero, 2008] (see Figure **2-12**). The area under the stress-separation curve is the amount of energy required to completely separate the two surfaces, this value is set to be equal to the fracture energy G_i of the material in one specific mode of load [Rose et al., 2013].

The cohesive elements act like springs that connect two adjacent continuum element representing two different surfaces, such connection is given by the stiffness of the cohesive elements, which prior to failure should be high enough so it does not disrupt the compliance of the structure [Hashin, 1983]. The cohesive element stiffness is defined by the penalty stiffness $\tilde{K}_i$, the failure stress σ_i^0 and, failure separation δ_i^0 define the onset stiffness degradation. An example of how these values are selected is given in the implementation of the models using cohesive elements in section 4.
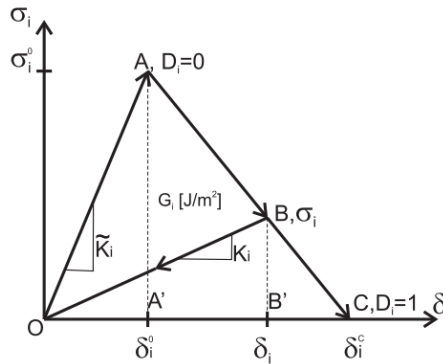
Figure 2-12.: Cohesive model stress-separation assumption [Barbero, 2008].

With all the background provided above, now we are in the position to explain how the hybrid materials can develop a gradual failure and how this phenomenon can be modelled.

2.9. Hybrid composite materials under tension loads

The problem at hand is related to pure bending load scenario, where the stress distribution represents a linear variation from tension to compression [Recupero et al., 2005] (see Figure **2-13**); so, the behaviour of hybrid composites specimen under pure tension can give insight into the behaviour of the tensile side of hybrid specimens under bending loads, besides, most of the failure mechanisms that aid gradual failure in tension also contribute to gradual failure in bending, and this is the main reason for the study in this section. As mentioned before, a lot of work has been done in unidirectional symmetric layups for tension tests; both in unidirectional as well as quasi-isotropic laminates. But as the problem in this project is related to bending, only three publications can be considerate to be relevant, and the reason for that is explained next:

- The first paper explains the methodology for modelling fragmentation of hybrid composites using the finite element method, this knowledge is useful as fragmentation is also expected in this kind of material under bending loads [Jalalvand et al., 2014].

- The second paper explains an analytical model that predicts fragmentation and stiffness reduction in hybrid composites, this theory is later used in the development of the analytical tool for bending [Jalalvand et al., 2015].

- The last publication is useful in the sense that provides the tabulated data and mechanical properties needed to validate numerical and analytical models [Idárraga, 2019].
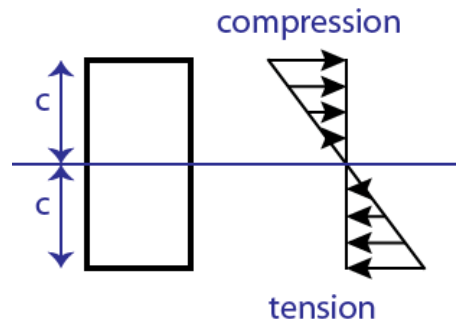
Figure 2-13.: Stress distribution under pure bending load [Recupero et al., 2005].

2.9.1.   Numerical model of Jalalvand et al [Jalalvand et al., 2014]

In this work, doctor Jalavand modelled unidirectional hybrid laminates made of SkyFlex USN020A thin carbon pre-pregs and standard thickness Hexcel 913/E-Glass pre-pregs under unidirectional traction load (problem described in section 2.4.1); the idea was to be able to capture all the possible damage modes in a glass/carbon/glass hybrid sandwich configuration; for that, he created a 2D plane-strain model using quadrilateral elements with quadratic formulation to model the stiffness; intralaminar and interlaminar cohesive elements to model fracture and delamination; he arranged the cohesive elements in as is shown in Figure **2-14**. The strength and fracture energy of the interlaminar cohesive elements is taken from the properties of the resin, he used a single value for the whole cohesive layer for delamination. The strength of the cohesive elements for carbon fragmentation is taken from a random distribution obtained in Equation 2-13 based on Weibull statistical distribution. Failure in the glass layer is assessed by considering both the size effect and stress concentration due to carbon fragmentation. Equation 2-14 is used to compute the equivalent stresses (σ_{eq}) in the glass layers and then it is compared with the characteristic strength given for the specific volume of glass.
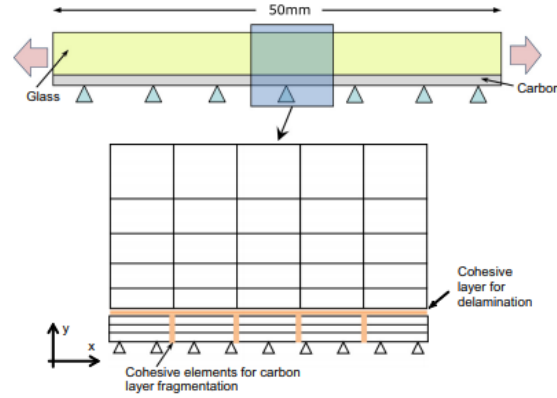
Figure 2-14.: Jalalvand numerical 2D model for hybrid composites under tension loads [Jalalvand et al., 2014].

$$T = T^0[ln(\frac{1}{1-n})]^{1/m} \tag{2-13}$$

Where according to Jalalvand T is the value of strength for one particular cohesive section, n is a random variable between 0 and 1, m is the Weibull modulus, and T^0 is a scale factor.

$$\sigma_{eq} = \sqrt[m]{\int_0^v (\sigma_1(x,y))^m dv} \tag{2-14}$$

Where σ_{eq} is the equivalent stress in the glass ply, and the integral represents the sum of all the stress in the fibre direction inside the volume of the glass layers.

The results he obtained were very accurate in most cases, as can be shown in Figure **2-15**.
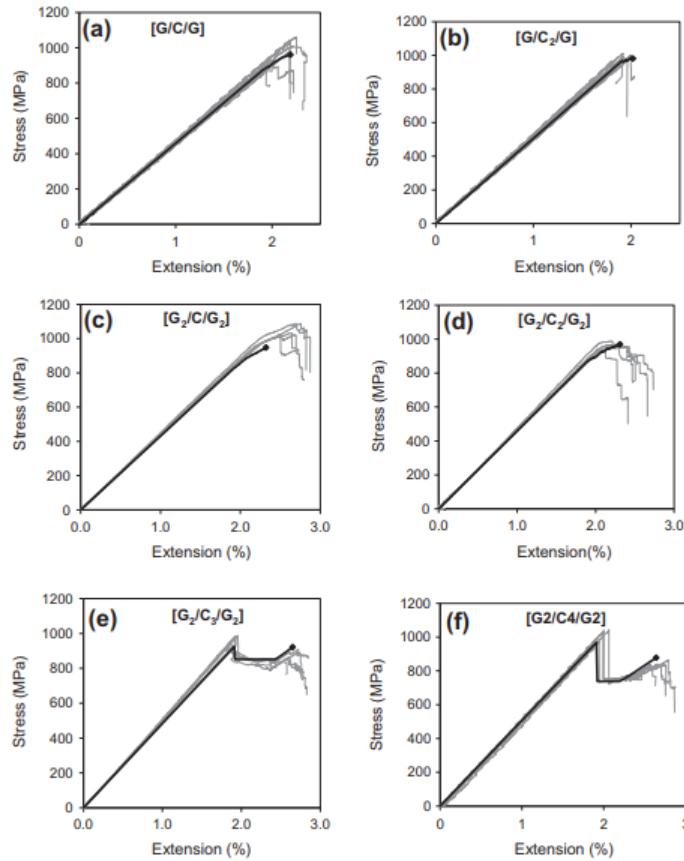
Figure 2-15.: Jalalvand numerical stress-strain results; numerical results in bolt and
experimental results in shaded grey [Jalalvand et al., 2014].

2.9.2.   Analytical model of Jalalvand et al [Jalalvand et al., 2015]

In this work, doctor Jalalvand developed an analytical solution for the problem described
in section 2.4.1. He found analytical expressions to compute the stress and strain curve for
each failure mode, each point can be found according to Table **2-1**, and explained in Table
2-2 Based on the laminate mechanical properties and dimensions, critical stress values can
be found for each damage mode, so following the algorithm detailed in Figure **2-16**, the
critical stress values are compared, this way the failure sequence can be obtained and plotted
as shown in Figure **2-17**. More details on this topic are given in the development of the
analytical solution for bending.

Table 2-1.: Coordinates for main points in stress-strain curve of hybrid composite layup in tension [Jalalvand et al., 2015].

Failure mode	Point 1	Point 2	Point 3	Point 4	Point 5
Premature high strain material failure	(0.0,0.0)	$(\epsilon_{FL}, \sigma_{@FL})$			
Catastrophic delamination and high strain material failure	(0.0,0.0)	$(\epsilon_{FL}, \sigma_{@FL})$	$(\epsilon_{FL}, \sigma_{@del})$	$\left(\frac{\sigma_{@del}}{E_{int}}, \sigma_{@del}\right)$	$\left(\frac{\epsilon_{FH}}{K_{t}*\sqrt[m]{V}}, \sigma_{@HF}\right)$
Low strain material fragmentation and high strain material failure	(0.0,0.0)	$(\epsilon_{FL}, \sigma_{@FL})$	$\left(\frac{\sigma_{@Frg}}{E_{sat}}, \sigma_{@Frg}\right)$	$(\epsilon_{HF-PS}, \sigma_{@HF})$	
Low strain material fragmentation, local delamination, and high strain material failure	(0.0,0.0)	$(\epsilon_{FL}, \sigma_{@FL})$	$\left(\frac{\sigma_{@Frg}}{E_{sat}}, \sigma_{@Frg}\right)$	$\left(\frac{\sigma_{@del}}{E_{int}}, \sigma_{@del}\right)$	$\left(\frac{\epsilon_{FH}}{K_{t}*\sqrt[m]{V}}, \sigma_{@HF}\right)$

Table 2-2.: Variables used in [Jalalvand et al., 2015].

ϵ_{FL}	Failure strain of the low strain material
$\sigma_{@FL}$	Laminate stress at low strain material failure
$\sigma_{@del}$	Stress in the laminate at which delamination propagates
$\frac{\sigma_{@Frg}}{E_{sat}}$	Laminate strain at low strain material fragmentation
$\sigma_{@Frg}$	Laminate stress at low strain material fragmentation
E_{sat}	Modulus of the laminate with randomly saturated fragmentation in the low strain material
$\frac{\sigma_{@del}}{E_{int}}$	Strain in the laminate at which delamination propagates
$\sigma_{@del}$	Stress in the laminate at which delamination propagates
E_{int}	Initial modulus of the UD hybrid laminate
ϵ_{HF-PS}	Strain in the laminate at the post-saturation phase when the high strain material fails
$\sigma_{@HF}$	Laminate stress at high strain material failure
$\frac{\epsilon_{FH}}{K_t * \sqrt[m]{V}}$	Laminate strain at high strain material failure
ϵ_{FH}	Failure strain of the high strain material
K_t	Stress concentration factor
V	Volume of the specimen
m	Weibull modulus of high strain material strength distribution

Where the variables such as α, β correspond to material and geometric constants defined in reference [Jalalvand et al., 2015].
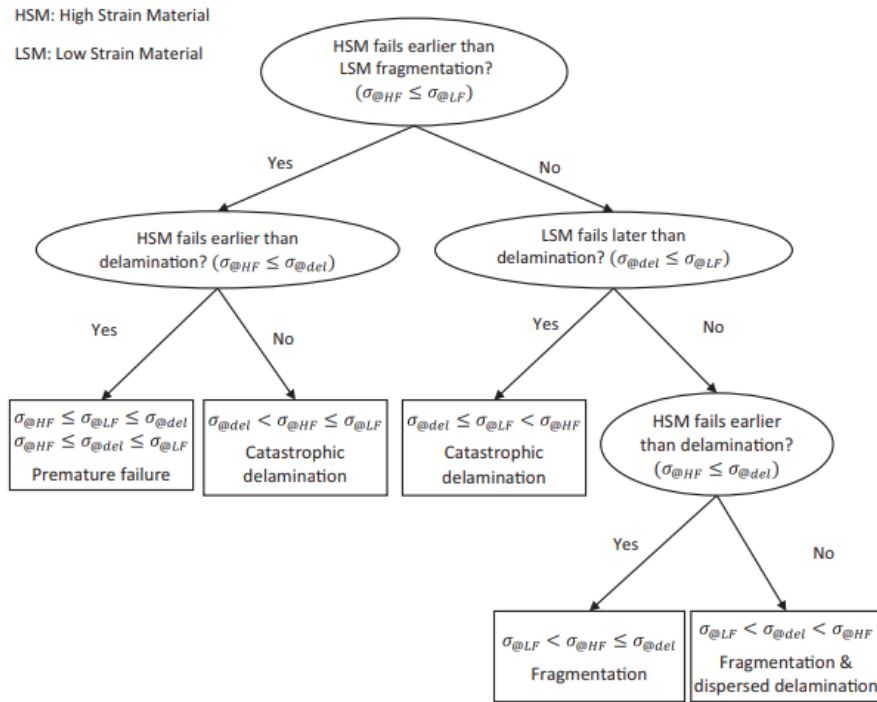
Figure 2-16.: Algorithm to find the failure sequence [Jalalvand et al., 2015].
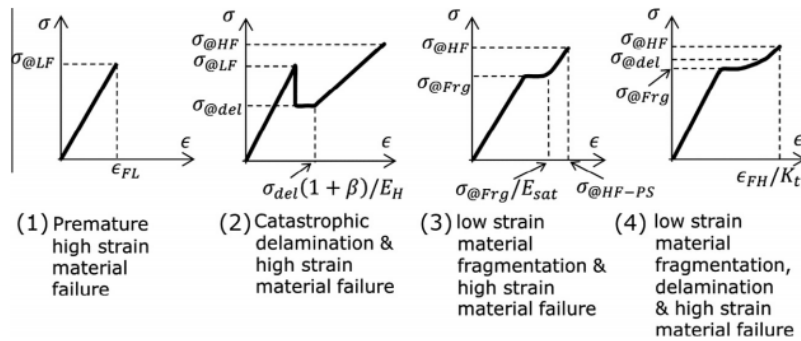
Figure 2-17.: Possible stress–strain responses in hybrid composite laminates [Jalalvand et al., 2015].

The results were accurate but slightly more limited than the numerical solution, see Figure **2-18**.
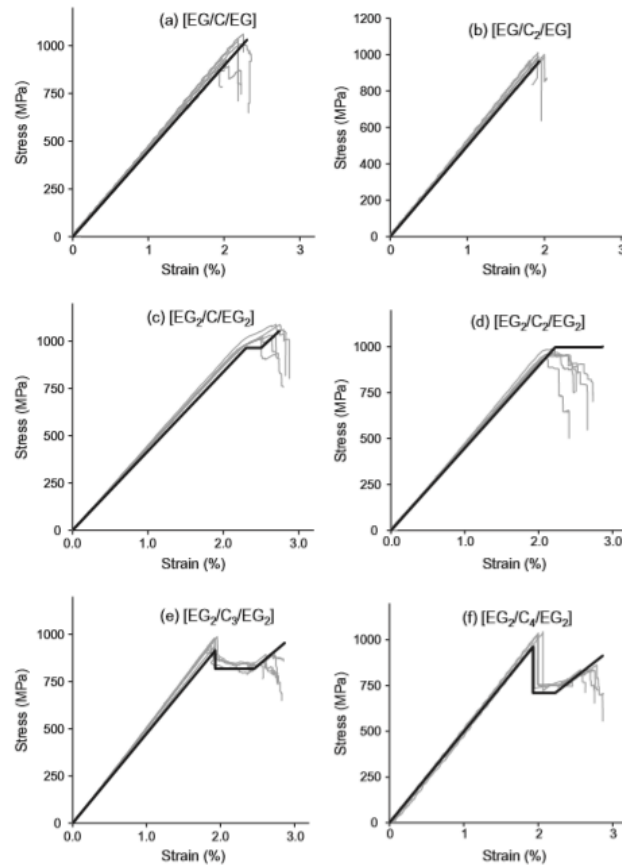
Figure 2-18.: Jalalvand analytical stress-strain results; analytical results in bolt and experimental results in shaded grey [Jalalvand et al., 2015].

2.9.3.   Experimental work done by Idarraga [Idárraga, 2019]

This work consists of a series of experiments using different layups and orientations, thanks to the collaboration of Idárraga, the load-displacement tabulated results are at hand for direct comparison. More details of this work are given in the background of this project, in section 3.

2.10.   Hybrid composite materials under bending loads

Hybrid composite materials have been studied almost exclusively using a three-point bending setup and just a few experimental and numerical results are found using a four-point bending setup to promote gradual failure, Idárraga [Idárraga, 2019] and Cusack [Cusack, 2018] works are mentioned in later sections. In this section there is an overview of the most relevant work performed on hybrid composite materials under bending loads, particularly in a three-point bending setup; the main authors, analysis approaches, and research focuses are addressed

here.

2.10.1.   Materials, layups, and fabric types

Most of the work performed in hybrid composite laminates under bending loads has been done in carbon/epoxy and glass/epoxy hybrid configurations [Idárraga, 2019, Jesthi et al., 2018, Dong and Davies, 2013, Sudarisman et al., 2009, Dong, 2016, Zhang et al., 2012, Kalantari et al., 2016a, Kalantari et al., 2016c, Sudarisman et al., 2009, Dong, 2016, Cusack, 2018, Dong and Davies, 2012, Ary Subagia et al., 2014, Dong and Davies, 2014]. It is possible to find hybridization in natural fibres and glass [Reis et al., 2007, Velmurugan and Manikandan, 2007], or glass and Basalt [Fiore et al., 2011]. The hybrid effect is the main subject of study, and it is found that can be presented in all the aforementioned material combinations. Pseudo-ductility is only mentioned in [Jalalvand et al., 2015], in the other publications failure is almost exclusively brittle, with no discussion beyond first ply failure. In the carbon/glass hybrid composites studies, the trend is to use unidirectional fabrics, but some author use woven [Jesthi et al., 2018, Zhang et al., 2012] or twill [Jesthi et al., 2018]. When the hybridization is not done with carbon, the glass fibre is usually used as mat [Reis et al., 2007, Fiore et al., 2011, Velmurugan and Manikandan, 2007]. A positive hybrid effect can be obtained in all scenarios, but the effect is stronger in unidirectional fabrics, because unidirectional fabrics have higher compressive strength than woven fabrics of the same material, a key factor in the design of hybrid composites under bending.

Research has focused mainly on unidirectional laminates (all layers oriented at 0 degrees), only one publication has been found to study reinforcement in more than one direction [Kalantari et al., 2016c], the results say that it is possible to obtain a positive hybrid effect, but more work needs to be done.

It has been proved that the staking sequence plays one the mayor roles when it comes to the performance of hybrid composites; for carbon/glass laminates, it has been found that unsymmetrical layups yield the highest positive hybrid effect, but only when the glass layers are placed in the compressive side; this is due to the lower flexural stiffness and higher failure strain of the glass fibre; so when in a pure carbon composite (material with a low failure strain in compression and high stiffness) some of the upper laminas in compression are replaced by glass, the overall composite strength can be increased [Lim et al., 2014, Kalantari et al., 2016c, Dong, 2016, Dong and Davies, 2014, Dong and Davies, 2013, Dong and Davies, 2015, Dong and Davies, 2012, Ary Subagia et al., 2014]. Dong et al [Lim et al., 2014, Kalantari et al., 2016c, Dong, 2016, Dong and Davies, 2014, Dong and Davies, 2013, Dong and Davies, 2015, Dong and Davies, 2012, Ary Subagia et al., 2014] have studied the effect of the staking sequence on the layup strength, resistance and energy absorption; besides, the effect of other parameters such as fibre volume fraction, price and density. The parameter he used to define the staking sequence and degree of hybridization is the hybrid ratio (r_h), which is basically the amount of glass in the glass/carbon hybrid, so $r_h = 0$ is a non-hybrid carbon

composite, and $r_h = 1$ is a non-hybrid glass composite. One of the most useful tools these authors designed are plots like the ones shown in Figure **2-19** and Figure **2-20**, where the variation of the laminate strength and stiffness is calculated according to the ASTM D790-07, as a function of the hybrid ratio. Besides, they compared the experimental results with the predictions done using finite element analysis (FEA) and using the Classical Laminate Theory (CLT).
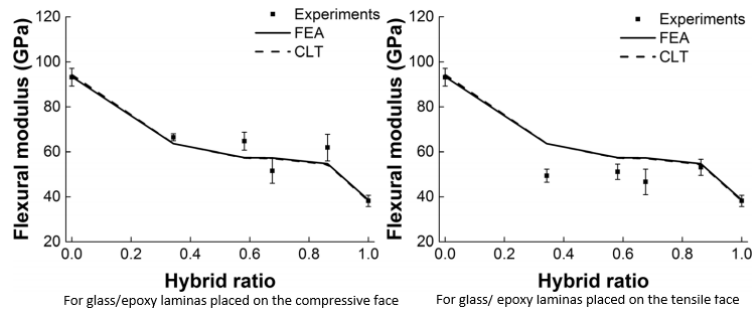
Figure 2-19.: Flexural modulus as a function of the hybrid ratio according to [Ary Subagia et al., 2014].
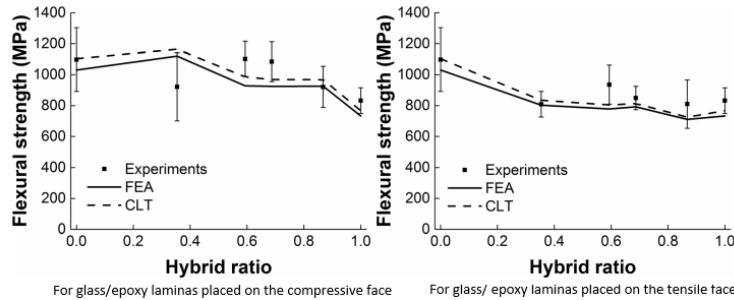
Figure 2-20.: Flexural strength as a function of the hybrid ratio according to [Kalantari et al., 2016a].

Some publications also work with symmetric layups [Jesthi et al., 2018, Dong and Davies, 2015, Zhang et al., 2012, Reis et al., 2007, Velmurugan and Manikandan, 2007], analysing the effect of having the high stiffness material on the outer or inner layers. The conclusion so far is that for symmetric laminates having the high stiffness material in the outer layers can increase the overall bending stiffness but promote failure at a low deformation.

2.10.2.   Standard test procedure for composite materials in bending

All the publications of hybrid composite analysis tested or modelled in a three-point bending setup have been in accordance with ASTM D7264/D7264M-15. The flexural strength and flexural modulus are calculated according to the equations in the standard, and even though

these equations only represent the maximum stress and Young's modulus in homogeneous non-hybrid materials, the equations are used as a mean of comparison.

2.10.3. Failure prediction and modelling approaches using finite elements and the Classical Laminate theory

It has been found that finite element analysis can help understand and predict failure in hybrid composite laminates (see Figure **2-19** and Figure **2-20**); the analysis are always done at lamina level, people usually use either a 3D shell element approach like the one used by Kalantari et al [Kalantari et al., 2016c] (see Figure **2-21**) or a 2D plane strain approach like the one of Dong et al [Lim et al., 2014, Kalantari et al., 2016c, Dong, 2016, Dong and Davies, 2014, Dong and Davies, 2013, Dong and Davies, 2015, Dong and Davies, 2012, Ary Subagia et al., 2014] (see Figure **2-22**). The trend is always to avoid contact modelling (the only paper found that modelled contact was the one of Reis et al [Reis et al., 2007]), and set load controlled simulations; most of the time non-linearities are not taken into account, the elastic mechanical properties of the materials are calculated according to Hashin theory [Hashin, 1983], failure in tension is based on the maximum strain of the fibre, and compressive strain is based on the Lo-Chim model [Naik and Kumar, 1999]. Finite element analysis as well as Classical Laminate Theory allow investigating the way the stress and strain distribution changes when the stacking sequence is modified or hybridized. Besides, it is necessary to mention that numerical and analytical analyses never go beyond first ply failure.
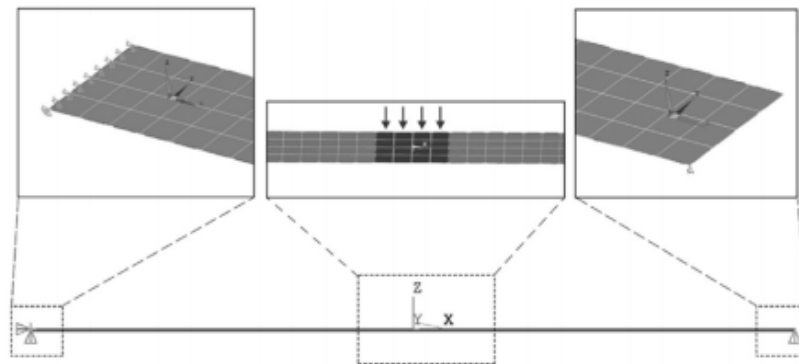
Figure 2-21.: 3D shell element model used by Kalantari et al [Kalantari et al., 2016c].
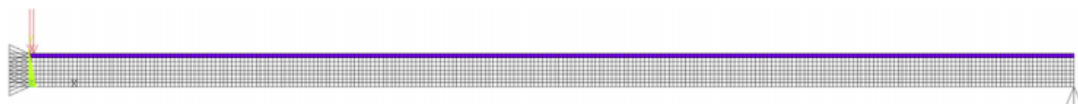
Figure 2-22.: 2D plane strain model used by Dong et al [Lim et al., 2014].

Ignoring contact and large deformations can still be accurate when the test is performed at a low span-to-depth ratio (in this context, a ratio of 32 is considered to be a low span to deep ratio), the experiment in [Dong et al., 2012] can prove that the load displacement curves at low span ratios are linear up to failure (see Figure **2-23**). But, when larger span-to-depth ratios are used (in this context, a ratio of 64 is considered to be a high span to deep ratio), non-linearities appear (see Figure **2-24**), and the effect of large deformations and contact starts to play an important role, evidence of this is later elaborated in the results.
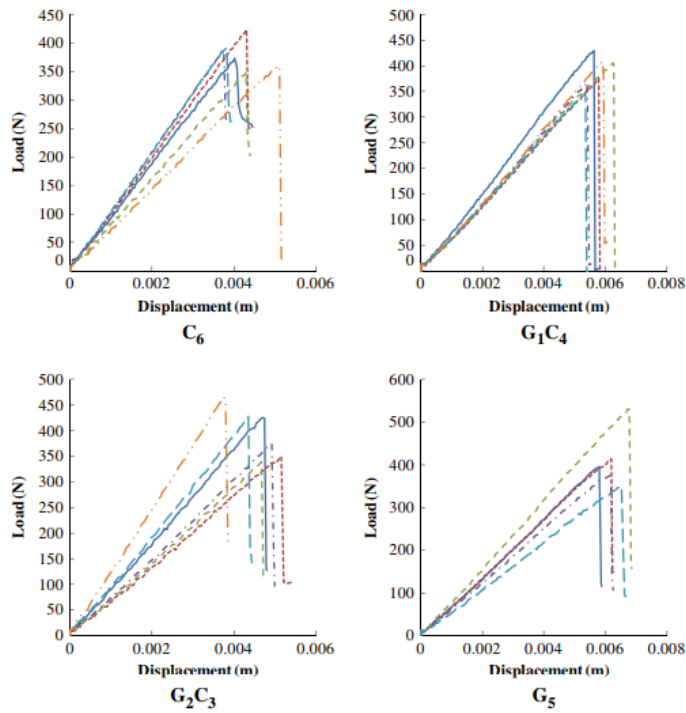
Figure 2-23.: Experimental load-displacement curves obtained for S-Glass(G) and T700S carbon (C) composites at a load-span-to-depth ratio of 32 [Dong et al., 2012].
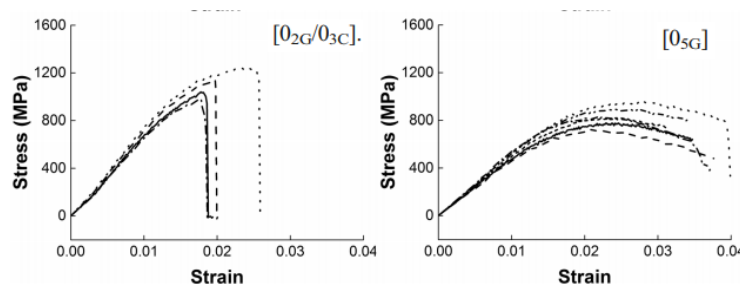
Figure 2-24.: Experimental load-displacement curves obtained for E-Glass(G) and IM7 carbon (C) composites at a load-span-to-depth ratio of 64 [Ary Subagia et al., 2014].

2.10.4.   Failure modes

According to all the papers but one [Idárraga, 2019] mentioned so far, failure in bending test is catastrophic and mainly in the area under compressive stresses; failure is mainly due to buckling and micro-buckling when large span-to-depth ratios are used, a transition to delamination may be present when the span-to-depth ratios are reduced, therefore, an apparent strength and stiffness reduction can be seen, this has been one of the major conclusions in the numerical [Dong and Davies, 2012] and experimental [Ary Subagia et al., 2014] studies on this topic, see Figure **2-25**. Besides, it can be said that, with the aid of light and electron microscopy important work has been done on an accurate characterization of the failure mechanisms that take place in hybrid composites [Idárraga, 2019, Lim et al., 2014].
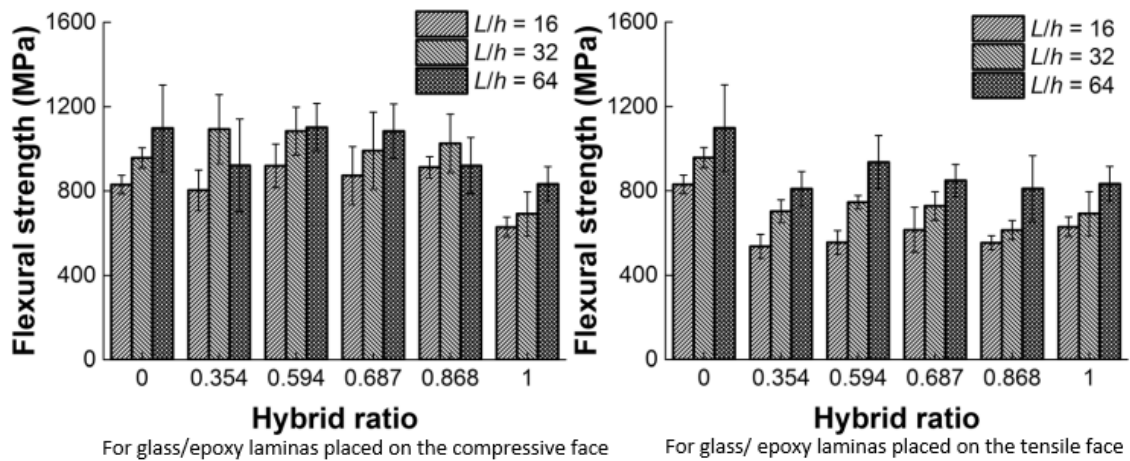
Figure 2-25.: Influence of the span-to-depth ratio on the flexural strength of IM7 and E-Glass / epoxy laminates [Ary Subagia et al., 2014].

3. Chapter 3: Background

3.1. Idárraga's results

The PhD student Guillermo Idárraga is part of the Design of Advanced Composite Materials Research Group (DADCOMP) at the National University and together with the former master students Jay Cusack and Ellis Hill from the University of Strathclyde (main collaborator institution) have done experimental, numerical, and analytical analysis in order to study the progressive failure in hybrid composite materials in a four-point-bending setup. As this thesis is a continuation and collaboration of their work, their previous results are analysed as the main background, mainly because they provide the data necessary to debug and verify the analytical and numerical models designed here.

3.1.1. Idárraga's results for tension

The first set of experiments done by Idárraga [Idárraga, 2019] on symmetric hybrid composite laminates were carried out in unidirectional (UD) and quasi-isotropic laminates in tension tests using SkyFlex USN020 spread tow carbon-reinforced thin prepreg from SK Chemicals as the low strain material; and a standard thickness UD S-Glass/913 Epoxy pre-preg supplied by Hexcel as the high strain material, see Table **3-1**. He proposed six different quasi-isotropic layups which all prove to fail gradually; and two unidirectional layups, see Figure **3-1**, which again proved to produce pseudo-ductility, see Figure **3-2** and Figure **3-3**. Figure **3-4** shows the typical stripes pattern presented in pseudo-ductile composites.
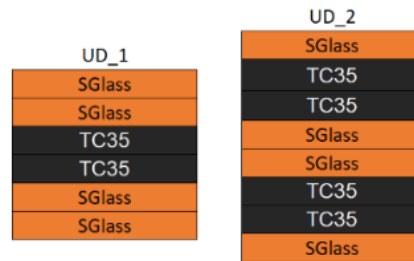
Figure 3-1.: Unidirectional laminates tested in tension by Idárraga [Idárraga, 2019].
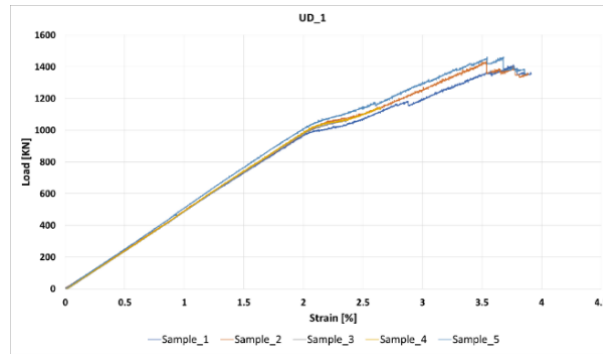
Figure 3-2.: Load vs Strain curve for layup UD_1 [Idárraga, 2019].
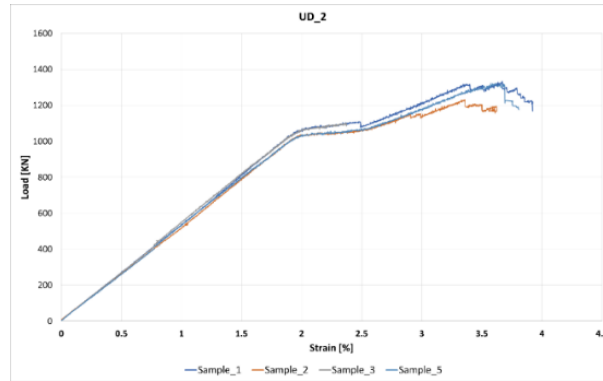
Figure 3-3.: Load vs Strain curve for layup UD_2 [Idárraga, 2019].
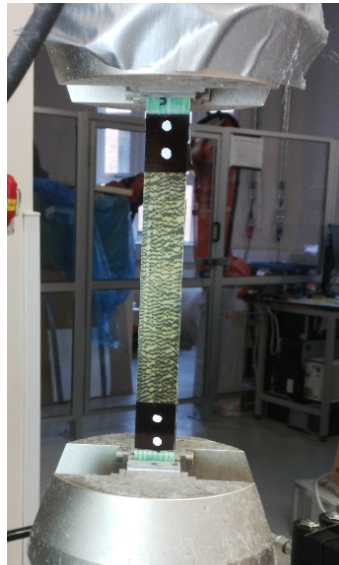
Figure 3-4.: Stripes pattern in a tensile specimen [Idárraga, 2019].

Table 3-1.: Mechanical properties of S-Glass-913/Epoxy, TC35/Epoxy, M55/Epoxy, T1000/Epoxy, and T800/Epoxy prepregs according to [Idárraga, 2019, Swolfs, 2019, X. Wu and Wisnom, 2017].

SGlass-913/Epoxy						
E_1 [GPa]	E_2 [GPa]	v_{12}	G_{12} [GPa]	Ply thickness [mm]	Tensile strain [%]	Compressive strain [%]
45.6	15.4	0.30	4.34	0.1551	3.98	2.33
TC35/Epoxy						
E_1 [GPa]	E_2 [GPa]	v_{12}	G_{12} [GPa]	Ply thickness [mm]	Tensile strain [%]	Compressive strain [%]
114.3	6.06	0.32	2.4	0.023	1.97	-
M55/Epoxy						
E_1 [GPa]	E_2 [GPa]	v_{12}	G_{12} [GPa]	Ply thickness [mm]	Tensile strain [%]	Compressive strain [%]
280.0	6.06	0.32	2.4	0.0305	0.8	0.46-0.56[1]
T1000/Epoxy						
E_1 [GPa]	E_2 [GPa]	v_{12}	G_{12} [GPa]	Ply thickness [mm]	Tensile strain [%]	Compressive strain [%]
143.3	6.06	0.32	2.4	0.0323	2.2	1.1
T800/Epoxy						
E_1 [GPa]	E_2 [GPa]	v_{12}	G_{12} [GPa]	Ply thickness [mm]	Tensile strain [%]	Compressive strain [%]
150.0	6.06	0.32	2.4	0.125	1.5	1.2-2

Idárraga tested specimens of layup UD 1 and UD 2, see Figure **3-5** and Table **3-2**. The data

---

[1]the value used in [Idárraga, 2019] was 0.56; but the value used in this work was 0.46, the one found in [Swolfs, 2019, X. Wu and Wisnom, 2017]

from the unidirectional laminates is used in the following sections to get a first validation of the finite element simulation of fragmentation in a simple load scenario; once the numerical model can accurately reproduce this phenomenon in tension, one can be sure it can be applied in bending.
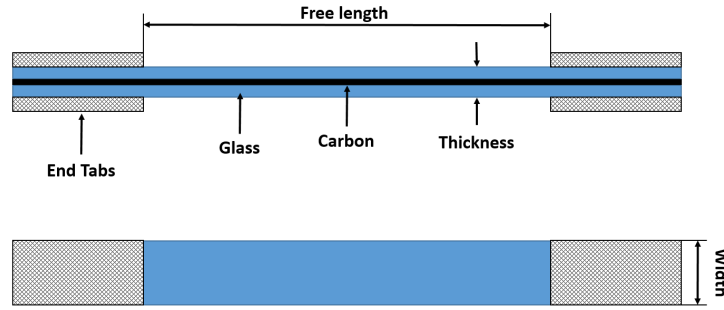
Figure 3-5.: Hybrid specimen dimensions for a tensile test [Idárraga, 2019].

Table 3-2.: Hybrid specimen dimensions for a tensile test [Idárraga, 2019].

Layup	Width [mm]	Thickness [mm]	Free length [mm]
UD 1	19,5	0,79	156,0
UD 2	19,9	0,84	161,0

3.1.2.   Idárraga's results for bending

The experiments done by Idárraga [Idárraga, 2019] on unsymmetrical hybrid composite laminates that proved to fail gradually under a four-point bending test were used for the debug and first validation of the numerical and analytical models developed in the next chapters. In that reference the author proposed two different hybrid composite layups that can fail in a gradual manner under bending loads. The layups consisted of seven layers of high strength S-Glass (SG) on the top of two different sequences of M55 and T1000 carbon fibres to form 61 layer hybrids: one layer of M55 followed by 4 layers of T1000 for Layup 1 $[SGlass_7/\text{T}1000/(M55/T1000_4)_{10}/\text{M}55/T1000_2]$; and one layer of M55 followed by 2 layers of T1000 for Layup 2 $[SGlass_7/T1000_2/(M55/T1000_2)_{18}]$, see Figure **3-6**. Specimens of these two configurations were manufactured using pre-pregs, autoclave for the curing process, and cut in rectangles of $190mm$ length, $20{,}38mm$ width and around $2{,}8mm$ thickness, the mechanical properties of these materials are shown in Table **3-1**. Then, the four-point bending tests were carried out according to the configuration shown in Figure **3-7** this configuration is not according to any ASTM standard, the support and load span are larger, and do not have the proportions recommended by ASTM D6272-17 [ASTM, 2019], according to

the author, the idea of having such a large support span was to avoid shear failure. The load and displacement of the upper noses (see Figure **3-8** and Figure **3-9**) and the strain in the lower lamina (see Figure **3-10** and Figure **3-11**) were recorded; besides, video record was used to have an approximation of the failure sequence of the laminas inside the laminates. The experimental failure analysis performed by Idárraga is summarized in Figure **3-8**, up to around 10 mm of vertical displacement the specimens have not reach damage, at this point fragmentation starts to take place generating the non-linear behaviour of the load-displacement curve. At around 24 mm of vertical displacement fracture and delamination of the T1000 blocks takes places creating the brush-like failure and the staircase shape in the gradual load drop, see Figure **3-14**. Compressive failure did not take place in the T1000 and S-Glass plies located in the upper compressive area. Some of the test were interrupted before the load drops; in these specimens, some of the upper most M55 plies fail by fragmentation in compression without delamination (see Figure **3-13**) and some of the lower most M55 plies also fail by fragmentation in tension (see Figure **3-12**).

a) Layout 1: [Sglass7/T1000/ (M55/T1000$_4$)$_{10}$ /T1000$_2$ /M55]   b) Layout 2: [Sglass7/(T1000$_2$ /M55)$_{18}$]
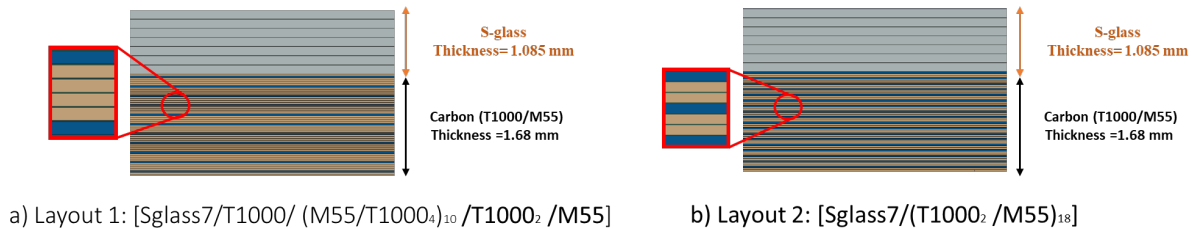
Figure 3-6.: Layup configuration for Idárraga's laminates in [Idárraga, 2019].
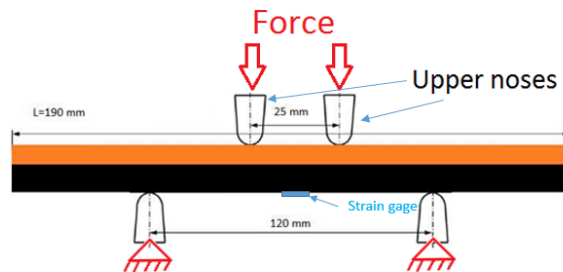
Figure 3-7.: Four point bending test configuration, the orange part of the laminate represents the S-Glass layers and the black the carbon layers [Idárraga, 2019].
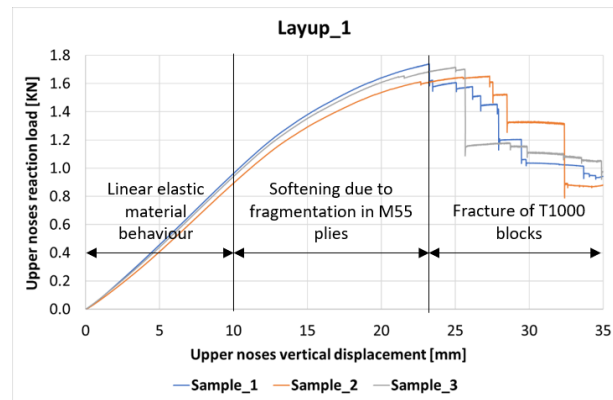
Figure 3-8.: Upper noses reaction force vs displacement of the upper noses for Layup 1 [Idárraga, 2019].
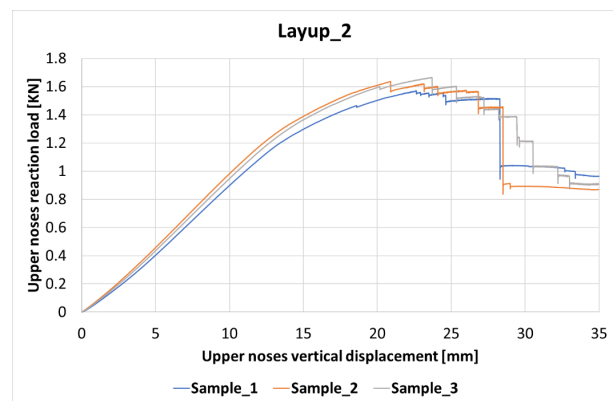
Figure 3-9.: Load vs displacement curve for layup 2 [Idárraga, 2019].
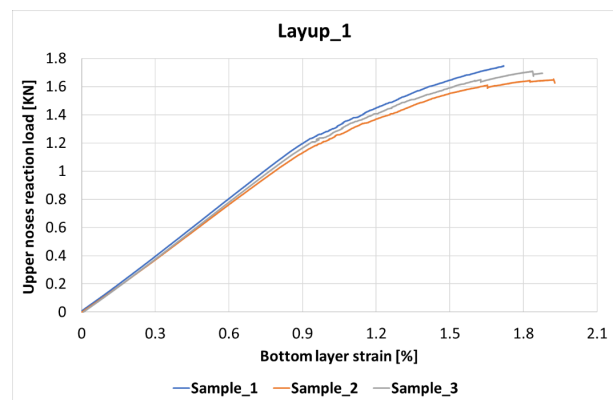
Figure 3-10.: Load vs strain in the lowest ply curve for Layup 1 [Idárraga, 2019].
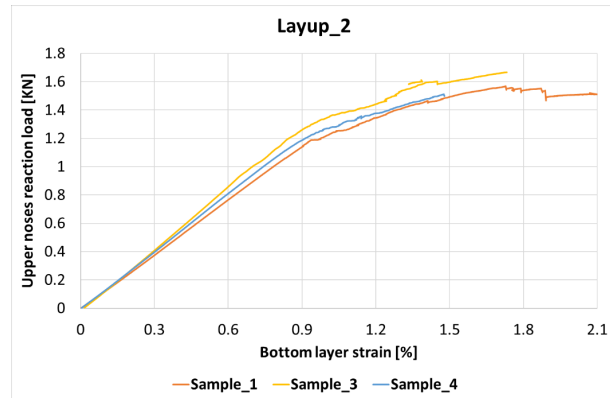
Figure 3-11.: Load vs strain the lowest ply curve for Layup 2 [Idárraga, 2019].
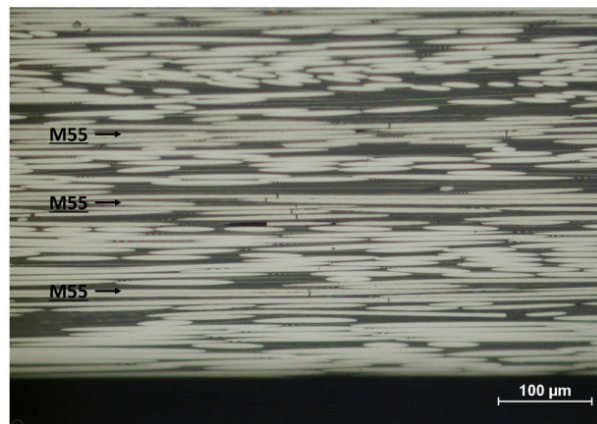
Figure 3-12.: Microscopy observation using 20X objective lens, tensile face of Layup 1
[Idárraga, 2019].
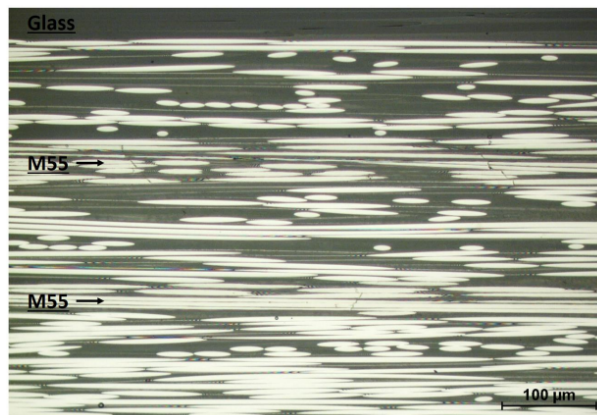
Figure 3-13.: Microscopy observation using 20X objective lens, compression face of Layup 1
[Idárraga, 2019].
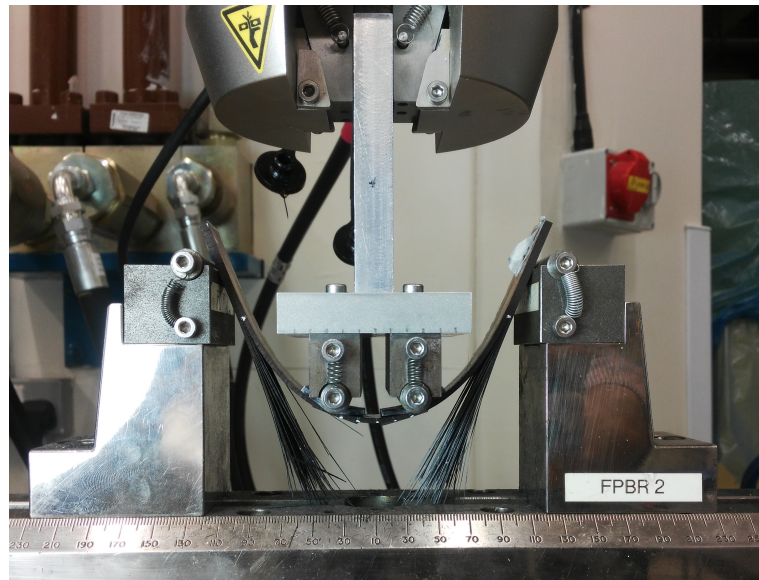
Figure 3-14.: Failure mode in the four point bending test of Layup 1 [Idárraga, 2019].

Idárraga defined gradual failure as the non-linearity first associated to softening due to fragmentation of the M55 plies and posterior staircase behaviour in the load-displacement curve due to brush-like failure, namely, the small load drops associated to gradual fracture and delamination of the T1000 blocks. He attributed the onset of non-linear behaviour in the load-displacement and load-strain curves to the initiation of fragmentation in the lower most and upper most M55 layers; but, as it will be shown later, the initial non-linear behaviour is dominated by large deformations, the contribution of fragmentation (internal damage) is barely perceived. Therefore, in this work, gradual failure is defined as the capacity of the specimen to bear a considerable amount of damage while still holding load, this definition overlaps with Idárragas definition on the capacity to have an staircase shape of the load-displacement curve.

The mechanical properties of these three materials are shown in Table **3-1**; most of these properties are taken from data-sheets using standard methods, and from experiments carried out by other researchers. The validity of some of these properties may be doubtful due to the procedures used for measurement; for instance, the properties in tension like the strain to failure are easy to measure and have low scatter; besides the strength in tension even when is affected by size effects is not heavily affected by the setup or layup configuration, it means, the failure strain in tension measured in pure tension is only slightly lower than measured in bending. But when it comes to the failure strain in compression, the real strength of a lamina inside a hybrid laminate in bending can be as much as double, compared with the failure strain measured in a standard unidirectional compression test. Taking the M55 carbon as an example, it can be seen in [Czél et al., 2017] that according to the data-sheet of the supplier, the maximum compressive strain is 0,26 %, but when the M55 ply is tested for

compression in a four point bending test, in the configuration shown in Figure **3-15** inside the laminate $[Sglass_2/Eglass_{13}/SGlass_2/M55_2/SGlass]$ the compressive failure strain can reach $0,46\%$ and, more important in this configuration M55 fails progressively, supporting load up to $2,2\%$ strain. According to [Idárraga, 2019] the value of this property could reach $0,56\%$. Performing estimations using the different strength values can yield different failure sequences; besides, if progressive failure can be presented, failure predictions using methods like the Ply Discount may overestimate the stiffness reduction of the laminate.

As it will be shown later, the compressive failure strain of the S-Glass/Epoxy should be higher than the value used by Idárraga and Hill in order to get an accurate failure sequence; this way, Idárragas results provide the necessary data to calibrate the properties used in the models of this work.
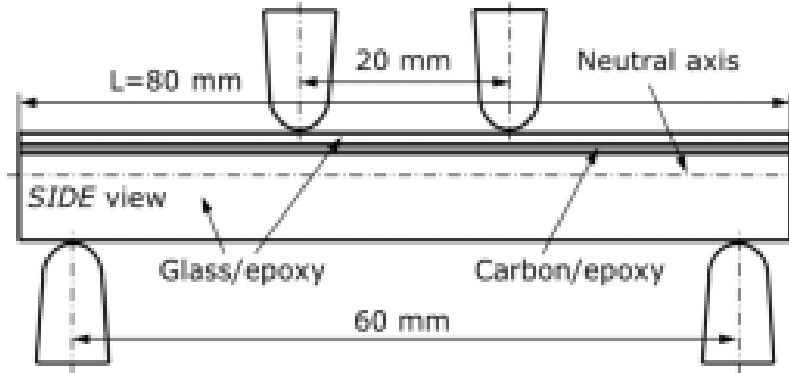
Figure 3-15.: Schematic of a four point bending test setup with an asymmetric interlayer hybrid specimen [Czél et al., 2017].

3.1.3.   Change Area Method (CAM)

The first method proposed by Idárraga and Hill, in an attempt to predicting the failure sequence of hybrid laminates, was called Change Area Method (CAM); this approach is grounded on the elemental beam theory which is based on linear elastic material response, infinitesimal strain and small deformations. They use the transformed section method described in [Hibbeler, 2001] to find the stiffness centroid of an equivalent beam of irregular cross-section; then, they use this centroid to compute the maximum bending moment that can be applied on each lamina based on its failure strain using Equation 3-1.

$$M_i = \frac{(\epsilon_i)_{max} * E_i * I_i}{c_i * N_i} \tag{3-1}$$

Where M_i is the failure bending moment, $(\epsilon_i)_{max}$ is the failure strain in the fibre direction for lamina i, E_i is the Young modulus in the fibre direction for lamina i, I_i is the moment of inertia of lamina i, c_i is the distance between the stiffness centroid and lamina i faces, and

N_i is the change area factor.

For each lamina, a different value for the maximum bending moment can be found, these values are then arranged to get an ordered list that works as a failure sequence. This is somehow equivalent to increase the bending moment applied to the laminate and check for failure in each lamina within each load increment using the maximum strain criteria. This is done without considering that the stiffness centre may change when laminas are gradually failing.

The results obtained in [Idárraga, 2019] using the CAM are shown in Figure **3-16** and Figure **3-17** for Layup 1 and Layup 2 respectively. The results obtained in [Cusack, 2018] using the CAM and lower compressive failure strain for the M55 layers (using 0.46 % instead of 0.56 %) are shown in Figure Table **3-3** and Table **3-4** for Layup 1 and Layup 2 respectively. The failure sequence in both references is similar, Idárraga uses a larger compressive strain for M55 and that is why he predicts tensile failure to take place first, Cusack uses a lower value of the same property, that is why he predicts failure to start in compression, they both agree that for layup 1, the first four laminas that fail are the three upper M55 plies (layers 9 and 14) in compression, the three lower M55 (layers 54 and 59) in tension; up to this point, except for T1000 compressive failure, the predictions are consistent with the post-mortem data. After that, the CAM predicts compressive failure of the first T1000 block (layers 10, 11, 12, 13) and part of the second block (layers 13 and 14); also, compressive failure in the S-Glass plies (layers 1 to 7) is expected; but there is no evidence of compressive failure of neither the T1000 blocks nor any of the S-Glass plies. On the contrary, the experimental results show that after fragmentation of the uppermost and lower most M55 plies in compression and tension, the bottom T1000 blocks fracture in tension (layers 60, 61, 55 to 58, and 50 to 53), and this happens while the S-Glass layers and T1000 blocks in the compressive area preserve their integrity. Something very similar happens for Layup 2, The CAM says that failure in compression in the S-Glass plies (layers 1 to 7) and upper T1000 blocks (layers 9, 10; 12, 13; 15, 16; and 18) is expected to take place earlier than in the bottom T1000 plies (layer 54, 55, 57, 58, 60, 61), but the experiments show that the S-Glass layers are not damaged while the lower most T1000 layers fail in tension. The main limitations of the CAM are summarised next:

- Change of stiffness centroid due to gradual failure of the laminas within the laminate is not considered.

- Delamination and failure due to shear is not considered.

- There are no in-situ corrections for the strength values to account for size effect or increased strength due to layup distribution.

- The failure sequence predicted by this method does not represent the actual failure sequence observed in the experiments.
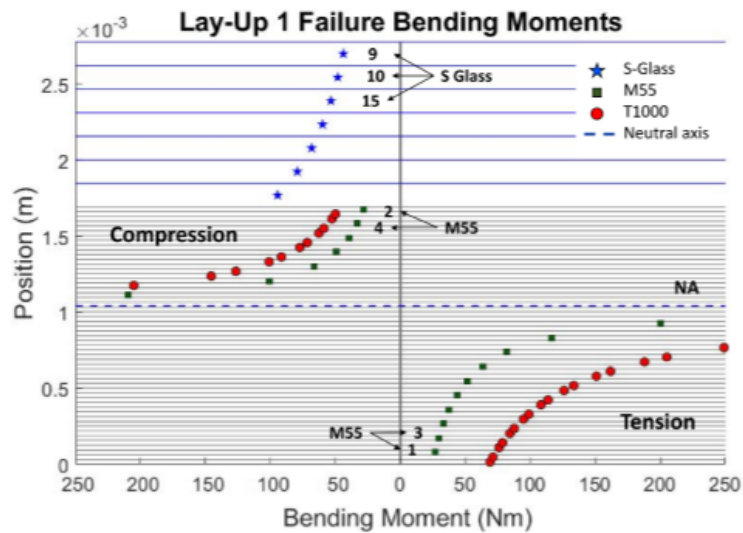
Figure 3-16.: Predicted failure sequence from the Change Area Method using the values of the failure bending moments and mechanical properties in [Idárraga, 2019] (0.56 % compressive failure strain M55/Epoxy), Layup 1.
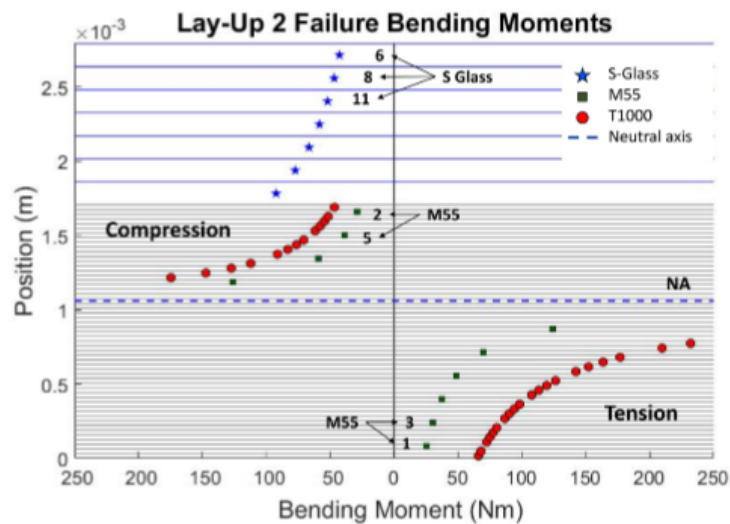
Figure 3-17.: Predicted failure sequence from the Change Area Method using the values of the failure bending moments and mechanical properties in [Idárraga, 2019] (0.56 % compressive failure strain M55/Epoxy), Layup 2.

Table 3-3.: Predicted failure sequence from the Change Area Method, Layup 1 using mechanical properties in [Cusack, 2018] (0.46 % compressive failure strain M55/Epoxy).

Layer	Material	Failure sequence	Layer	Material	Failure sequence
1	Sglass	15	32	T1000	58
2	Sglass	17	33	T1000	57
3	Sglass	19	34	TM55	37
4	Sglass	22	35	T1000	55
5	Sglass	25	36	T1000	54
6	Sglass	30	37	T1000	53
7	Sglass	36	38	T1000	52
8	T1000	5	39	TM55	20
9	TM55	1	40	T1000	49
10	T1000	8	41	T1000	48
11	T1000	9	42	T1000	47
12	T1000	10	43	T1000	45
13	T1000	11	44	TM55	12
14	TM55	2	45	T1000	44
15	T1000	13	46	T1000	43
16	T1000	14	47	T1000	42
17	T1000	16	48	T1000	41
18	T1000	18	49	TM55	7
19	TM55	6	50	T1000	40
20	T1000	23	51	T1000	38
21	T1000	27	52	T1000	35
22	T1000	33	53	T1000	34
23	T1000	39	54	TM55	4
24	TM55	21	55	T1000	32
25	T1000	46	56	T1000	31
26	T1000	51	57	T1000	29
27	T1000	56	58	T1000	28
28	T1000	61	59	TM55	3
29	TM55	50	60	T1000	26
30	T1000	60	61	T1000	24
31	T1000	59			

Table 3-4.: Predicted failure sequence from the Change Area Method, Layup 2 using mechanical properties in [Cusack, 2018] (0.46 % compressive failure strain M55/Epoxy).

Layer	Material	Failure sequence	Layer	Material	Failure sequence
1	Sglass	18	32	M55	49
2	Sglass	21	33	T1000	58
3	Sglass	23	34	T1000	57
4	Sglass	25	35	M55	37
5	Sglass	27	36	T1000	55
6	Sglass	33	37	T1000	54
7	Sglass	39	38	M55	26
8	M55	1	39	T1000	52
9	T1000	8	40	T1000	51
10	T1000	10	41	M55	20
11	M55	2	42	T1000	50
12	T1000	13	43	T1000	48
13	T1000	14	44	M55	15
14	M55	3	45	T1000	46
15	T1000	16	46	T1000	45
16	T1000	17	47	M55	12
17	M55	6	48	T1000	44
18	T1000	22	49	T1000	42
19	T1000	24	50	M55	9
20	M55	11	51	T1000	41
21	T1000	29	52	T1000	40
22	T1000	34	53	M55	7
23	M55	19	54	T1000	36
24	T1000	43	55	T1000	35
25	T1000	47	56	M55	5
26	M55	38	57	T1000	32
27	T1000	56	58	T1000	31
28	T1000	59	59	M55	4
29	M55	53	60	T1000	30
30	T1000	61	61	T1000	28
31	T1000	60			

3.1.4. Comparison between the Change Area Method and the Classical Laminate Theory

It is possible to calculate an approximation for the failure sequence using the Classical Laminate Theory, see Figure **3-18**. Failure is evaluated by imposing a gradual bending moment in the reference direction, which is also the fibre direction M_x or a gradual mid-surface curvature k_x; applying boundary condition either on the in-plane forces N_{xy}, N_y or in the in-plane strains ε_{xy}, ε_y; and checking either the maximum strain or maximum stress criteria are satisfied, similar to what was done in [Kalantari et al., 2016a, Kalantari et al., 2016c, Ary Subagia et al., 2014]. This allows a direct comparison between the change area method and Classical Laminate Theory.

Two failure sequences are obtained, the first one is obtained by setting the in-plane forces and bending moments as zero (see Figure **3-19**, force constrained), this way the laminate is free to stretch as well as bend when is loaded. For the second one, the in plane strains are constrained (see Figure **3-19**, strain constrained), so in plane forces and bending moments

appear as reactions.

The failure sequence using the force constrained condition is the same obtained in the Change Area Method using the mechanical properties in [Cusack, 2018], it predicts failure by collapse of the laminate due to compression on the S-Glass laminas. The failure sequence using the strain constrained condition yields slightly different results, but once again, compressive failure in the S-Glass plies is expected.
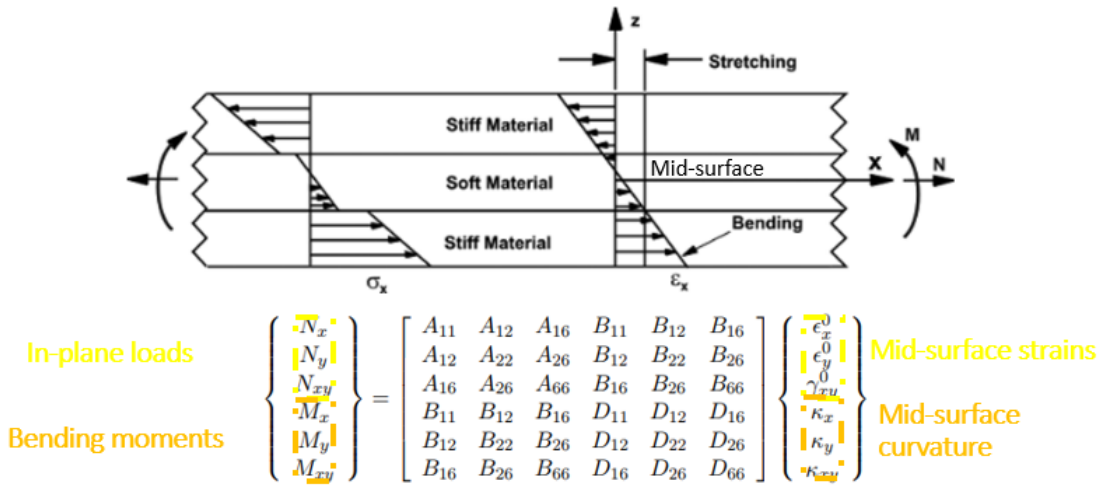
Figure 3-18.: Summary of the Classical Laminate Theory.

Figure 3-19.: Outline of the strain and force constrained border conditions that were used for implementing the Classical Laminate Theory.

So far it is possible to conclude that the Change Area Method does not add or contribute significantly to the analysis of laminates under bending loads, because it is equivalent to

the Classical Laminate Theory but far more limited. The main limitations of the Classical Laminate theory are the following:

- Change of stiffness centroid due to gradual failure of the laminas within the laminate is not considered.

- Delamination and failure due to shear is not considered.

- The failure sequence predicted by this method does not represent the actual failure sequence observed in the experiments.

3.1.5. Final conclusions on Idárragas work

The progression of gradual failure according to [Idárraga, 2019] is believed to proceed as follows:

It is concluded that Layup 1 and Layup 2 in Idárraga's work present gradual failure due to the fact that the fragmentation of the M55 layers inside the block structure creates a weak interface between blocks, this promotes delamination of the T1000 blocks once the intralaminar fracture advances inside them; it means, once the fracture in the T1000 layers starts to progress, it cannot go beyond the first layer of M55, because the previous failure and fragmentation of this layer (M55) promotes delamination and compel the initial intralaminar crack to migrate to delamination, see Figure **3-20**. The main issue is that the models proposed so far need to account for more failure mechanisms and the way they interact in these kind of layups.
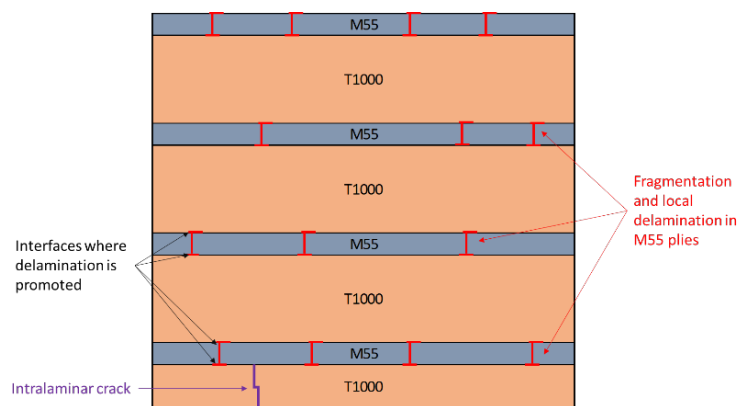
Figure 3-20.: Mechanisms for gradual failure in bending.

3.2. Cusack´s results

Following Idárraga´s results, Cusack attempt to design new hybrid composite laminates, using the same testing methodology and dimensions, his idea was to design laminates that

can also fail in a gradual fashion but improving the stiffness of Idárraga´s laminates [Cusack, 2018]. Cusack based his work in Layup 1 designed by Idárraga $[SGlass_7/T1000/(M55/T1000_4)_{10}/M55/T1000_2]$ and, according to that, he proposed two laminates, the first of them increases the number of $T1000/M55$ blocks to get the laminate $[SGlass_4/T1000/(M55/T1000_4)_{13}/M55/T1000_2]$ named Layup 7, in the second one he added T800 CF carbon/epoxy plies (whose properties can be seen in Table **3-1** in the compressive area to get the laminate $[SGlass_3/T800_2/SGlass/T800_2/T1000/(M55/T1000_4)_{10}/M55/T1000_2]$ named Layup 5. The new laminates of Cusack were calculated using the CAM, and even though compressive failure was expected he carried on with the experimentation. The vertical load vs displacement curves are shown in Figure **3-21** and Figure **3-22**; it can be seen that there is non-linear behaviour; however, no staircase-like failure was achieved. According to Cusack's conclusions, in Layup 7, failure was completely catastrophic, it started as compressive failure in the T1000 upper layers followed by severe delamination. For Layup 5 the behaviour was the same, but the compressive failure was presented in the T800 plies. From this work it can be concluded that the methodology and the CAM as a tool for designing hybrid laminates need further improvement.
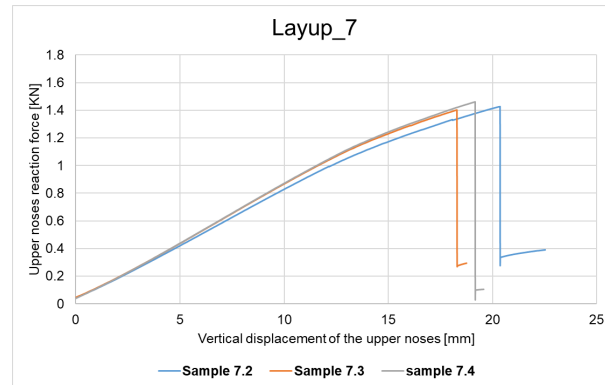
Figure 3-21.: Upper noses reaction load vs upper noses vertical displacement for Layup 7 [Cusack, 2018].
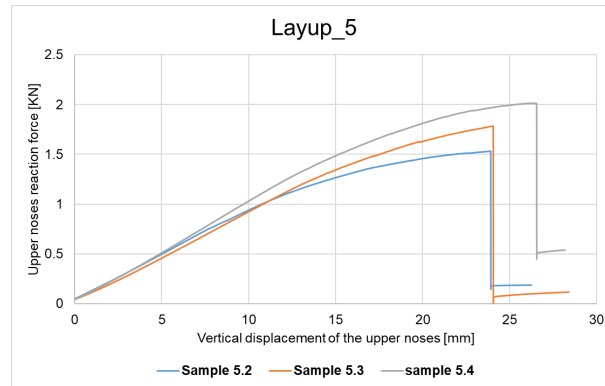
Figure 3-22.: Upper noses reaction load vs upper noses vertical displacement for Layup 5 [Cusack, 2018].

As the previous sections show, a lot of work has been done on hybrid composite materials under bending; so far, it can be concluded that there is reasonable understanding of the way the stress redistribution due to hybridization can be used to improve the overall strength of a laminate, and the way this redistribution affects the stiffness. Besides, there is a good identification of failure mechanisms at least up to first ply failure; but there is an evident need to identify the way failure progress, because once it is understood, it can be controlled. A good identification of the failure mechanisms and the way they interact allow to design laminates with increased damage-tolerance; but, in order to reach this kind of understanding, more complex models need to be developed, to include all sorts of non-linearities such as contact, large displacements, intralaminar and interlaminar damage, and this is main purpose of the present work.

4. Chapter 5: Development of the Numerical model

This section is dedicated to the gradual generation of the finite element model able to predict the internal fragmentation, gradual failure response, and non-linear behaviour of hybrid specimens under four-point bending tests; the model is verified at each step by using the experimental available data. Then, this model is used to design new laminates.

4.1. 3D Finite element analysis using shell elements and linear elastic material behaviour

According to Figure **3-8** and Figure **3-9** (see section 3.1.2) the load displacement curves, for the layups tested by Idárraga [Idárraga, 2019], show large non-linear behaviour. Therefore, the question at this point is how much of this non-linear behaviour is due to geometric large deformations and how much is due to damage or fracture (non-linear material response). This is why, the first finite element model is set to capture the non-linear response produced by contact interactions and large deformations only, this to identify the influence of this condition in the non-linear behaviour of the load-displacement curves.

The specimen test can be modelled by a single layer of shell elements with quadratic formulation and reduced integration, the same element type used in [Kalantari et al., 2016c]. The base geometry of the specimen needs to be a rectangular surface with no thickness, because the thickness as well as the stiffness are given by the assignment of the layup section, see Figure **4-1**. The model is set to account for geometric non-linearities and contact interaction (frictionless tangential behaviour and hard contact normal behaviour, separation is allowed); the material is always linear-elastic no matter how high the stress values are.

The boundary conditions are imposed by frictionless-contact interaction with the upper noses and side supports (rigid shell bodies). The simulation is displacement controlled; so the side supports are fixed while the upper noses have a set displacement in the vertical direction, see Figure **4-2**.
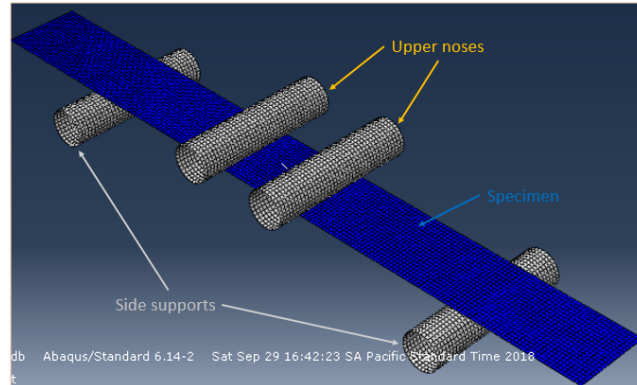
Figure 4-1.: First finite element model.
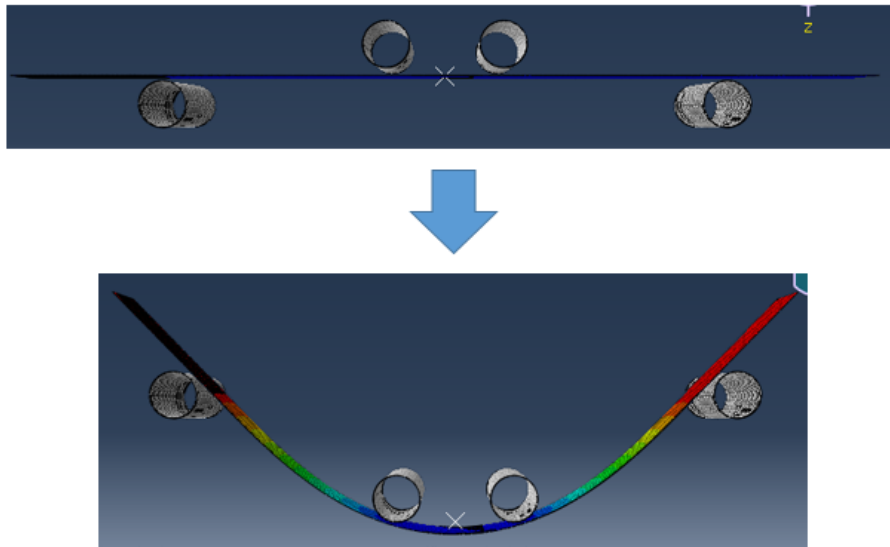
Figure 4-2.: Deformation of the first element model.

The results of the first simulation that correlate the force reaction and displacement in the upper rigid bodies (upper noses in Figure **3-7**) are compared with the measurement of the vertical displacement and load-cell data in the experiments (see Figure **4-3**). Besides, the strain in the lower carbon ply is compared with the strain measured by the strain gauge depicted in Figure **3-7**, (see Figure **4-4**). It is shown that most of the non-linear response is caused by large deformations, softening due to damage is expected to give a very small contribution, because the numerical model predicts a very similar stiffness up to around 25 mm of vertical displacement, the load drop onset.

Figure 4-3.: Upper noses reaction force vs vertical displacement of the upper noses; finite element model using shell elements, large deformations, and linear elastic material response (damage is not considered) for Layup 1.

Figure 4-4.: Upper noses reaction force vs strain at the bottom ply; finite element model using shell elements, large deformations, and linear elastic material response (damage is not considered) for Layup 1.

4.2.   3D Finite element analysis using shell elements and Hashin damage

The first approach to damage modelling considers intralaminar damage only and it is implemented by using the Hashin Damage model. Hashin takes the onset of damage as the point where the stress reaches its maximum value, from then a linear elastic softening follows, the slope of the softening curve is computed based on the fracture energy of the material which is the area under the stress strain curve in a simple tension or compression test [Simulia, 2014], see Figure **4-5**. The properties for the Hashin model are shown in Table **4-1**.
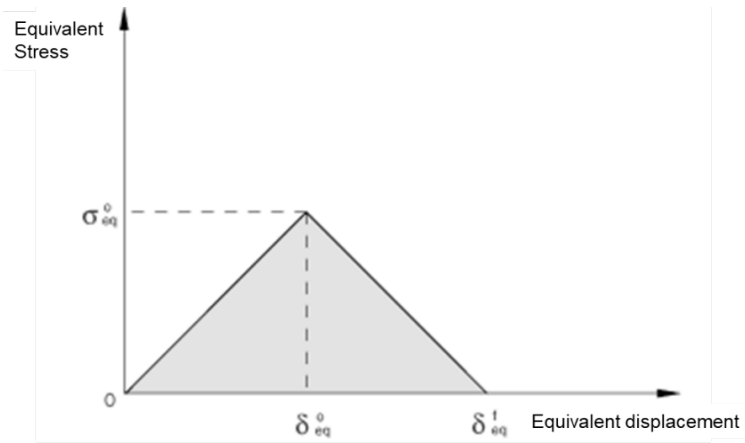
Figure 4-5.: Hashin Model equivalent stress-equivalent displacement curve [Simulia, 2014], where σ_{eq}^0 is the equivalent strength (damage onset), and δ_{eq}^0 the equivalent displacement at damage onset; δ_{eq}^0 is the equivalent displacement after full degradation.

Where the equivalent stress σ_{eq} and the equivalent displacements δ_{eq} are given in terms of the lamina in-plane stress and strain components; and element characteristic length.

Table 4-1.: Properties for Hashin damage model according to [Idárraga, 2019, Hexcel, 2018, Torayca(R), 2012].

SGlass-913/Epoxy			
Longitudinal tensile strength [MPa]	Longitudinal compressive strength [MPa]	Longitudinal tensile fracture energy [KJ/m^2]	Longitudinal compressive fracture energy [KJ/m^2]
1850.7	1083.5	91.6	79.9
M55/Epoxy			
Longitudinal tensile strength [MPa]	Longitudinal compressive strength [MPa]	Longitudinal tensile fracture energy [KJ/m^2]	Longitudinal compressive fracture energy [KJ/m^2]
2240.0	1288.0	81.5	106.5
T1000/Epoxy			
Longitudinal tensile strength [MPa]	Longitudinal compressive strength [MPa]	Longitudinal tensile fracture energy [KJ/m^2]	Longitudinal compressive fracture energy [KJ/m^2]
3152.6	1576.3	81.5	106.5

The Hashin damage model is built inside Abaqus, so no subroutine is needed. Besides, this model can only be applied to regular shell or continuum shell elements; therefore, the damage model uses the same mesh, border conditions, non-linearities, and contact interaction described in section 4.1 and shown in Figure **4-1**; only the material formulation changes.

The results are again compared to the experimental data and they can be seen in Figure **4-6** and Figure **4-7**. Hashin damage model can be more accurate than the previous models up to 25 mm approximately; namely, the new approximation can follow the tendency only when failure proceeds inside the laminas, but it cannot model the load drops. So, in order to elucidate this hypothesis, a more accurate finite element model must include interlaminar damage, as it will be seen next.

The through-thickness damage distribution for Layup 1 once the vertical displacement reaches $25,0mm$, which is the displacement at average peak load, as shown in Figure **4-8**, here damage is presented as a percentage value, where $100\,\%$ represents a fully broken material and $0\,\%$ represents no damage. According to this graph compressive failure is ex-

pected in the S-Glass layers (layer 1, 2, and 3 in Table **3-3**) on the top of the layup, and the top M55 layers (layer 9,14 and 19 in Table **3-3**) close to the S-Glass layers; which according to the post-mortem analysis makes sense for the M55 plies, but it does not for the S-Glass. In Idárraga´s specimens there was never evidence of compressive failure of the S-Glass plies; therefore, the actual compressive strength of this material must be higher than the values expected in [Idárraga, 2019, Hill, 2018]. On the other hand, tensile failure proceeded as expected in the bottom M55 plies.

It can be seen that at least up to peak load, the large non-linear behaviour is mainly created by the large deformations of the specimens rather than caused by damage; Figure **4-6** shows that softening due to damage accounts for a very small reduction on the overall specimen's stiffness. This could have been foreseen because up to peak load only four of the eleven M55 plies (layers with the lowest thickness) have fragmented, it means that only a very small portion of the layup is damage, and the laminas that are damaged are still able to hold load.

Figure 4-6.: Upper noses reaction force vs vertical displacement of the upper noses; finite element model using shell elements, large deformations, and Hashin damage model for Layup 1.
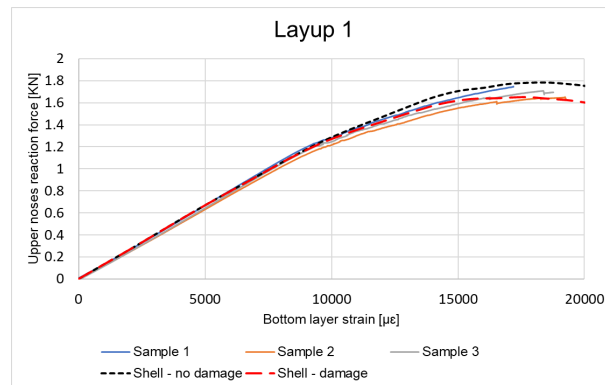
Figure 4-7.: Upper noses reaction force vs strain at the bottom ply; finite element model using shell elements, large deformations, and Hashin damage model for Layup 1.
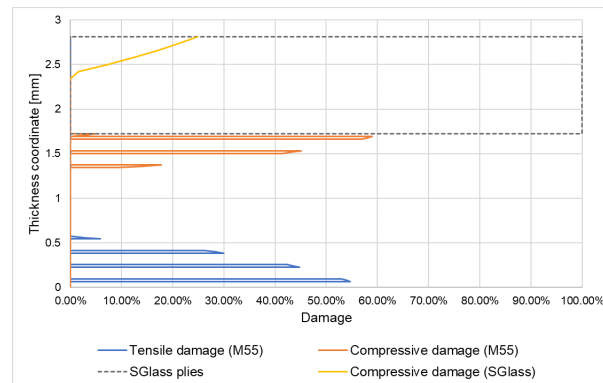
Figure 4-8.: Through-thickness damage distribution for Layup 1 (vertical displacement $= 25{,}0mm$).

Knowing that the two previous models yield similar and accurate results on load-displacement and load-strain in the bottom lamina data, it is possible to assume that the strain prediction on the top lamina is at least realistic as well; if it is also known that the top lamina (S-Glass ply) did not fail in the test, the S-Glass layer should endure at minimum the strain reached at the point where the failure strain in the lower T1000 ply is achieved (point of load drop), all this while accounting for the softening due to failure in the M55 plies; this is defined as the critical point because once the lower ply fails (T1000 ply), the strain in the upper layer (S-Glass ply) either holds or decreases.

Therefore, a new model is set using the Hashin damage formulation to account for softening in the M55 plies only (layers that gets fragmented, and therefore lose their stiffness gradually), no damage model is used for the remaining materials but the strain is monitored in the upper S-Glass layer and the bottom T1000 one (layers that are more prone to failure). From the experimental analysis, it can be see that for gradual failure to take place, first the M55 layers should fail and fragment inside the layup, then the bottom layer should reach its tensile strength before any of the top layers reach their compressive strengths; so the strain at the top ply at the point of failure of the bottom ply is a measure of the minimum compressive deformation that the material (S-Glass) can withstand. The load-displacement and load-strain results compared to the experimental data can be seen in Figure **4-9** and Figure **4-10**. The strain in the bottom and top plies vs vertical displacement of the upper noses is shown in Figure **4-11**, according to this analysis, the compressive failure strain of the S-Glass should be at least higher than $3.65\,\%$.
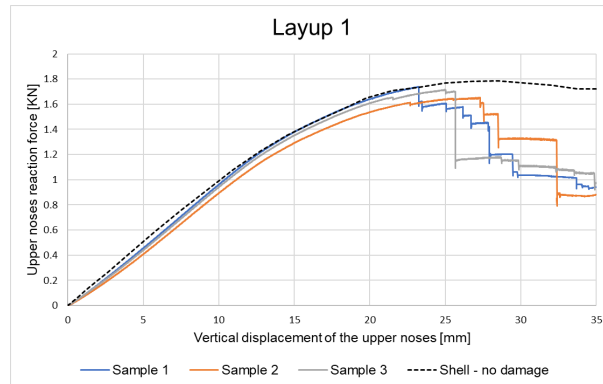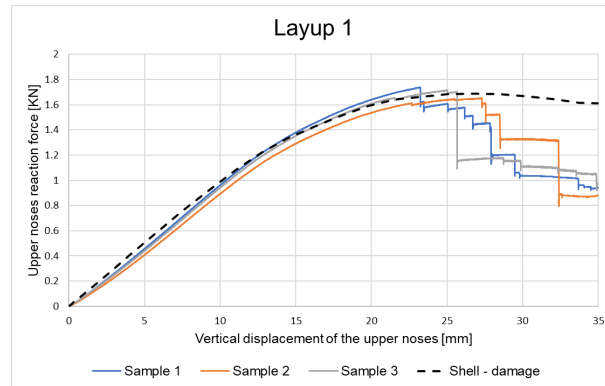
Figure 4-9.: Upper noses reaction force vs vertical displacement of the upper noses; finite element model using shell elements, large deformations, and Hashin damage model for failure in the M55 plies only in Layup 1.
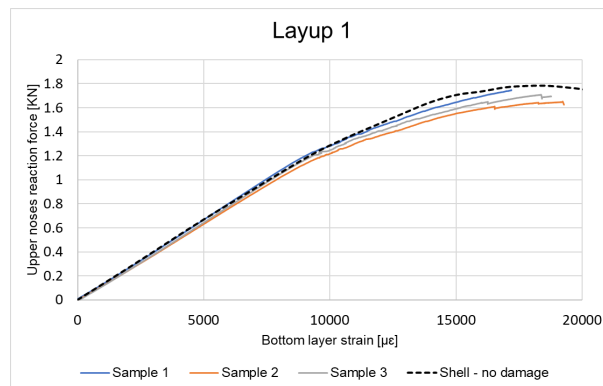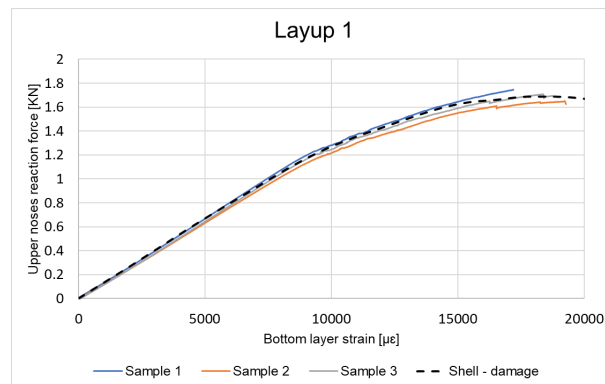

Figure 4-10.: Upper noses reaction force vs strain at the bottom ply; finite element model using shell elements, large deformations, and Hashin damage model for failure in the M55 plies only in Layup 1.
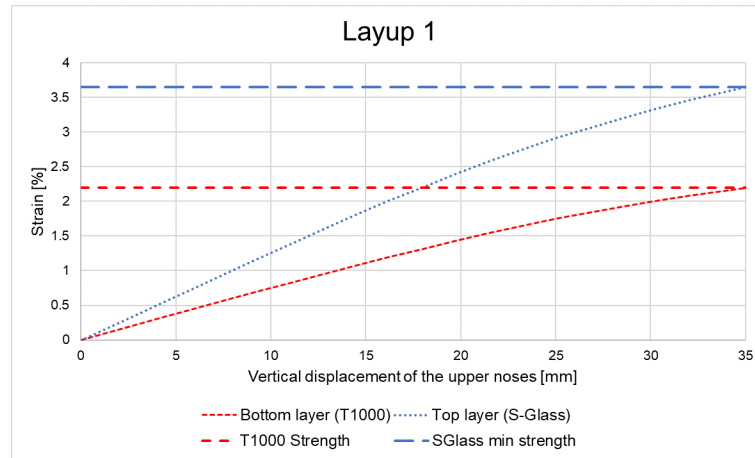
Figure 4-11.: Top and bottom layer strain vs vertical displacement of the upper noses for
Layup 1; where the horizontal line "T1000 Strength" represents the strain at the
point where the T1000 layer reaches its tensile strength, and the horizontal line
"S-Glass min strength" represents the strain at the maximum stress reached by
the top S-Glass layer.

4.3. 2D finite element analysis using plane strain elements and linear elastic material behaviour

Even when the Hashin damage model using shell elements can yield accurate results up to peak load, it can neither model the load drops caused by delamination, nor the fragmentation of the M55/Epoxy plies and fracture of the bottom T1000/Epoxy plies; this approach shows average degradation of properties rather than specific failure mechanisms.

The way to include intralaminar damage and get a better approximation of the intralaminar nature of failure is by modelling each ply separately. This way, each ply can be joined to its neighbours by cohesive elements to model delamination (interlaminar failure), and other cohesive elements can be placed inside each lamina to model fracture inside the laminas (intralaminar failure).

In order to use interlaminar as well as intralaminar cohesive elements in the whole specimen while keeping low running times, it makes sense to change from a 3D modelling approach to a 2D one; so, the idea is to model a single section of the width of the specimen, subjected to the same deformation; such section is considered as subjected to plane strain and according to [Lim et al., 2014, Kalantari et al., 2016c, Dong, 2016, Dong and Davies, 2014, Dong and Davies, 2013, Dong and Davies, 2015, Dong and Davies, 2012, Ary Subagia et al., 2014], it yields an accurate representation of the behaviour of the whole specimen; the first way to verify this is by setting a 2D model using plane strain elements only, and check that the results match the results of the 3D shell model of section 4.1.

The initial 2D elastic model also accounts for large deformations and contact interaction (normal contact "Hard", tangential frictionless contact); besides, the deformation of this model, similar to the one in section 4.1, is set by imposing a controlled displacement on the upper noses and fixing the lateral supports, see Figure **4-12**. The model uses plane strain eight nodes quadrilateral elements for the specimen and rigid lines to model the upper noses and lateral supports; its results agree with the 3D shell model as shown in Figure **4-13** and Figure **4-14**; therefore, the plane strain assumption is still valid for the specimens and test configuration at hand.
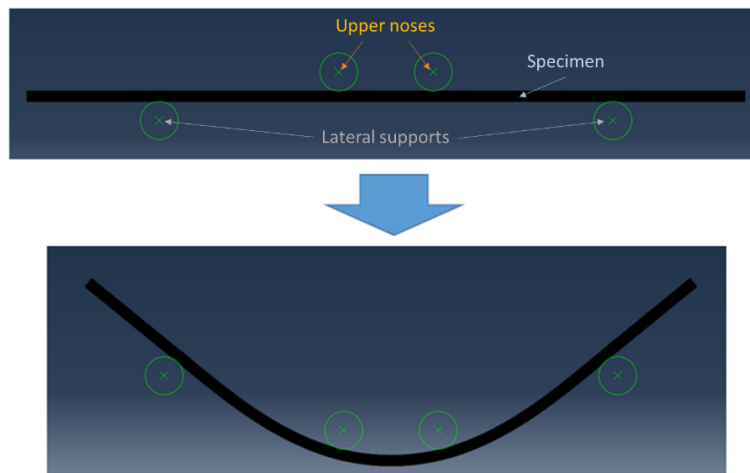
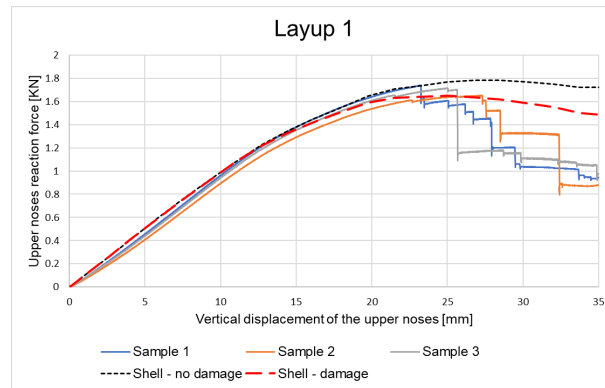**Figure 4-12**.: Deformation in the 2D plane strain finite element model.
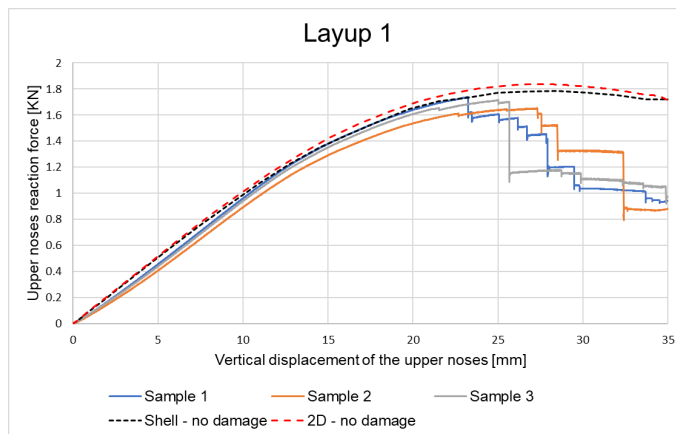
Figure 4-13.: Upper noses reaction force vs vertical displacement of the upper noses; finite element model using plane strain 2D elements for Layup 1.

4.4 2D Plane-strain finite element approach using intralaminar
fragmentation and interlaminar cohesive damage, unidirectional tension
test   61
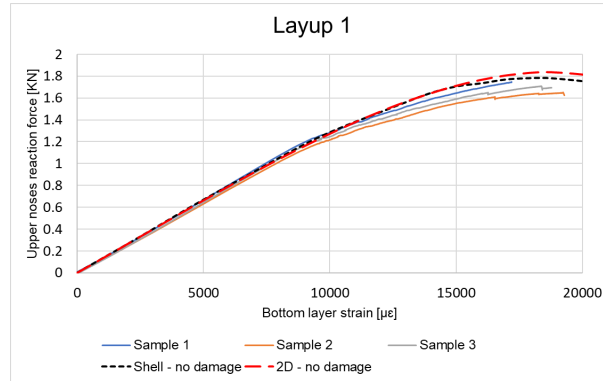
Figure 4-14.: Upper noses reaction force vs strain at the bottom ply; finite element model using plane strain 2D elements for Layup 1.

## 4.4. 2D Plane-strain finite element approach using intralaminar fragmentation and interlaminar cohesive damage, unidirectional tension test

Due to the complexity that involves modelling fragmentation; before applying this behaviour to the bending test, it must be debugged in a much simpler scenario; in this case unidirectional tension. As explained previously, the unidirectional experiments done by Idárraga [Idárraga, 2019] are used to validate the following model, specifically layup UD_1 $[SGlass_2/TC35_2/SGlass_2]$. The approach followed in this section is similar to the one of Jalalvand [Jalalvand et al., 2014], where only one section of the specimen is modelled using 2D plane-strain elements (see Figure **4-15**). The distribution of cohesive elements is shown in Figure **4-16**, the stiffness of the 2D plane strain elements is taken from Table **3-1** for S-Glass/Epoxy and TC35/Epoxy prepregs; the properties for the interlaminar cohesive elements are defined according to [Idárraga, 2019], see Table **4-2**. The mesh size was defined according to the required interlaminar cohesive length following the recommendation in [Turon Travesa, 2007].

The intralaminar strength is found using the same methodology in [Jalalvand et al., 2014], see section 2.9.1, for a Weibull modulus of 40 for the carbon plies and 25 for the glass plies; namely, this time intralaminar cohesive elements are used in both the carbon and the glass layers. The simulation models only a fraction of the actual specimen length ($30cm$), within this space 300 intralaminar cohesive sections where added. To study the amount of cohesive sections required and the way the results vary with this parameter an external sensitivity analysis was performed, the results show that the number of cohesive sections does not disrupt the final results, see **4-17**.

The model uses cohesive part elements instead of cohesive surface interaction, and the way it is done is by creating cohesive parts with coincident nodes on the thickness, then tie cons-

trains are defined on the cohesive part faces and the solid element faces; this configuration was found to yield better convergence when compared with cohesive surface interaction.
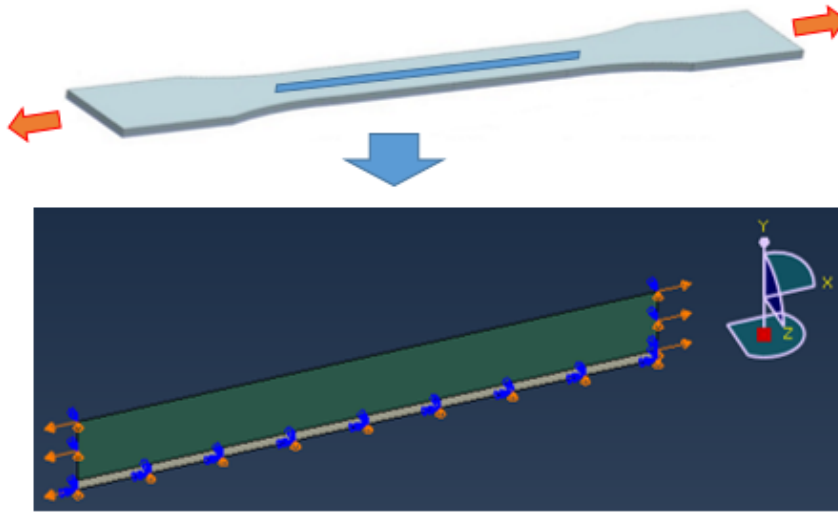
Figure 4-15.: Tension test model assumptions.
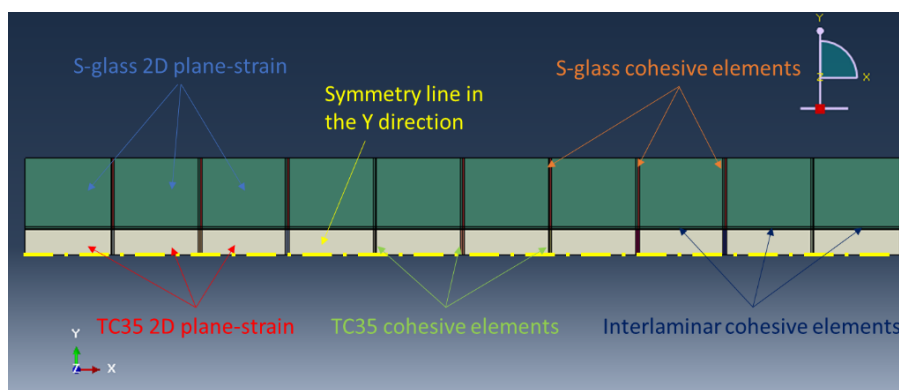
Figure 4-16.: Tension test model set-up.

4.4 2D Plane-strain finite element approach using intralaminar
fragmentation and interlaminar cohesive damage, unidirectional tension
test   63

FEM 1: Free length = 30 mm
Number of cohesive sections = 300

FEM 4: Free length = 30 mm
Number of cohesive sections = 500

FEM 6: Free length = 50 mm
Number of cohesive sections = 500

FEM 7: Free length = 100 mm
Number of cohesive sections = 1000

Figure 4-17.: Mesh sensitivity analysis (influence of the number of intralaminar cohesive
sections).

Table 4-2.: Interlaminar cohesive element properties according to [Idárraga, 2019, Jalalvand et al., 2014, Hexcel, 2018, Torayca(R), 2012].

Interlaminar cohesive properties T35C/Epoxy to SGlass/Epoxy				
Strength in the normal direction $[MPa]$	Strength in the transverse direction $[MPa]$	Penalty stiffness $[N/mm^2]$	Fracture toughness mode I $[N/mm]$	Fracture toughness mode II $[N/mm]$
34,0	67,0	10^5	0,2	1,0
Interlaminar cohesive properties M55/Epoxy to T1000/Epoxy				
Strength in the normal direction $[MPa]$	Strength in the transverse direction $[MPa]$	Penalty stiffness $[N/mm^2]$	Fracture toughness mode I $[N/mm]$	Fracture toughness mode II $[N/mm]$
34,0	68,0	10^5	0,1	0,5
Intralaminar cohesive element for M55/Epoxy plies				
Strength in the normal direction $[MPa]$	Strength in the transverse direction $[MPa]$	Penalty stiffness $[N/mm^2]$	Fracture toughness mode I $[N/mm]$	Fracture toughness mode II $[N/mm]$
2240,0	68,0	10^9	0,01	0,01
Intralaminar cohesive element for T1000/Epoxy plies				
Strength in the normal direction $[MPa]$	Strength in the transverse direction $[MPa]$	Penalty stiffness $[N/mm^2]$	Fracture toughness mode I $[N/mm]$	Fracture toughness mode II $[N/mm]$
3152,6	68,0	10^9	0,01	0,01

The load vs overall longitudinal strain results of this model compared to the experimental data are shown in Figure **4-18**; the stress distribution (stress in the fiber direction) when the specimen is fragmented is shown in Figure **4-19** only for qualitative representation. The simulation can accurately predict fragmentation, local delamination, and final collapse of the laminate; therefore, fragmentation modelling can be considered as verified and can be implemented in bending.
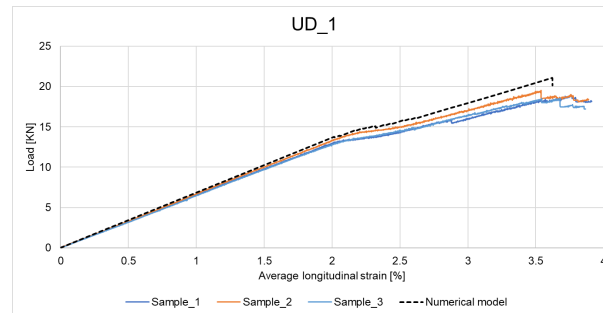
Figure 4-18.: Load vs average tensile strain in the longitudinal direction results for layup UD_1.
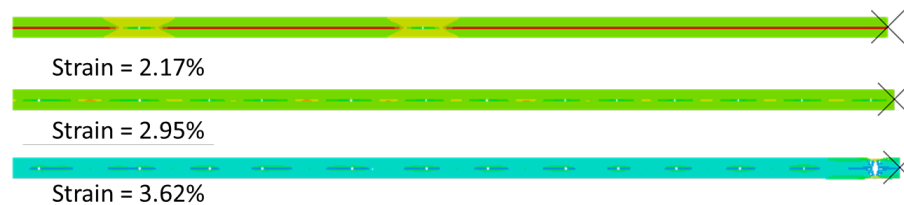
Figure 4-19.: Fragmentation and failure of layup UD_1 (qualitative representation of the stress
in the fibre direction).

4.5. 2D Plane strain finite element approach using intralaminar fragmentation and interlaminar cohesive damage, bending test

The setup of this model consist of adding several rows of cohesive elements in the vertical
position (representing places where fibre failure is likely to take place), while keeping the
horizontal cohesive elements (representing places where delamination can take place), see
Figure **4-20**. The intralaminar strength distribution of the T1000 and M55 layers is found
using the same methodology of Jalalvand [Jalalvand et al., 2014], see section 2.9.1, for Weibull
modulus of 40 in both materials; 200 cohesive sections (cohesive pars) were placed for each
carbon layer. The section of the specimen where all the cohesive elements are located is only
between the loading noses ($25cm$ of span), as this is the area of maximum tensile stresses
and it is necessary in order to keep the computation expenses at a minimum. The border
conditions and elastic material properties are the same introduced before in section 4.3, the
cohesive properties are shown in Table **4-2**, large deformation and contact modelling are
considered.
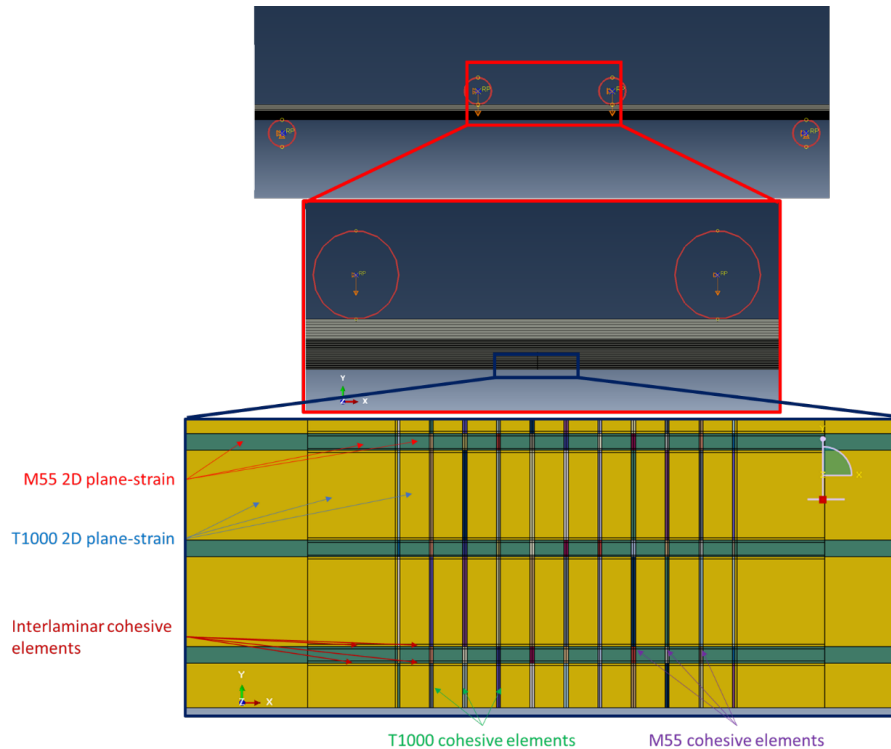
Figure 4-20.: Cohesive element distribution inside the specimen.

The load vs displacement and load vs strain results are shown in Figure **4-21** and Figure **4-22** respectively, it can be seen in the initially elastic part that the stiffness of the cohesive sections where properly selected because they do not disrupt the overall specimen stiffness. The final deformation of the specimen in the numerical model and test are shown in Figure **4-23**. Fragmentation of the three bottom M55 layers (layers 44, 46, and 54 in Table **3-3**) can be observed before failure of the bottom T1000 block (layers 60 and 61 in Table **3-3**) at around $21mm$ of vertical displacement, see Figure **4-24**; at this point there is a first load drop that goes from $1{,}64KN$ to $1{,}34KN$, the deformation keeps on and more fragmentation is observed in the following M55 plies before failure on the next block; this is the same failure process observed in the test but is presented at an earlier displacement than the average experimental one, the reason for this is the fact that the intralaminar cracks modelled with cohesive elements are sharp, meanwhile the actual physical intralaminar failure in composite materials can hardly be considered as crack-shaped, failure in the fibre direction is given as bundles of fibres that delaminate once they break; modelling this type of failure using cohesive elements overestimates the stress concentration and produces an earlier failure.
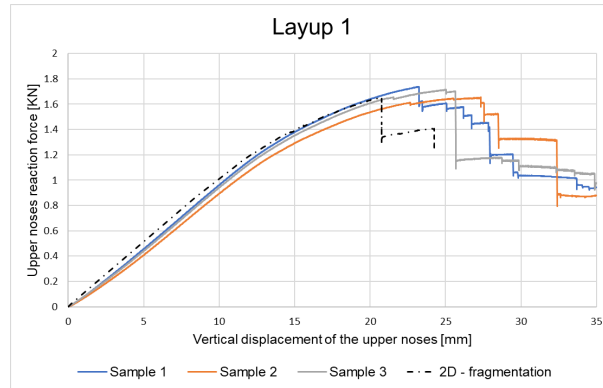
Figure 4-21.: Upper noses reaction force vs vertical displacement of the upper noses; finite
element model using plane strain 2D elements, cohesive intralaminar
fragmentation and interlaminar damage for Layup 1.
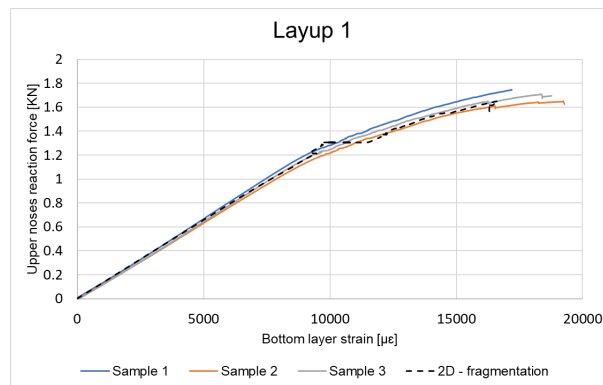
Figure 4-22.: Upper noses reaction force vs strain at the bottom ply; finite element model using
plane strain 2D elements, cohesive intralaminar fragmentation and interlaminar
damage for Layup 1.
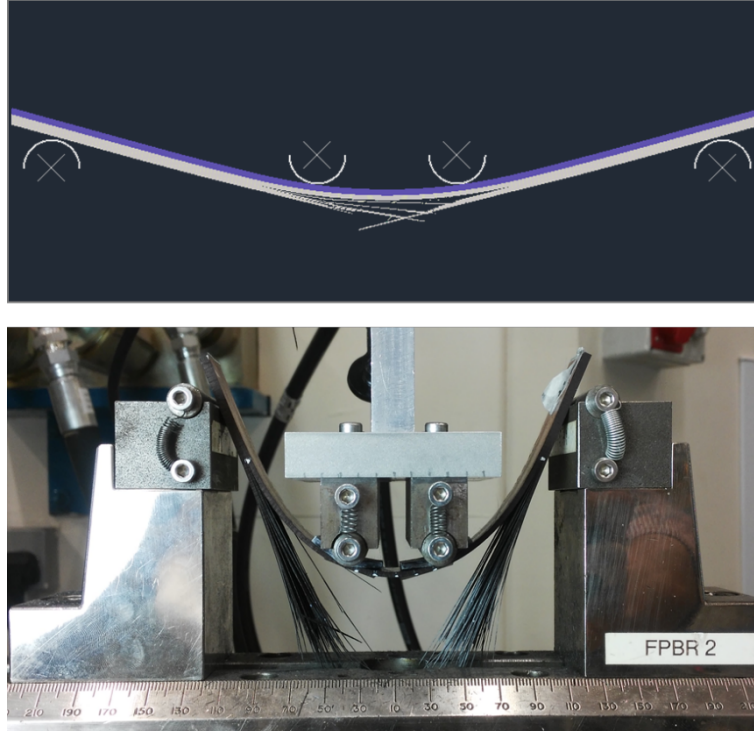
Figure 4-23.: Numerical and experimental look of gradual failure in bending.
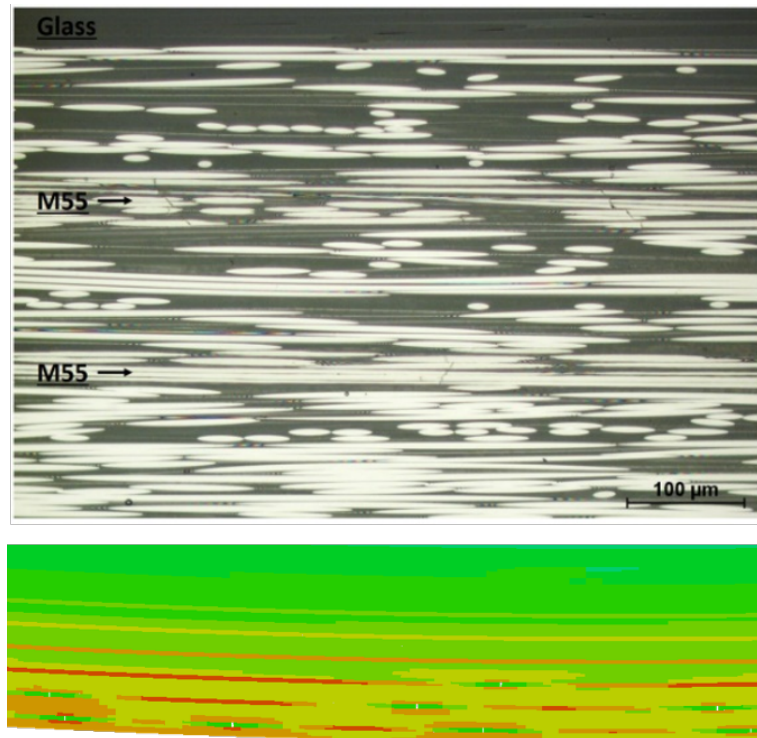
Figure 4-24.: Numerical and experimental look of fragmentation.

Compressive failure in the top M55 plies is expected but their failure behaviour is out of the scope of this work, for that continuum damage models will be implemented in the future, so far, it can be said that knowing that the stiffness reduction due to fragmentation is so small that can be ignored without heavily disrupting the results obtained.

According to this model, the maximum compressive strain on the top S-Glass layers is 3,0 %.

5. Analytical model implementation

The main purposes of this chapter are to obtain a failure sequence and replicate the experimental load-displacement and load-strain curves; the stress distribution and damage mechanisms in the laminate needs to be computed as well as the vertical displacement and force reaction at several stages of the deformation process. In this sections, the stiffness, failure sequence, and damage process of the specimens are given according to the Classical Laminate Theory and some modifications; the load-displacement curve is obtained by using the solution of S. I. Paolinelis and R. M. Ogorkiewicz at [Paolinelis and Ogorkiewicz, 1976] with some modifications as well. The model developed here takes the layup stiffness and deformation from the Classical Laminate Theory (where it defines the failure sequence and damage modes) as an input for the non-linear four-point bending test theory and computes the vertical displacement and load reactions of an equivalent isotropic beam. The process is explained gradually, to include all the variables needed to model the complete damage process.

5.1. Four point bending analytical solution according to S. I. Paolinelis and R. M. Ogorkiewicz [Paolinelis and Ogorkiewicz, 1976]

According to S. I. Paolinelis and R. M. Ogorkiewicz at [Paolinelis and Ogorkiewicz, 1976] for the problem of the four point bending beam under large displacements depicted in Figure **5-1** the supports reactions and beam stiffness can be related to the geometric parameters of the deformations as shown in Equation 5-1 and Equation 5-2 (see Figure **5-1** Figure **2-10**).

$$\left(\frac{2R}{EI}\right)^{1/2} a = 2cos(\alpha)sin^{1/2}(\alpha - \beta) + sin(\alpha)P(\alpha - \beta) \tag{5-1}$$

$$\left(\frac{2R}{EI}\right)^{1/2} y_a = 2sin(\alpha)sin^{1/2}(\alpha - \beta) + cos(\alpha)P(\alpha - \beta) \tag{5-2}$$

Where R is the support reaction, a is the distance between the support and the upper noses, y_a is the vertical displacement of the upper noses, α and β are the angles measured with respect to the horizontal line at the point of contact with the support and the upper noses respectively (see Figure **2-10**), the function $P(\alpha - \beta)$ is defined in Equation 5-3, the product

EI is originally defined as the isotropic material Young modulus times the second moment
of area of cross-section of the beam referred to its neutral axis, this product represents the
stiffness of the beam, accounting for both material and cross-section shape.

$$P(\alpha - \beta) = \int_{\phi=0}^{\phi=\alpha-\beta} sin^{1/2}\phi * d\phi \tag{5-3}$$

The curvature of the beam in the central region (area between the upper noses) is defined
by Equation 5-4.

$$\frac{1}{r} = \left[\frac{2R}{EI} * \frac{sin(\alpha - \beta)cos(\theta)}{cos(\beta)} \right]^{1/2} \tag{5-4}$$

Where $^1/r$ is the curvature of the beam, and θ is the angle with respect to the horizontal line
at any point in the beam between the upper noses (see Figure **2-10**).
The Bernoulli-Euler hypothesis holds, so "the plane sections originally normal to the cen-
troidal axis of the beam remain plane and normal to its deformed axis" [Paolinelis and
Ogorkiewicz, 1976] giving Equation 5-5.

$$M = \frac{EI}{r} \tag{5-5}$$

Where M is the applied bending moment due to the force and support loads. The geometric
relationship between the angles α and β, the distance between the upper noses and supports
a, and support span L is given by Equation 5-6.

$$\frac{L}{2a} - 1 = \frac{\left\{ \frac{cos(\beta)}{sin(\alpha-\beta)} \right\}^{1/2} M(\beta)}{2cos(\alpha) * sin^{1/2}(\alpha - \beta) + sin(\alpha)P(\alpha - \beta)} \tag{5-6}$$

Where the function $M(\psi)$ is defined by Equation 5-7.

$$M(\psi) = \int_{\phi=0}^{\phi=\psi} cos^{1/2}(\phi) * d\phi \tag{5-7}$$

The relationship between the upper noses load and support reaction is given by the equili-
brium condition according to Equation 5-8.

$$Fcos(\beta) = Rcos(\alpha) \tag{5-8}$$

Where R is the reaction load in the supports.
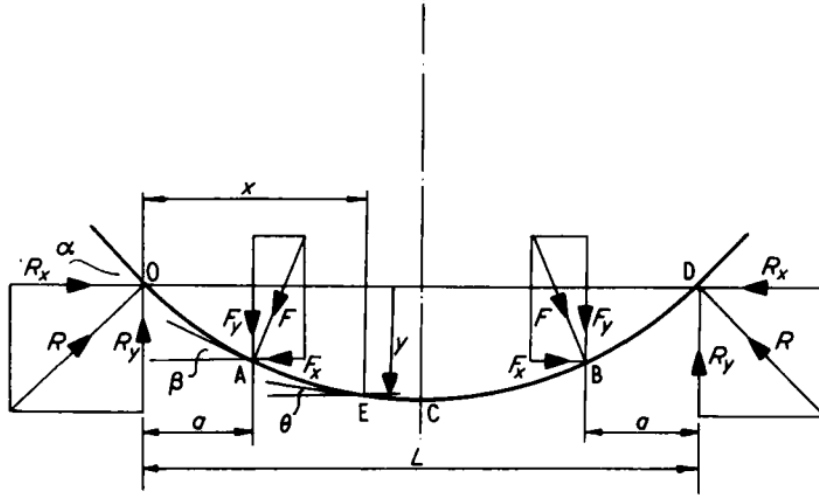
Figure 5-1.: Schematic of a thin beam under large displacements in a four point bending test
[Paolinelis and Ogorkiewicz, 1976]

The main modification to this solutions is to account for the contact condition, as the upper noses and supports have a radius r_p, the values of L, a, and y_a are functions of α and β, so the notation changes according to Figure **5-2**. Here, the values of a and L are replaced by a_n and L_n respectively; with the new conditions, the values of a_n and L_n are not fixed anymore, they vary according to Equation 5-9 and Equation 5-10 respectively. The vertical displacement of the upper noses y_n also needs to account for the change in the contact point according to Equation 5-11.

$$L_n = L_o - 2r_p sin(\alpha) \tag{5-9}$$

$$a_n = a_o - r_p sin(\alpha) - r_p sin(\beta) \tag{5-10}$$

$$y_n = y_a + r_p(1 - cos(\alpha)) + r_p(1 - cos(\beta)) \tag{5-11}$$
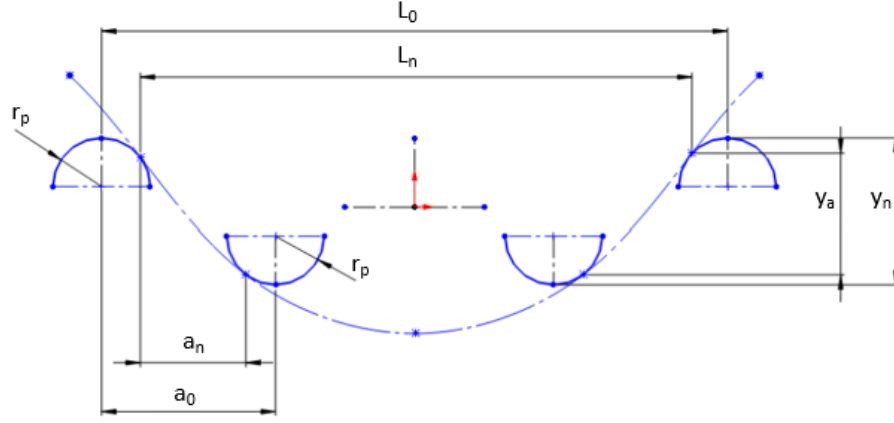
Figure 5-2.: Schematic of a thin beam under large displacements in a four-point bending test accounting for contact condition.

5.2. Four point bending analytical solution adapted for a composite material without accounting for failure

In this section, the load-displacement curve of a four-point bending test using a composite material is obtained, in this section failure is ignored; the material is considered to be linear elastic up to any deformation; therefore, similar results to the ones in sections 4.1 and 4.3 are found. The computation works as follows:

The vertical displacement is gradually increased, this is done indirectly, by imposing increasing values of α; so, for every value of α, L_n is updated according to Equation 5-9, a first estimation of β can be found solving numerically Equation 5-6 (using L_n, and approximating the first value of a_n as a_o, then with an initial estimate of β, a_o can be recalculated using Equation 5-11, this is an iterative process that is repeated until convergence is achieved in the values of a_n and β. Then, the value of the relation $^{2R}/_{EI}$ can be obtained from Equation 5-1, this value is replaced in Equation 5-4, setting θ to zero, to find the curvature in the centre of the specimen.

If the specimen is made of a thin composite material, where the x coordinate in Figure **2-10** corresponds to the laminate x direction, and the y coordinate in Figure **2-10** to the thickness direction, the curvature $^1/_r$ in Equation 5-4 corresponds to the term κ_x in Equation 2-6. If the values of N_x, N_y, N_{xy}, M_y, and M_{xy} are set to zero (the layup is free to stretch as well as bend when the deformation κ_x is imposed), the value of M_x can be found from Equation 2-9, which is equivalent to M in Equation 5-5. So, having $^1/_r$ and M, the product EI can be found from Equation 5-5. The value of EI can be used to find the reaction load R of the supports using Equation 5-1. Then, y_a can be found from Equation 5-2, and y_n from Equation 5-12. Besides, having the reaction load in the supports, it allows to compute the reaction force F in the upper noses by Equation 5-8. This process is better explained in appendix A, in the

form of pseudo-code, if the code is run without checking failure nor updating the stiffness matrices A, B, D this solution can be obtained.

In an experimental four-point bending test, the vertical displacement of the upper noses registered by the machine corresponds to the variable y_n, and the load captured by the load cell corresponds to the vertical component of the force reaction in the upper noses F_y. As shown previously, the same variables can be extracted from a finite element model. So, if these two variables are plotted from experiments, numerical analysis, and the previous algorithm, the accuracy of the algorithm can be assessed.

The load vs displacement and load vs strain results are shown in Figure **5-3** and Figure **5-4** respectively; they compare experimental, numerical, and analytical analysis with a linear elastic material model. The analytical model uses the elastic mechanical properties shown in Table **3-1**.
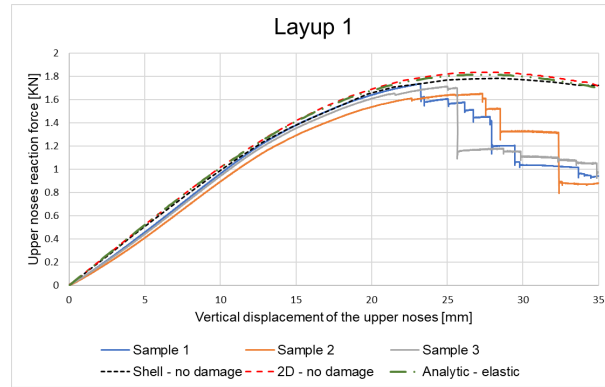
Figure 5-3.: Upper noses reaction force vs vertical displacement of the upper noses; finite element models using plane strain 2D elements and shell elements; analytic elastic solution for Layup 1.
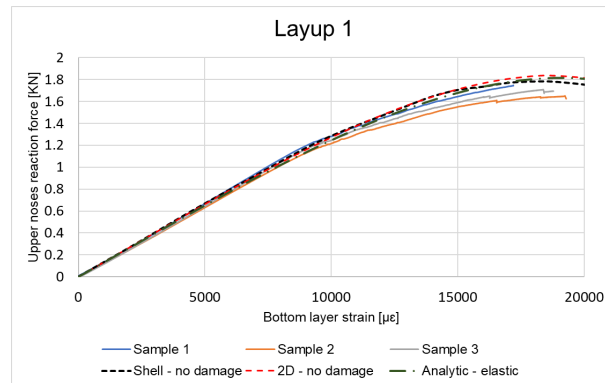
Figure 5-4.: Upper noses reaction force vs strain at the bottom ply; finite element models using plane strain 2D elements and shell elements; analytic elastic solution for Layup 1.

So far, the analytical and numerical results match, this means the non-linearities due to the

large deformations can be accurately captured; therefore, there is green light to continue and
include various damage mechanisms, as it is seen in the next sections.

5.3. Four point bending analytical solution adapted for a composite material using the ply discount method

As explained in section 2.6.1, the ply discount method is the first way one can approximate
the failure sequence of the laminate; and even though it has many limitations, in this work
can give insight into a first approximation of the actual failure sequence.

The load vs displacement and load vs strain results are shown in Figure **5-5** and Figure
5-6 respectively; they compare experimental results and results from the previous algorithm
augmented to implement the ply discount method according to the description in section
2.6.1. The analytical model uses the mechanical properties shown in Table **3-1**, the only
property that is modified is the compressive failure strain of the S-Glass fiber, which is set
to be 4,0 % according to the analysis performed in sections 4.2 and 4.5

The failure sequence is also presented along the load-displacement curves for Layup 1 in
Figure **5-7** and Table **5-1**; for the sake of a better understanding it is necessary to remember
that the layer´s numbering is mentioned in Table **3-3**.
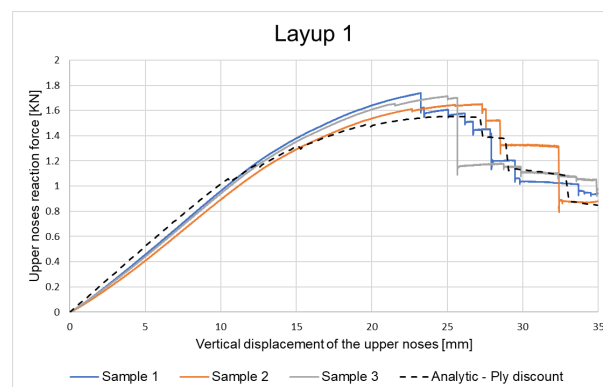
Figure 5-5.: Upper noses reaction force vs vertical displacement of the upper noses; analytic ply
discount model for Layup 1.
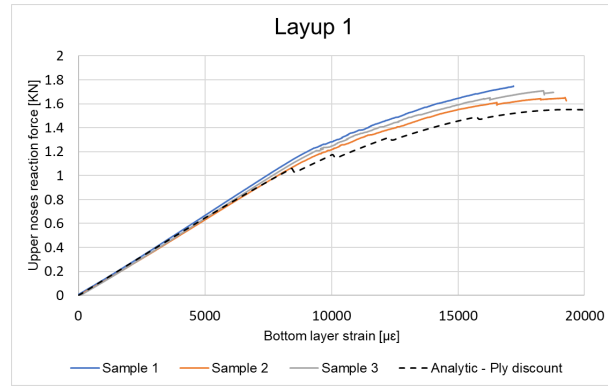
Figure 5-6.: Upper noses reaction force vs strain at the bottom ply; analytic ply discount model for Layup 1.
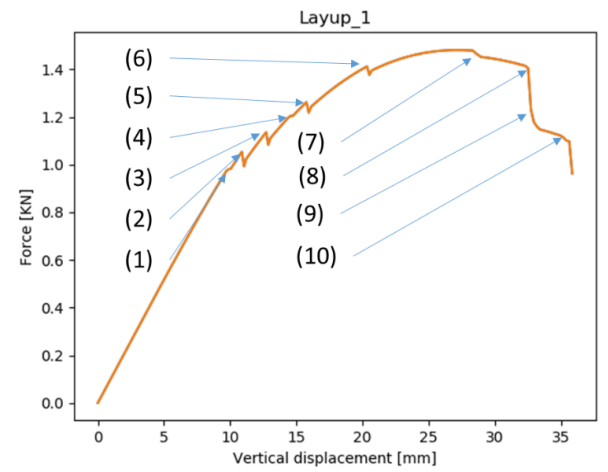
Figure 5-7.: Upper noses reaction force vs strain at the bottom ply and failure sequence using the ply discount method for Layup 1.

Table 5-1.: Failure sequence using the ply discount method for Layup 1.

Layup_1			
Failure order	layer number	Layer's material	Failure type
1	9	M55	Compression
2	59	M55	Tension
3	54	M55	Tension
4	14	M55	Compression
5	49	M55	Tension
6	44	M55	Tension
7	8	T1000	compression
8	19	M55	Compression
9	10	T1000	Compression
10	1	Sglass	Compression

The first conclusion that can be drawn from the ply discount method is that the failure
progression of the M55 layers cannot be considered as brittle, fragmentation in these plies
produces a smooth reduction in stiffness, and such a phenomenon cannot be captured by
this method. When it comes to the failure sequences, for Layup 1, compressive failure in
the S-Glass and T1000 layers is predicted but there is no experimental evidence of such a
failure; so, the prediction is wrong. Assuming that the M55 plies lose all their stiffness when
they reach their compressive failure strain causes an immediate shift of the neutral axis to
the compressive upper area, increasing the compressive deformation so much that failure is
reached in the upper S-Glass and T1000 layers.

5.4.   Analytical modelling of the fragmentation in the high modulus material

As shown by Idárraga [Idárraga, 2019], fragmentation is present in the high modulus material
(M55 layers), both in tension and compression areas of specimens under bending loads;
as the material is fragmented its stiffness decreases in a gradual manner. Fragmentation
can only take place if the other failure mechanisms such as delamination and fracture in
the low modulus material do not happen first. Therefore, if any failure theory can predict
fragmentation, it is because this theory accounts for the remaining failure mechanisms. In
the following sections, a sound analysis regarding the fragmentation presented both in tensile
and compressive areas is explained.

The block structure in the hybrid composite materials in bending proposed in [Idárraga,
2019] can be analysed separately, the lower bottom side under tension can be modelled using
some equations from the analytical solution proposed by Jalalvand at [Jalalvand et al.,
2015], and the upper compressive side modelled according to the available experimental data

in [Czél et al., 2017].

5.4.1. Tensile fragmentation

Fragmentation in tension has been successfully modelled by Jalalvand et at [Jalalvand et al., 2015], allowing to predict the stress-strain curves of hybrid composite laminates based on the materials properties, the relative, and absolute thicknesses. Taking into account the block structure of Layup 1 tested by Idárraga, the bottom tensile part can be viewed as a collection of symmetric hybrid sub-layups under tension, see Figure **5-8**. Each sub-layup is assumed to have the staking sequence $[T1000_2/M55/T1000_2]$; therefore, the hybrid stress-strain curve can be computed using the equation of Jalalvand shown in Table **2-1**. The amount of load taken by the sub-layup F_{hyb} must the equal to the sum of the load taken by each of its constituents, F_{M55} load in the M55 plies and F_T load in the T1000 plies, see Equation 5-12.

$$F_{hyb} = F_{M55} + F_T \tag{5-12}$$

Equation 5-12 can be expressed in terms of the average stresses within each ply, as shown in Equation 5-13, where A_{hyb} is the transversal area and σ_{hyb} the average stress of the sub-layup; A_{M55} is the transversal area and σ_{M55} the average stress of the M55 plies; A_T is the transversal area and σ_T the average stress of the T1000 plies.

$$A_{hyb}\sigma_{hyb} = A_{M55}\sigma_{M55} + A_T\sigma_T \tag{5-13}$$

If the average tensile strain within each lamina is the same, and no stiffness reduction is assumed in the T1000 plies, the stress strain relation within each ply and within the sub-layup can be expressed as Equation 5-14, Equation 5-15, and Equation 5-16, where ε is the average strain, $E_{hyb}(\varepsilon)$ is the stiffness of the hybrid and is a function of the strain, obtained from Table **2-1**, E_T is the stiffness of the T1000 plies and is a constant, $E_{M55}(\varepsilon)$ is the stiffness of the M55 ply inside the hybrid and is also a function of the strain, it can be obtained by expressing Equation 5-13 in terms of the stiffness, see Equation 5-17, and then clearing the term $E_{M55}(\varepsilon)$, see Equation 5-18.

$$\sigma_{hyb} = E_{hyb}(\varepsilon)\varepsilon \tag{5-14}$$

$$\sigma_{M55} = E_{M55}(\varepsilon)\varepsilon \tag{5-15}$$

$$\sigma_T = E_T\varepsilon \tag{5-16}$$

$$A_{hyb}E_{hyb}(\varepsilon)\varepsilon = A_{M55}E_{M55}(\varepsilon)\varepsilon + A_TE_T\varepsilon \tag{5-17}$$

$$E_{M55}(\varepsilon) = \frac{A_{hyb}E_{hyb}(\varepsilon) - A_TE_T}{A_{M55}} \tag{5-18}$$

In summary, knowing the block structure $[T1000_2/M55/T1000_2]$, the stress-strain curve of this sub-layup and the properties of the constituents, it is possible to identify the way

the constituents degrade and fail, see Figure **5-9**. The hybrid layup $[T1000_2/M55/T1000_2]$
presents pseudo-ductility; it is linear elastic up to the plateau, and then it becomes linear
again; this behaviour implies that the M55 layer inside such hybrid configurations starts
to degrade once the plateau in the hybrid is reached, this degradation stops once the load
starts to increase again, the remaining strength is sustained up the fracture of the T1000 side
layers. The behaviour of the M55 layers in tension can be included in the previous algorithm,
so the stiffness of the M55 plies is a function of the strain, and the laminas that surround
the M55 layer.
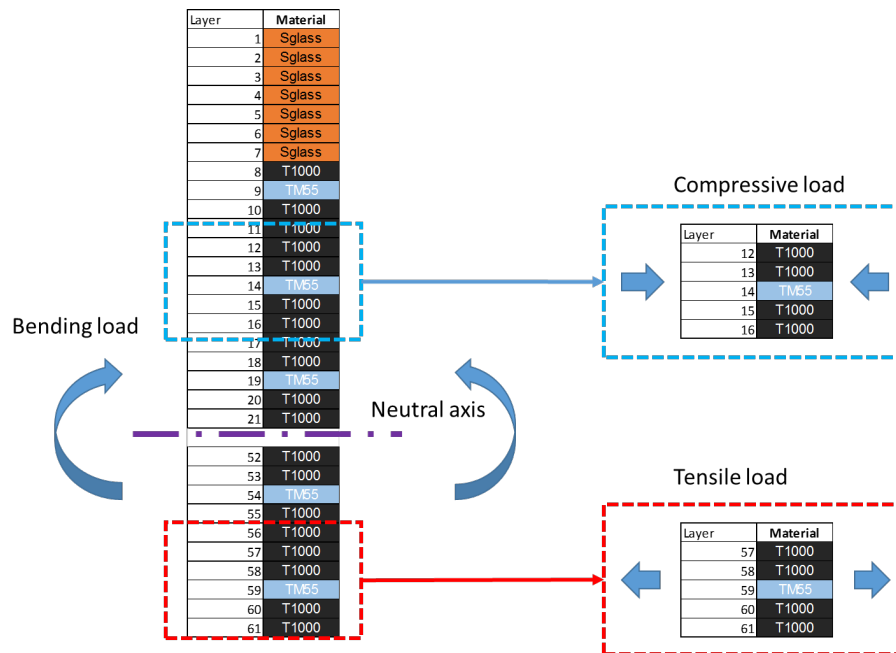
Figure 5-8.: Analytical model assumptions
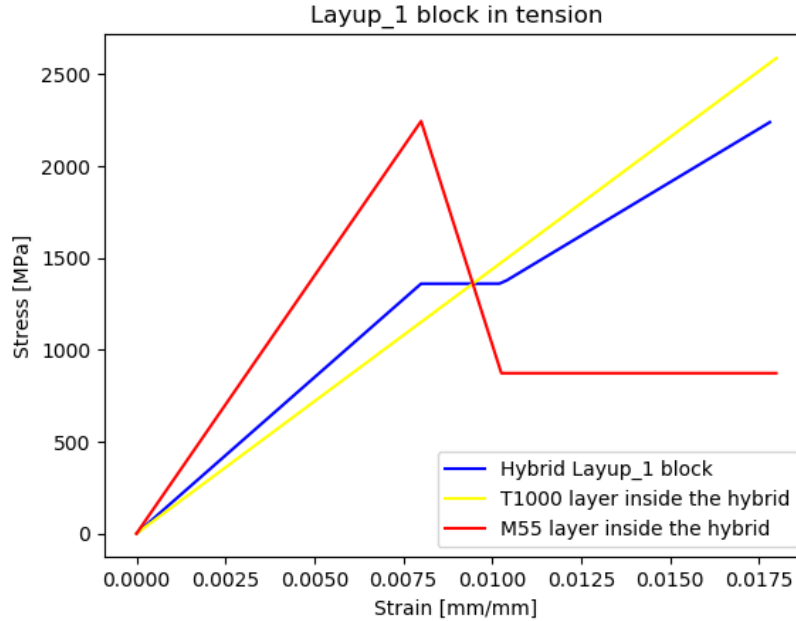
Figure 5-9.: Stress-strain curve of Layup 1 block ($[T1000_2/M55/T1000_2]$), and the layers inside of it (M55 and T1000).

5.4.2. Compressive fragmentation

Compressive fragmentation for hybrid materials has not been modelled in the literature, but there are experimental results that show the conditions needed for it to happen. The results in [Czél et al., 2017] show that the M55 plies in the laminate $[SG_2/EG_{13}/SG_2/M55_2/SG_1]$, where SG represents S-Glass and EG the E-Glass, start to fragment at a strain of 0,46 %, preserving up to 20 % of its initial stiffness at a strain of 2,2 %. A procedure similar to one explained in 5.4.1 can be applied to obtain the stress-strain response of the M55 in compression inside a hybrid layup, the one shown in Figure **5-10**, as in the case of tension, this stress-strain behaviour can be included in the previous algorithm to model the M55 degradation in compression.
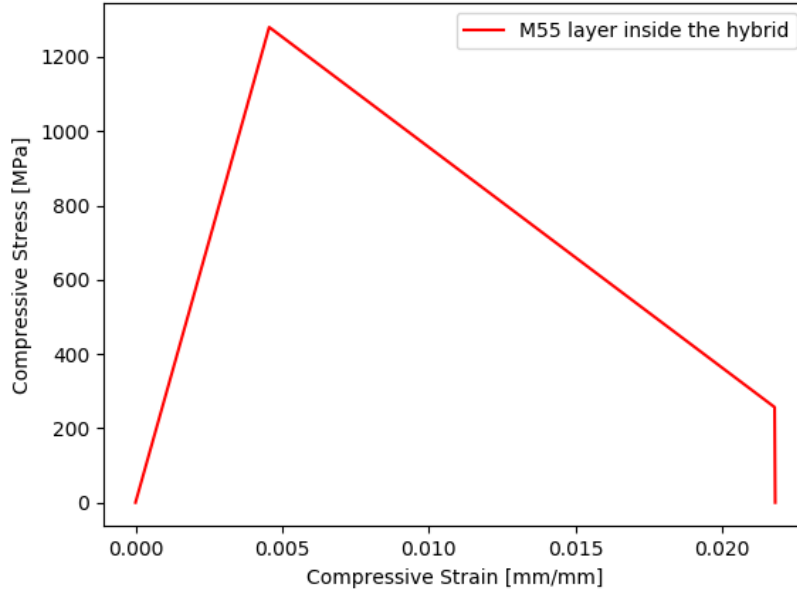
Figure 5-10.: Stress-strain curve for M55 ply inside the laminate [SG2/EG13/SG2/M552/SG1],
extracted from [Czél et al., 2017].

5.4.3.   Delamination

According to [this document is confidential], the energy release rate for mode II (G_{II}) for
a lamina that has fractured inside a laminate, see Figure **5-11**, can be computed from
Equation 5-19, where the terms in the difference are defined in Equation 5-20 and Equation
5-21, explained in Figure **5-12**.

$$G_{II} = \frac{t}{2}\big(\tilde{u}_{after} - \tilde{u}_{before}\big) \tag{5-19}$$

$$\tilde{u}_{before} = \frac{1}{2}\int_{-t/2}^{t/2} \sigma\varepsilon dz \tag{5-20}$$

$$\tilde{u}_{after} = \frac{1}{2}\int_{-t/2}^{t/2} \acute{\sigma}\acute{\varepsilon} dz \tag{5-21}$$
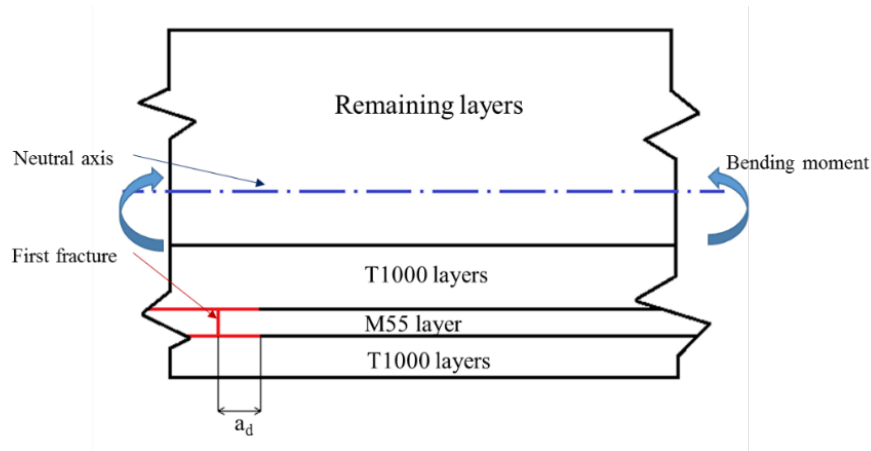
Figure 5-11.: Schematic of Layup 1 where the first fracture in the M55 layers just took place [confidential].
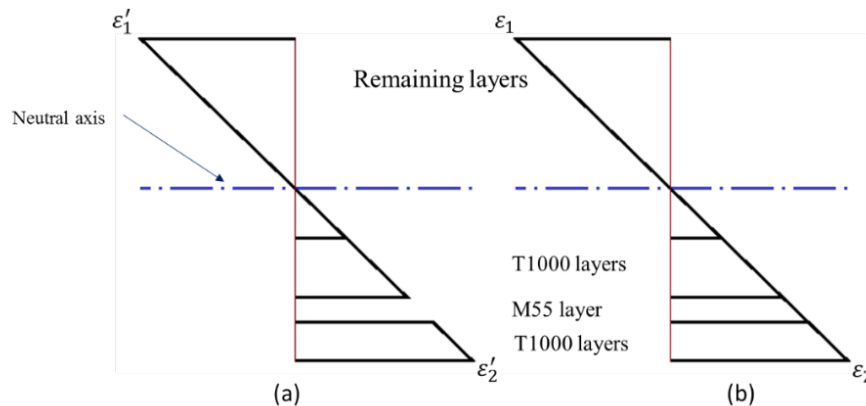
Figure 5-12.: Axial strain distribution along the thickness (a) after and (b) before crack propagation [confidential].
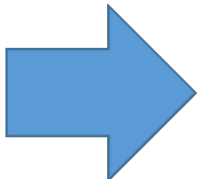
Using Equation 5-19 at every increment allows to assess if the lamina that has fractured posses enough energy to delaminate, or if it rather gets fragmented.

5.4.4.   High strain material failure

Once a lamina either gets the first fracture or is fragmented, the laminas next to it have to keep carrying the load, the cracks in the lamina that has fractured create stress concentration in the adjacent laminas. According to [Jalalvand et al., 2015], for a unidirectional hybrid composite in tension the stress concentration factor is close to 1,1, due to the similarities with the problem at hand, the same value is used here; so, once a lamina gets its first fracture the stress value for failure assessment of the adjacent laminas is increased according to the stress intensity factor.

For every strain increment the stresses in all layers are evaluated and compared to the maximum values to assess failure, once a layer reaches its strength, delamination is checked, if there is no delamination, a degradation response can be implemented and the stress concentration factor is applied for the adjacent laminas. However, if a layer fails in tension and has enough energy to delaminate the whole block where such layer belongs is discarded in the stiffness matrix of the whole laminate. On the other hand, if a lamina fails in compression and is prone to delaminate, full collapse is expected. This process is better explained in appendix A in the form of a pseudo-code.

One important consideration is that the blocks of laminas of the same material are taken as single thicker laminas; for example, for the laminate structure of Layup 1, the basic block structure $[T1000_4/M55]$ where each T1000 layer has thickness of 0,0323mm is now assumed as a structure $[T1000/M55]$ where the T1000 layer has thickness of 0,1292mm (see Figure **5-13**). This is because once the four layers of T1000 thin prepreg are cured, they behave and fail (as it was proved experimentally) as a single lamina.

Figure 5-13.: New numbering stile for Layup 1.

The previous failure assessment is incorporated to the original algorithm; and this way, it is possible to obtain the load vs displacement and load vs strain results in Figure **5-14** and Figure **5-15** respectively, and the failure sequences obtained up to $35mm$ of vertical displacement in Table **5-2**. The failure sequence obtained and load drops can accurately describe the failure progression and damage mechanisms found in the experimental tests, it can be verified that for the gradual failure to be obtained compressive failure of the S-Glass and T1000 blocks needs to be avoided; and more important the algorithm needs to be able to account for them.

The main limitation of the solution designed here is the fact that as the specimen is treated in a homogenized manner, the predicted softening is larger than expected, and this is due to the fact that the fragmentation and delamination occur only in a portion of the specimen, but the algorithm assumes it happens in the region of the specimen between the supports, see Figure **5-16**.
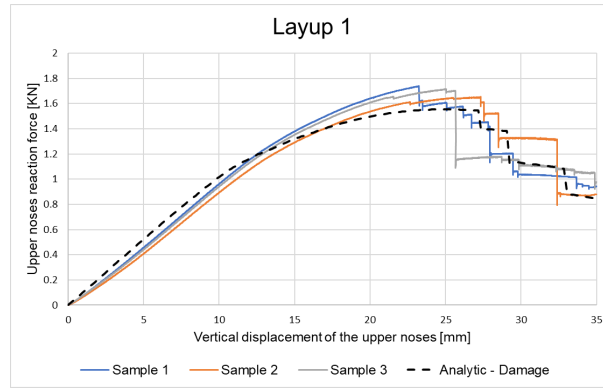
Figure 5-14.: Upper noses reaction force vs vertical displacement of the upper noses; analytic
model for Layup 1.
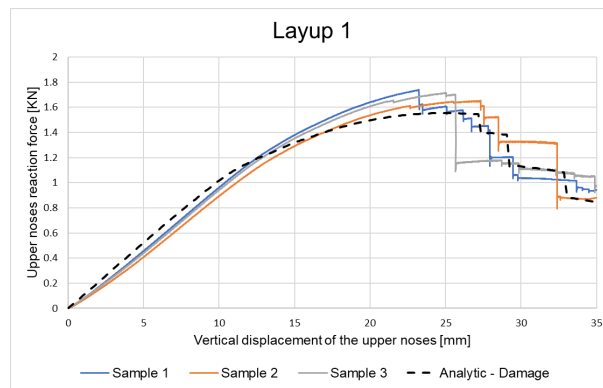
Figure 5-15.: Upper noses reaction force vs strain at the bottom ply; analytic model for Layup
1.

Table 5-2.: Failure sequence according to the analytical method for Layup 1.

Layup_1			
Layer	Material	Failure order (fragmentation)	Failure order (Delamination)
1	Sglass		
2	Sglass		
3	Sglass		
4	Sglass	--	--
5	Sglass		
6	Sglass		
7	Sglass		
8	T1000	--	--
9	M55	1	
10	T1000	--	--
11	M55	4	
12	T1000	--	--
13	M55	7	
14	T1000	--	--
15	M55	--	
16	T1000	--	--
17	M55	--	
18	T1000	--	--
19	M55	--	
20	T1000	--	--
21	M55	9	
22	T1000	--	--
23	M55	6	
24	T1000	--	--
25	M55	5	
26	T1000	--	11
27	M55	3	
28	T1000	--	10
29	M55	2	
30	T1000	--	8
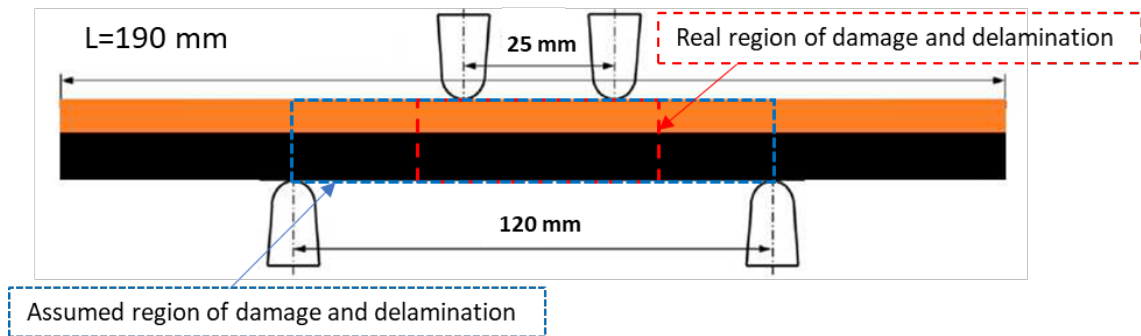
Figure 5-16.: Real and assumed regions of damage and delamination.

6. Summary of verification against other test data

For the sake of simplicity, the Finite elements analysis done in section 4.2 using Hashin damage and the analytical model proposed in present work in section 5.4 is now performed for Layup 2 investigated by Idarraga, and also for the Layup 5 and Layup 7 investigated by Cusack.

Gradual failure was experimentally achieved in Layup 2. As shown in Figure **6-1** and Figure **6-2** the analytical model in 5.4 accurately predict both the load vs displacement and load vs strain results. The numerical model in section 4.2 can also predict the stiffness response of the layup, at least up to the point of maximum load; according to this analysis, the compressive failure strain of the S-Glass should be at least higher than 3.68 %, because at this point, the failure strain in the bottom (T1000 layer) is reached, see Figure **6-3**. The required compressive strain for Layup 2 is higher than the one found in the analysis of Layup 1, therefore, it will stay as the design and verification parameter for the remaining layups to be analysed.

On the other hand, gradual failure was not experimentally achieved for Layup 5 and Layup 7 of Cusack. The analytical model of section 5.4 anticipates such behaviour because it stops at the point where compressive catastrophic failure is expected, see Figure **6-4** and Figure **6-6**. The numerical model is first verified using the stiffness plot of Figure **6-4** and Figure **6-6**; it can accurately predict the initially linear behaviour and the following non-linearity; the softening due to intralaminar damage in the M55 plies is also captured, it ignores delamination and failure due to compressive fracture of the other materials; but the strain measured in the remaining laminas gives insight in the failure sequence; namely, for Layup 5 according to the strain measured, the upper T800 ply reaches its failure strain before the bottom T1000 ply does; so, failure is focused in the compressive side, it is expected to be catastrophic, see Figure **6-5**. For layup 7, the results are similar, failure on the top T1000 ply is reached before failure on the tensile side, yielding compressive sudden failure, see Figure **6-7**.
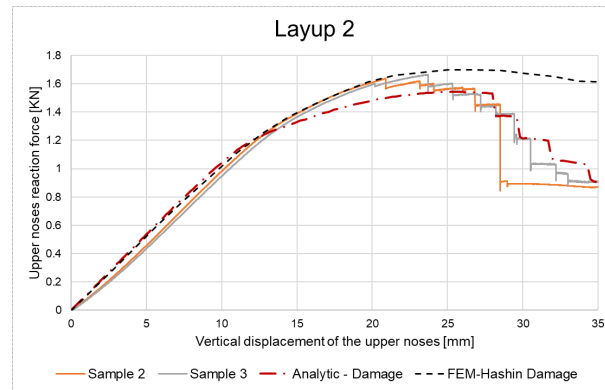
Figure 6-1.: Upper noses reaction force vs vertical displacement of the upper noses; analytic model and finite element model using Hashin damage for Layup 2.
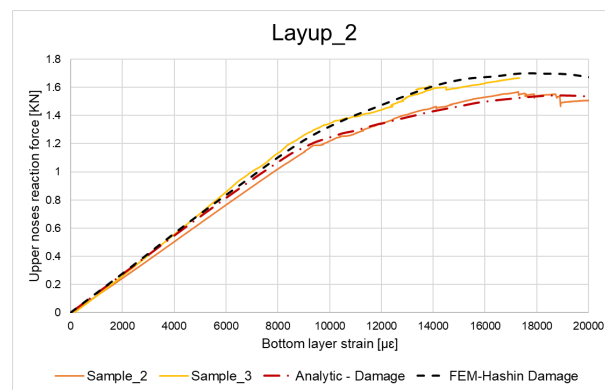
Figure 6-2.: Upper noses reaction force vs strain at the bottom ply; analytic model and finite element model using Hashin damage for Layup 2.
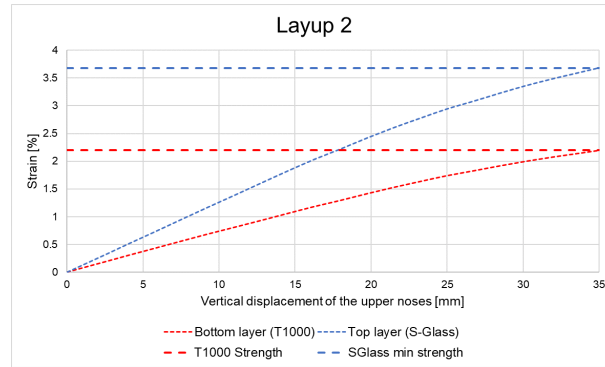
Figure 6-3.: Top and bottom layer strain vs vertical displacement of the upper noses for Layup 2 ; where the horizontal line "T1000 Strength" represents the strain at the point where the T1000 layer reaches its tensile strength, and the horizontal line "SGlass min strength" represents the strain at the maximum stress reached by the top S-Glass layer.
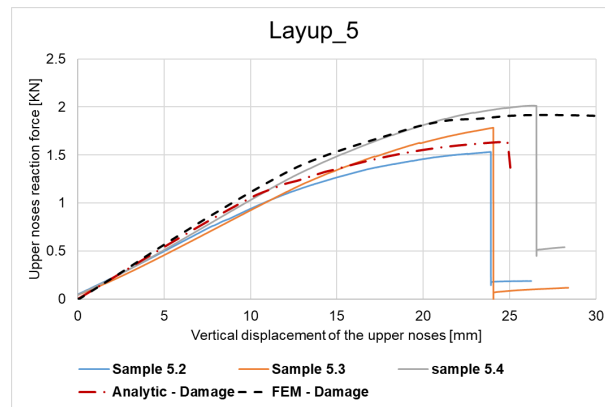
Figure 6-4.: Upper noses reaction force vs vertical displacement of the upper noses; analytic model and finite element model using Hashin damage for layup 5.
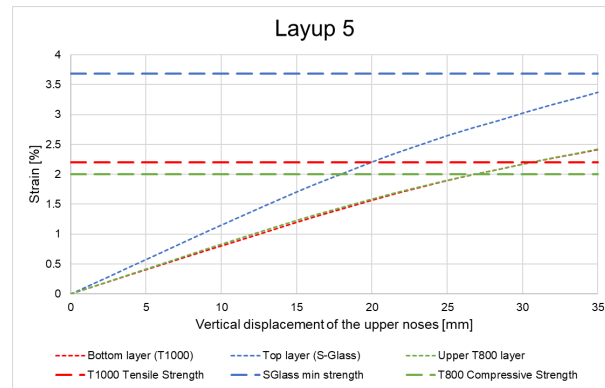
Figure 6-5.: Top, upper T800, and bottom layer strain vs vertical displacement of the upper noses for Layup 5; where the horizontal line "T1000 Tensile Strength" represents the strain at the point where the T1000 layer reaches its tensile strength, the horizontal line "T800 Compressive Strength" represents the strain at the point where the T800 layer reaches its compressive strength, and the horizontal line "SGlass min strength" represents the strain at the maximum stress reached by the top S-Glass layer in Layup 2.
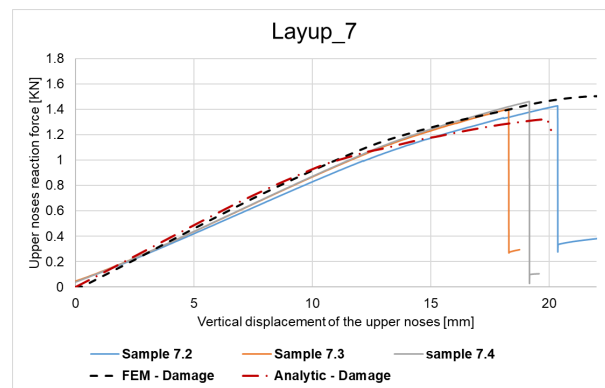
Figure 6-6.: Upper noses reaction force vs vertical displacement of the upper noses; analytic model and finite element model using Hashin damage for Layup 5.
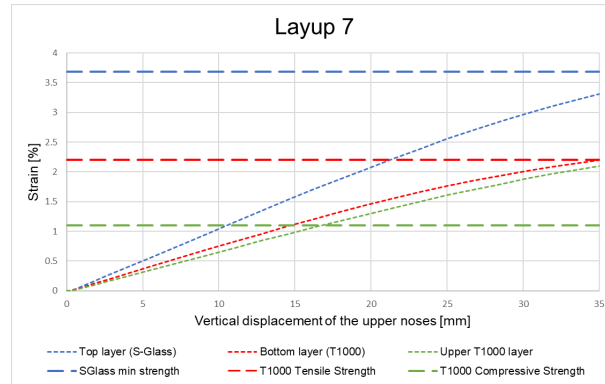
Figure 6-7.: Top, upper T1000, and bottom layer strain vs vertical displacement of the upper
noses for Layup 7; where the horizontal line "T1000 Tensile Strength" represents
the strain at the point where the T1000 layer reaches its tensile strength, the
horizontal line "T1000 Compressive Strength" represents the strain at the point
where the T1000 layer reaches its compressive strength, and the horizontal line
"SGlass min strength" represents the strain at the maximum stress reached by the
top S-Glass layer in Layup 2.

7. Experimental validation

The analytical solution that works in the algorithm can run in seconds while the numerical simulation using cohesive elements can take hours and even days to get results, for this reason, the layup proposal for experimental validation is chosen analysing several options using the algorithm and then verifying the best option using the numerical model in 4.2.

As the experimental results from Idárraga and Cusack already help in the validation of the models, the new experimentation is meant to assess both the assumptions that were made in the development of these work and the conclusions that were reached in the previous ones; as it is shown later on, this ends up in more efficient and economical layups compared with the ones from the previous works. The new layups and their main purpose are explained in the following.

7.1. Layup proposals

7.1.1. Layup A (S-Glass/IM7/M55)

For Layup 1 in [Idárraga, 2019], one of the main assumptions in the development of the analytical solution is that the four layers of thin-ply T1000 carbon in the block structure fail as a single thicker lamina; because once the laminate is cured the four layers in the block act as a single one; therefore, if the four thin layers of T1000 can be replaced by a single layer of a standard thickness material of similar properties and the new hybrid can show the same kind of failure response such an assumption can be considered as proved.

The UD IM7/913 Epoxy prepreg supplied by Hexcel has a post-cured thickness of approximately $0,13mm$ [Hexcel, 2018], and the mechanical properties are shown in Table **7-1**, which can be considered similar to the ones of the T1000 shown in Table **3-1**; so, if one layer of this material can be considered as an approximation of several layers of T1000, a new layup of the type $[SGlass_m/(IM7/M55)_p/IM7]$ should be able to exhibit the same kind of response. Now, consider Layup A is a laminate of the type $[SGlass_m/(IM7/M55)_p/IM7]$, where m and p are chosen such that Layup A has a similar thickness to the one of Layup 1, fails gradually, and obtain the maximum possible strength and stiffness. Using the algorithm and systematically changing the values of m and p, it is found that the best configuration is $[SGlass_7/(IM7/M55)_{10}/IM7]$, see appendix A for more details on the design methodology.

7.1.2. Layup B (S-Glass/IM7/M46J)

Layup B has the same function of Layup A, this configuration was created mainly due to limitations in the availability of the M55/Epoxy prepregs in Layup A. Layup B has the purpose of emulating the behaviour of Layup 1 in [Idárraga, 2019], where the effect of the four blocks of T1000/Epoxy is changed by the single layer of regular thickness IM7/Epoxy pre-preg, and the thin M55/Epoxy replaced by UD thin-ply M46J/Epoxy pre-preg which has comparatively larger modulus than the IM7/Epoxy, see Table **7-1**. Following the process explained previously, the optimum configuration for this layup in bending is found to be $[SGlass_7/(IM7/M46J)_{10}/IM7]$.

The resulting layups optimise the amount of material, it also reduces the time for manufacture and the cost of the hybrid layup, as one standard ply replaces four thin plies inside each block, Layup 1 and Layup 2 having 61 plies each, can be substituted by Layup A and Layup B, having 28 plies each. The cost reduction is significant as the price of the thin-ply material is more than double of the standard thickness per square meter.

7.1.3. Layup C (IM7)

The main objective of the design of hybrid composite layups is to overcome the inherent fragile behaviour of single constituent layups, this is why Layup C is set as the baseline, to probe that the hybridisation of carbon composites can change the nature of failure from brittle, in pure carbon composites made of unidirectional carbon $[IM7_{21}]$, to gradual and controlled in glass/carbon hybrid configurations.

Table 7-1.: Material properties for IM7/Epoxy and M46J/Epoxy prepregs according to [Hexcel, 2018, Torayca(R), 2012].

IM7/Epoxy						
E_1 [GPa]	E_2 [GPa]	v_{12}	G_{12} [GPa]	Ply thickness [mm]	Tensile strain [%]	Compressive strain [%]
152,0	6,06	0,32	2,4	0,13	1,6	1,23
M46J/Epoxy						
E_1 [GPa]	E_2 [GPa]	v_{12}	G_{12} [GPa]	Ply thickness [mm]	Tensile strain [%]	Compressive strain [%]
265,0	6,06	0,32	2,4	0,029	0,8	0,6

The numerical and analytical results (Load vs displacement and Load vs compressive strain) prior to testing are shown in Figure **7-1**, Figure **7-2**, Figure **7-4**, Figure **7-5**, Figure **7-7**, and Figure **7-8** for Layup A, Layup B, and Layup C. Layup A is expected to fail gradually, the analytical models shows the staircase gradual failure due to fragmentation of the M55 layers and tensile fracture of the blocks of IM7/M55; this is verified by the numerical model, where it can be seen that failure in the lower IM7 ply takes place earlier than in the top layers, see Figure **7-3**. Layup B proceeds in the same way that Layup A does, see Figure **7-6**; the analytical model in these two scenarios is set up to 35 mm of vertical displacement because the loading fixture should not go far beyond that; so, load-displacement data as well as load-strain data are recorded up to that displacement. On the other hand, Layup C is not expected to fail gradually, the analytical models stops at the point where catastrophic compressive failure is computed, besides, the numerical models predicts failure by compression rather than by tension, see Figure **7-9**.

Figure 7-1.: Upper noses reaction force vs vertical displacement of the upper noses; analytic model and finite element model using Hashin damage for layup A.

Figure 7-2.: Upper noses reaction force vs strain at the top ply; analytic model and finite element model using Hashin damage for layup A.

Figure 7-3.: Top, upper IM7, and bottom layer strain vs vertical displacement of the upper noses for Layup A; where the horizontal line "IM7 Tensile Strength" represents the strain at the point where the IM7 layer reaches its tensile strength, the horizontal line "IM7 Compressive Strength" represents the strain at the point where the IM7 layer reaches its compressive strength, and the horizontal line "SGlass min strength" represents the strain at the maximum stress reached by the top S-Glass layer in Layup 2.

Figure 7-4.: Upper noses reaction force vs vertical displacement of the upper noses; analytic model and finite element model using Hashin damage for layup B.

Figure 7-5.: Upper noses reaction force vs strain at the top ply; analytic model and finite element model using Hashin damage for Layup B.

Figure 7-6.: Top, upper IM7, and bottom layer strain vs vertical displacement of the upper noses for Layup B ; where the horizontal line "IM7 Tensile Strength" represents the strain at the point where the IM7 layer reaches its tensile strength, the horizontal line "IM7 Compressive Strength" represents the strain at the point where the IM7 layer reaches its compressive strength, and the horizontal line "SGlass min strength" represents the strain at the maximum stress reached by the top S-Glass layer in Layup 2.
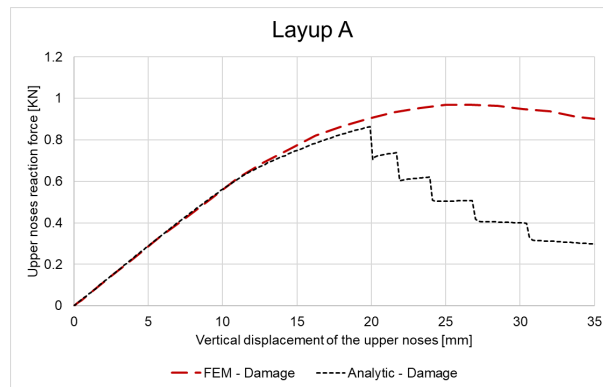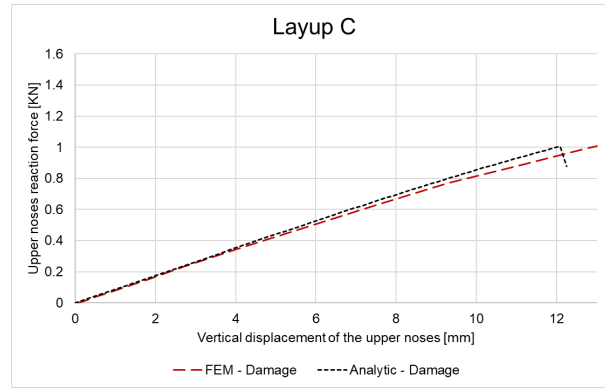
Figure 7-7.: Upper noses reaction force vs vertical displacement of the upper noses; analytic model and finite element model using Hashin damage for layup C.
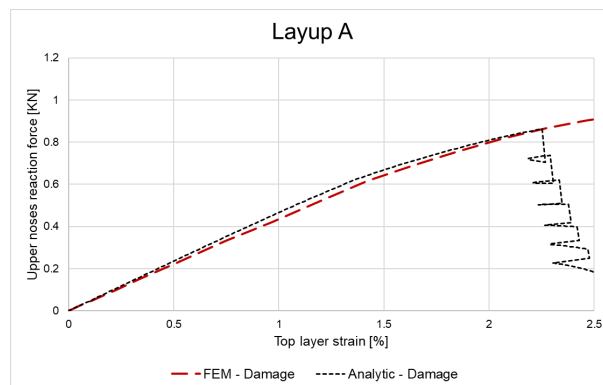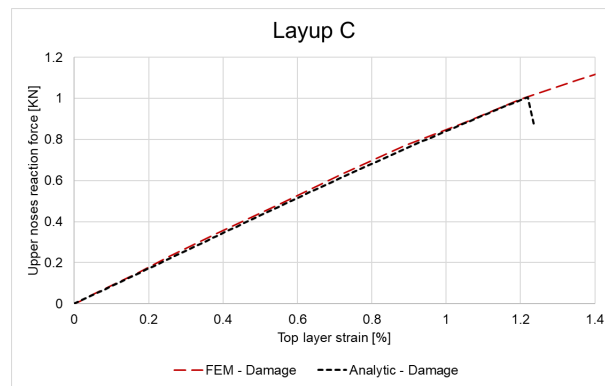

Figure 7-8.: Upper noses reaction force vs strain at the top ply; analytic model and finite element model using Hashin damage for Layup C.
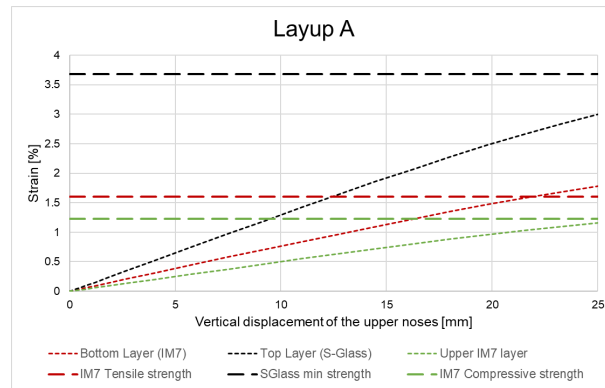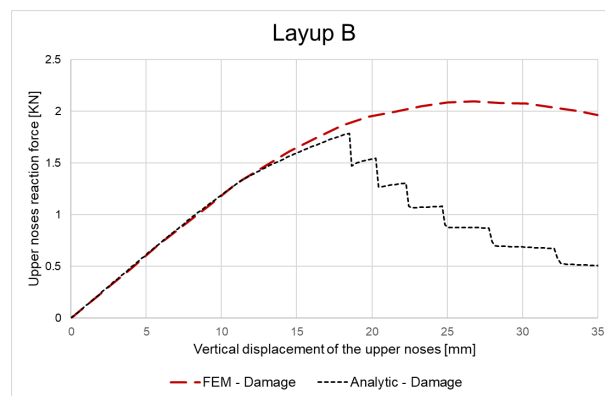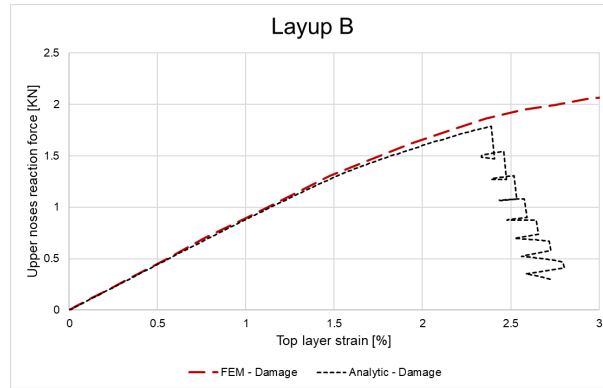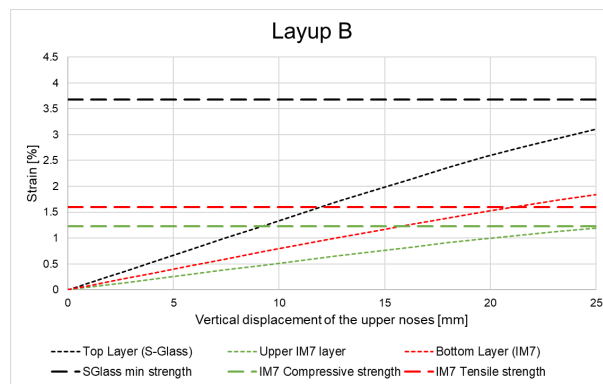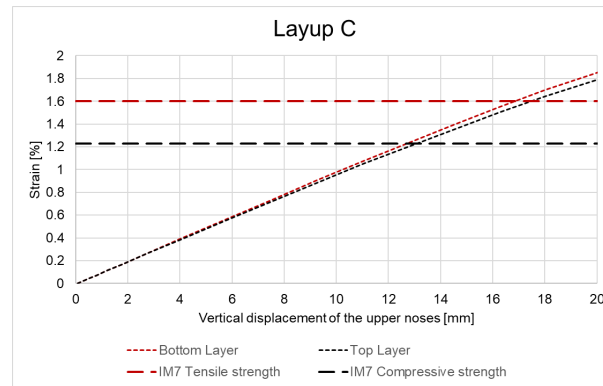
Figure 7-9.: Top and bottom layer strain vs vertical displacement of the upper noses for Layup
C; where the horizontal line "IM7 Tensile Strength" represents the strain at the
point where the IM7 layer reaches its tensile strength and the horizontal line "IM7
Compressive Strength" represents the strain at the point where the IM7 layer
reaches its compressive strength.

7.2. Experimental campaign

The layups were manufactured in the facilities of the University of Strathclyde, in the laboratories of the department of mechanical and airspace engineering. The specimen dimensions are shown in Table **7-2**, as can be seen the specimens made using the configuration of Layup A and Layup C are smaller than the rest, this is due to the low availability of materials. Layup B is manufactured according to the recommendations of Idárraga and Cusack.

Due to limited resources, measurement using strain gauges was possible only for Layup A and Layup C, upper noses reaction load vs top ply compressive strain and upper noses reaction load vs upper noses vertical displacement data were recorded. The load vs strain curve is used for validation of the stiffness and failure prediction, and agreement between expected and experimental results is found; but load vs displacement results are not compared neither with analytic nor numerical predictions, as the recorded displacement was not accurately measured its results can only be used qualitatively to visualize gradual failure tendency. For the case of Layup B, no strain gauges could be used, so, only upper noses reaction load vs upper noses vertical displacement was recorded; again, due to the low accuracy of the displacement measurement, its results can only be used qualitatively to visualize gradual failure tendency. In summary, the results from the testing on these layups are mainly focused on the failure mechanisms and failure progression, rather than exact prediction of the load-displacement or load-strain curves, it was already done with Layup 1, Layup 2, Layup 5, and Layup 7. Layup B was tested using the configuration of Idárraga shown in Figure **3-7**, without strain gauges; while testing on Layup A and Layup C had to be done in a different machine, placement of the strain gauges forced to change such configuration, namely, the upper noses distances went from $25mm$ to $28,5mm$, besides, the strain gauges were placed

on the upper layer rather than in the lower bottom one.

Table 7-2.: Average dimensions of the specimen types.

Specimen type	Width [mm]	Thickness [mm]	Length [mm]
Layup A (S-Glass/IM7/M55)	10,18	2,74	190,0
Layup B (S-Glass/IM7/M46J)	20,18	2,96	220,0
Layup C (IM7)	10,19	2,74	220,0

7.3. Results

The upper noses reaction load vs upper noses vertical displacement curves for Layup A, Layup B, and Layup C can be seen in Figure **7-10**, Figure **7-11**, and Figure **7-12**
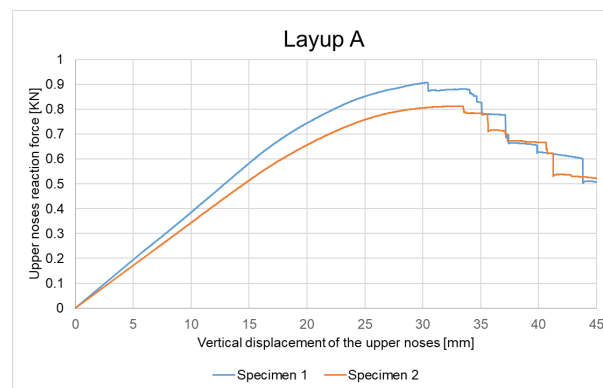
Figure 7-10.: Upper noses reaction force vs vertical displacement of the upper noses; Layup A.
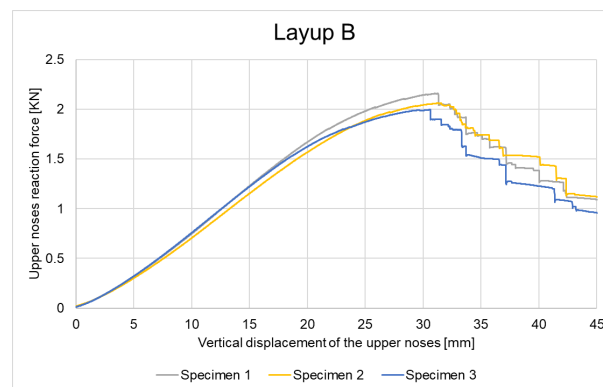
Figure 7-11.: Upper noses reaction force vs vertical displacement of the upper noses; Layup B.
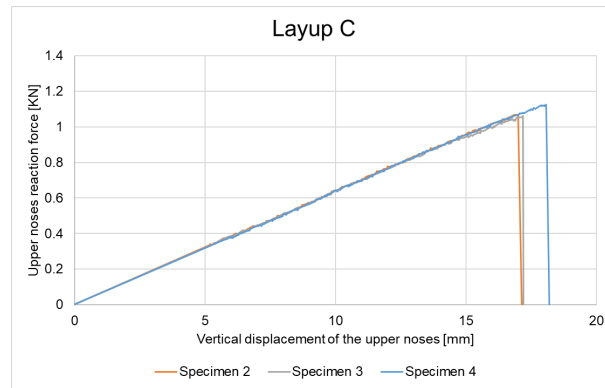
Figure 7-12.: Upper noses reaction force vs vertical displacement of the upper noses; Layup C.

The upper noses reaction load vs strain in the top lamina curves for Layup A and Layup C alongside with the analytic results used for its design can be seen in Figure **7-13** and Figure **7-14** respectively.
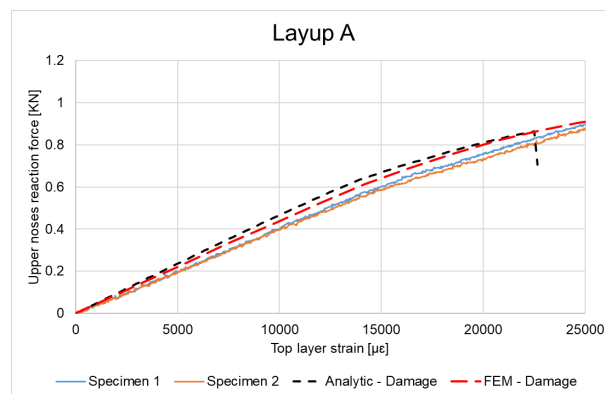
Figure 7-13.: Upper noses reaction force vs strain at the top ply; analytic model for Layup A.
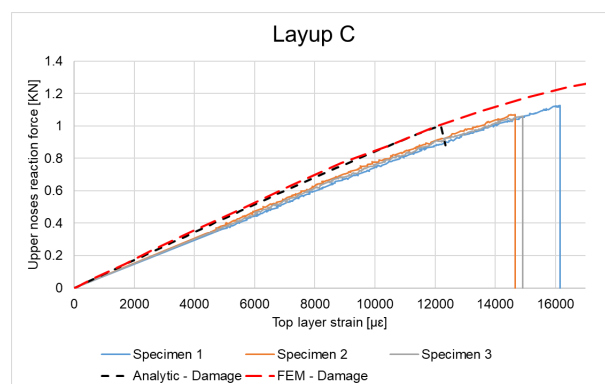
Figure 7-14.: Upper noses reaction force vs strain at the top ply; analytic model for Layup C.

Hybrid specimens failed as expected, first fragmentation took place in lower bottom thin ply materials, M55 in Layup A and M46J in Layup B, then gradual tensile fracture and delamination of the bottom blocks created the brush like failure shown in Figure **7-15** and Figure **7-16** respectively, the integrity of the top compressive part of the laminates was held as predicted by the algorithm.

The single constituent specimen also failed as expected; compressive failure of brittle nature took place, in this case, a single fracture travelled through the thickness of the specimen and broke it in two parts, see Figure **7-17**.

The analytical model was able to accurately predict the behaviour in both hybrid and non-hybrid composite layups; it shows a clear matching between the failure sequence and failure mechanisms in experimental and analytic results.

All the experimental results and its corresponding numerical and analytical predictions are summarized in table **7-3**

Figure 7-15.: Failure mode in the four-point bending test of Layup A.

Figure 7-16.: Failure mode in the four-point bending test of Layup B.
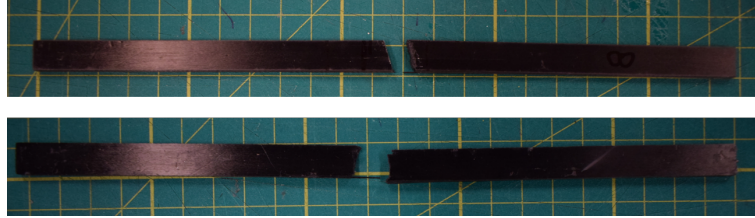
Figure 7-17.: Failure mode in the four-point bending test of Layup C.

Table 7-3.: Summary of experimental, numerical, and analytical results.

Specimen type	Experimental failure mode	Numerical failure prediction	Analytical failure prediction
Layup A (S-Glass/IM7/M55)	Brush-like-failure	Tensile failure	Brush-like-failure
Layup B (S-Glass/IM7/M46J)	Brush-like-failure	Tensile failure	Brush-like-failure
Layup C (IM7)	Catastrophic compressive failure	Compressive failure	Catastrophic compressive failure

8. Conclusions and recommendations

8.0.1. Conclusions

- The present methodology using analytical and numerical tools can accurately predict the failure sequence and failure mechanisms inside hybrid and standard composite layups with both gradual failure capabilities and brittle failure nature, no matter specimen and test dimensions, and degree of non-linear behaviour.

- The analytic solution developed through the implementation of the algorithm can save a considerable amount of time, compared to the numerical solution, when it comes to both running time and time for setting up. This makes the analytical solution more appealing for design purposes.

- All the main hypothesis done for the design of the numerical and analytical tools were properly verified by experimental evidence on different kinds of hybrid configurations.

- Accurate prediction of failure in hybrid and standard composite materials demands to be able to capture all possible failure mechanisms that can take place in such materials.

- The new layups show that gradual failure in bending can be achieved by using blocks created by thin-ply and standard-ply thickness prepregs, instead of using only thin-ply prepregs; namely, the new configuration of Layup A and Layup B proved to yield the same failure behaviour of Layup 1 and Layup 2 in [Idárraga, 2019] but at a much lower cost (only one type on thin-ply material used) and lower manufacture resources (lower amount of plies). This implies a considerable optimization on the design of hybrid composites for bending applications.

8.0.2. Recommendations

- The verification of the models was done using much finer experimental results that the ones used for its validation, this was due to lack of resources; but the ideal process is the opposite.

- In order to reach the implementation of this kind of material in real structures, the next step is to consider and multidirectional hybrid layups, this would require further testing for validation the modelling methodology in such scenario.

- During the test of the hybrid specimens fragmentation in the thin-plies was evidenced by sound the fibres do when they break, sound that could be heard before peak load. The proper way to verify it is by performing the post-mortem analysis done in [Idárraga, 2019].

- The python scripts for the numerical models developed here should be further parametrised in order to reduce the pre-processing time of the numerical analysis.

- The current 2D numerical approach uses several parts whose surfaces are connected using "Tie constrains", this should be replaced by a single mesh constructed from a script.

- CDM should be added to capture compressive fragmentation.

- Abaqus cohesive elements should be replaced by the cohesive subroutine in [Turon Travesa, 2007] that proved to yield faster convergence.

9. Additional experimentation

The total experimental campaign shown in the previous chapter was not the complete set of tests. In this section, some extra results to help understand and clarify the experimental results will be presented. Also, some interesting results on S-glass will be briefly discussed.

9.0.1. Laminate IM7 only

Comparison between experimental, analytical, and numerical models for the laminate $[IM7_{21}]$ is shown in Figure **9-1** for load/displacement data, and in Figure **9-2** for load/top-strain data.

Figure 9-1.: Upper noses reaction force vs vertical displacement of the upper noses; analytic model and finite element model using Hashin damage for laminate IM7 only.
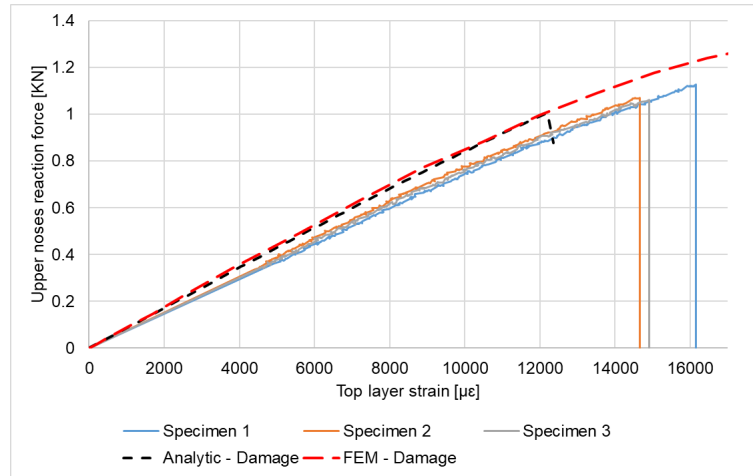
Figure 9-2.: Upper noses reaction force vs strain at the top ply; analytic model and finite element model using Hashin damage for laminate IM7 only.

9.0.2.   Laminate S-Glass only

Comparison between experimental and analytical model for the laminate $[SGlass_{18}]$ is shown in Figure **9-3** for load/displacement data, and in Figure **9-4** for load/top-strain data. Due to the low modulus and high failure strain of this material, the load and support dimensions had to be modified according to the recommendations in ASTM D6272 – 17; so, the new load and support span are 28.5 mm and 85.5 mm respectively. It means, these plots cannot be compared directly with rest, because the degree of non-linear behaviour is different and it would yield and apparent distorted stiffness and failure load.
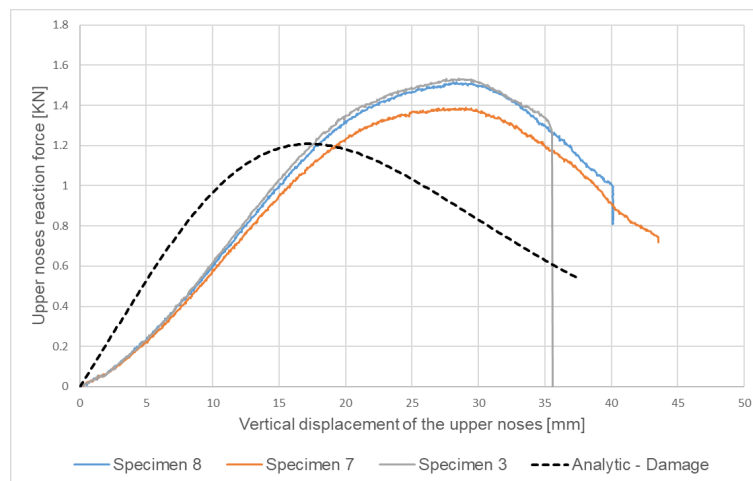
Figure 9-3.: Upper noses reaction force vs vertical displacement of the upper noses; analytic model and finite element model using Hashin damage for laminate SGlass only.
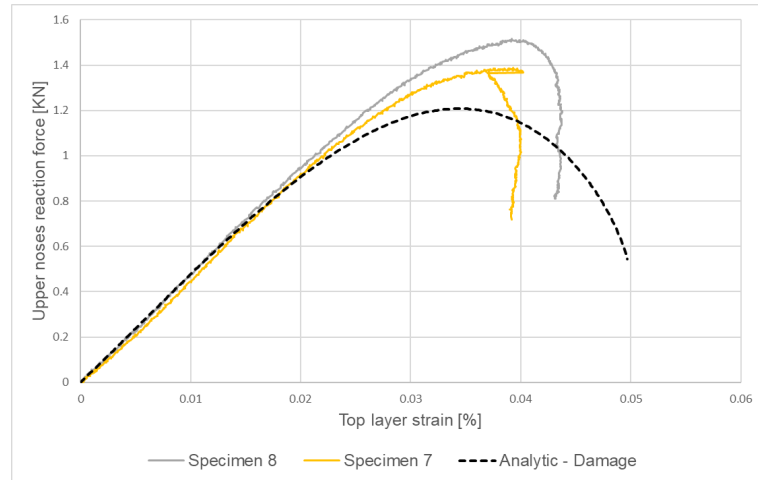
Figure 9-4.: Upper noses reaction force vs strain at the top ply; analytic model and finite element model using Hashin damage for laminate SGlass only.

9.0.3. Laminate SGlass-IM7-M55

Comparison between experimental and analytical model for the laminate $[SGlass_7/(IM7/M55)_{10}/IM7]$ is shown in Figure **9-5** for load/displacement data, and in Figure **9-6** for load/top-strain data.
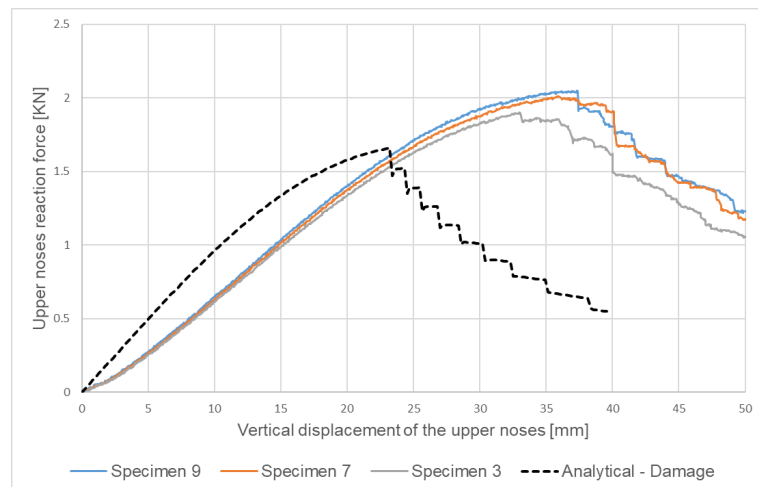
Figure 9-5.: Upper noses reaction force vs vertical displacement of the upper noses; analytic model and finite element model using Hashin damage for laminate SGlass/IM7/M55.
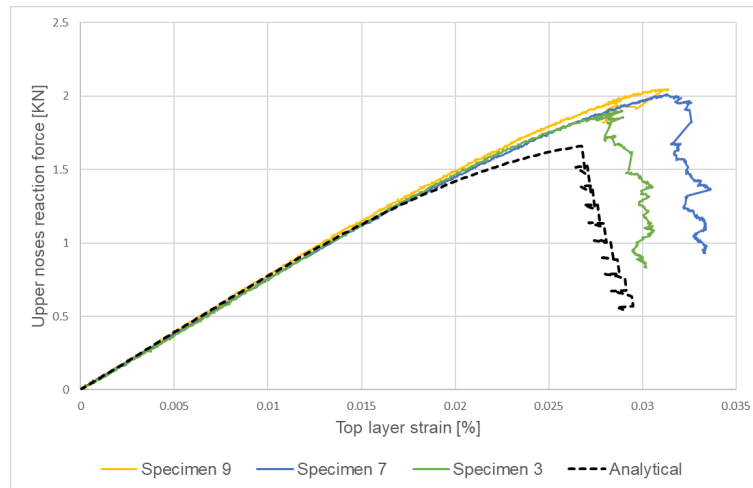
Figure 9-6.: Upper noses reaction force vs strain at the top ply; analytic model and finite element model using Hashin damage for laminate SGlass/IM7/M55.

9.0.4. Laminate SGlass-IM7-M46J

Comparison between experimental and analytical model for the laminate $[SGlass_7/(IM7/M46J)_{10}/IM7]$ is shown in Figure **9-7** for load/displacement data.
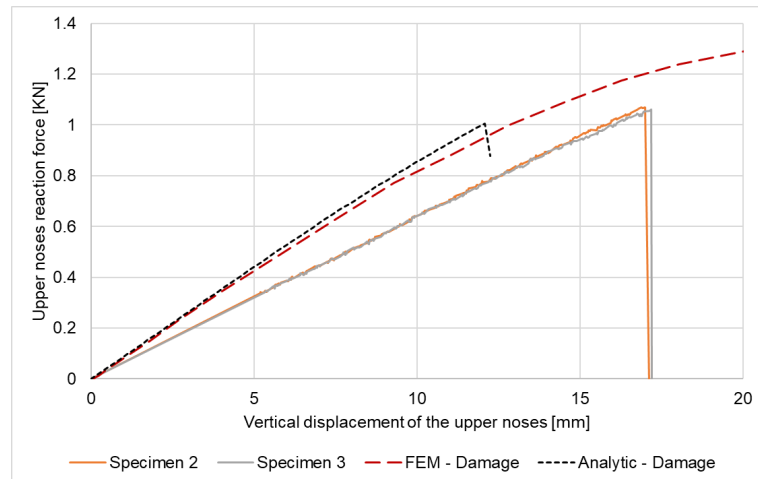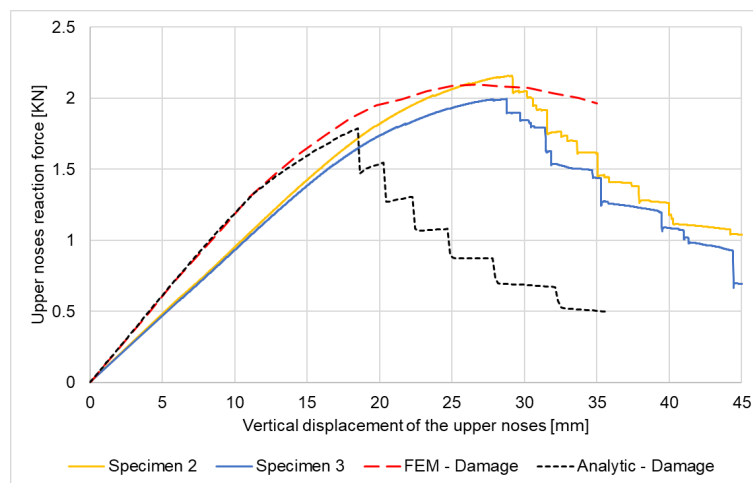

Figure 9-7.: Upper noses reaction force vs vertical displacement of the upper noses; analytic model and finite element model using Hashin damage for laminate SGlass/IM7/M46J.

The validation is performed using the load-strain curves, good agreement is found when these parameters are compared with the experimental results, also damage mechanisms and failure sequence agree with the experimental evidence; on the other hand, large error is found in the cross-head displacement measurement, so the displacement results are only used qua-

litatively to help visualise tendencies. Also, as explained previously, the analytical method over-predicts softening due to its inherent homogenised nature, this is why the predicted failure loads are lower than the experimental ones.

For IM7 laminate failure was always brittle and given in the compressive side; the intralaminar crack went through the specimen thickness without causing severe delamination. This is the kind of compressive collapse predicted by both methodologies explained in the numerical and analytical models.

For SGlass laminate the results are not conclusive, some of the specimens were tested without strain gauges, all of them failed by fracture in compression but with some degree of tensile failure before the specimen collapse, see Figure **9-8**. On the other hand some specimens were tested using strain gauges in the compressive side, all of this specimen failed gradually, presenting the same brush-like pattern but with a more controlled delamination, see Figure **9-9**. As mentioned earlier the compressive strength of the SGlass/Epoxy was higher than expected, that is why the first simulations using Layup 1 were used to calibrate this property; but the results of this campaign show that the compressive failure strain is so close to the tensile one, that the addition of the strain gauges can potentially act as a reinforcement, avoiding failure by compression and focus it in the tensile side; thus, achieving failure modes similar to the desired ones in hybrid composites. For the moment these are just hypothesis, in order to truly understand what triggers the change from compressive to tensile failure more testing needs to be performed following an accurate measure of strain in both faces of the laminate and using instruments that measure the deformation without potentially disrupting the specimen strength or stiffness.

Failure in the hybrid laminates was properly explained and discussed previously. The load-strain curves, damage mechanisms, and failure sequences validate the accuracy of the models; inaccuracy of the load-displacement data can be ignored accounting for the previous validation using the data in Idárragas and Cusacks tests, where an accurate measure of the same parameters perfectly agreed with the predictions.

Figure 9-9.: Failure in SGlass specimen with strain gauge.
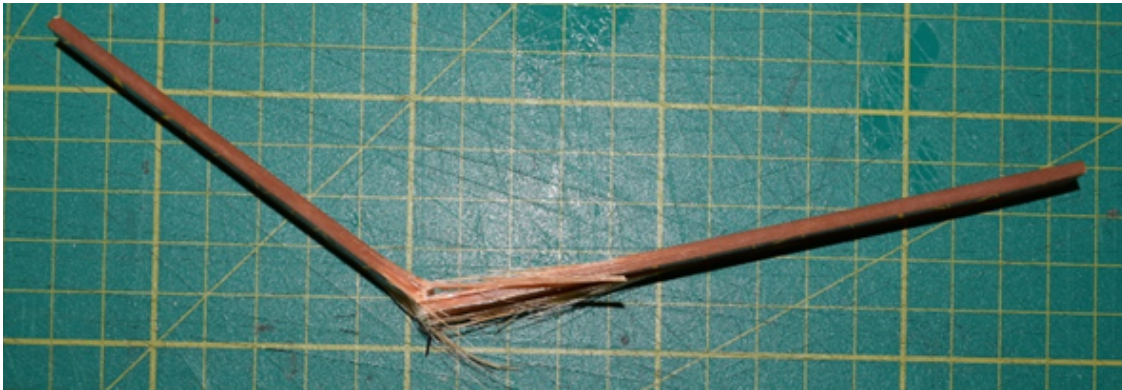
Figure 9-8.: Failure in SGlass specimen without strain gauge.

A. Annex: Pseudo-code for the analytical solution algorithm

- Define the material properties E_1, E_2, G_{12}, and v_{12} for each material (Glass, high modulus carbon, low modulus carbon).

- Calculate the local matrix $[Q]$ and global matrix $[\bar{Q}]$ for each material using Equation 2-5 and Equation 2-7 respectively.

- Define the layup sequence, orientations and thicknesses.

- Calculate the initial $[A]$, $[B]$, $[D]$ matrices according to Equation 2-10, Equation 2-11, and Equation 2-12.

- Define the values of upper noses and support radius r_p, the initial support span L_0 and noses-support distance a_0.

- Create a list of values of α (α_{list}), from a low value (α_0), close to zero; up to a value lower than $^{pi}/_2$ (α_N).

- Set the first value of the contact noses-support distance (a_n) to be equal to the noses-support distance (a_0) $a_n = a_0$

- Iterate through all the values of α in (α_{list}). For α_n in (α_{list}):

  - Calculate the contact support-span (L_n), as function of α_n, r_p, and L_0, using Equation 5-9

  - Find a first approximation of the current value of beta (β_n), solving numerically Equation 5-6, using α_n as α, L_n as L, and the first estimate of a_n as a

  - Set a variable named a_{new} as the new approximation of a_n using Equation 5-10 based on the current value of α_n, r_p, and the first estimate of β_n

  - Set a variable named (a_{old}) as zero; $a_{old} = 0,0$

  - Iteratively find the current values of β_n and a_n, check convergence in the value of a_n. While the absolute value of ($a_{new} - a_{old}$) > $tolerance$:

    - Set a_{old} equal to a_{new}; $a_{old} = a_{new}$

- ○ Find a new approximation of (β_n), solving numerically Equation 5-6 using α_n as α, L_n as L, and a_{old} as a

- ○ Calculate a_{new} using Equation 5-10 based on α_n, and the previous estimation of β_n

- Set a_n equal to a_{new}; $a_n = a_{new}$

- Set θ equal to zero; $\theta = 0$

- Calculate the value of $2R/EI$ from Equation 5-1 based on a_n, α_n, and β_n

- Use the value of $2R/EI$ to calculate the curvature $1/r$ at the centre of the using Equation 5-4

- Set the laminate bending curvature in the x direction κ_x to be equal to the beam curvature $1/r$; $\kappa_x = 1/r$

- For each lamina in the layup:

  - ○ Solve Equation 2-3 and Equation 2-4 to find the stress in the upper and lower surfaces of the lamina

  - ○ Check if the stress state is compression or tension

  - ○ If there is a tension stress state:

    - ◇ If the current stress is larger than the material strength: Evaluate possible delamination using Equation 5-19 and the critical energy release rate in mode II of the interface between the two materials

    - ◇ If delamination is NOT expected: Use a degradation mechanism in the current lamina according to Figure **5-9** and apply a stress concentration on the adjacent laminas.

    - ◇ If external delamination is expected: Discard the block of laminas where the current lamina belongs to.

    - ◇ If internal delamination is expected: Stop and alert delamination collapse.

    - ◇ If the current stress is NOT larger than the material strength: Jump to the next lamina

  - ○ If there is compressive stress:

    - ◇ If the current stress is larger than the material strength: Evaluate possible delamination using Equation 5-19 and the critical energy release rate in mode II of the interface between the two materials

    - ◇ If delamination is NOT expected: Use a degradation mechanism in the current lamina according to Figure **5-10** and apply a stress concentration on the adjacent laminas.

⬦ If internal delamination is expected: Stop and alert delamination collapse.

⬦ If external delamination is expected: Stop and alert compressive collapse.

- Update the A, B, D matrices according to the previous loop

- Set the variables N_x, N_y, N_{xy}, M_y, and M_{xy} equal to zero

- Solve Equation 2-9 to find the bending moment reaction in the x direction M_x, using κ_x, N_x, N_y, N_{xy}, M_y, and M_{xy}

- Calculate the product "EI" from equation 5-5 using M_x and κ_x

- Calculate the reaction force in the supports R from Equation 5-1 using α_n, β_n, EI, and a_n.

- Calculate the reaction force on the upper noses in the vertical direction (F_y), as a function of R, α_n, and β_n.

- Save the value of F_y in a list called F_{y_list}

- Calculate the contact vertical displacement y_a using Equation 5-2 based on $^{2R}/_{EI}$, a_n, α_n, and β_n.

- Calculate the actual vertical displacement of the upper noses yn using Equation 5-11 based on y_a, r_p, α_n, and β_n

- Save the value of y_n in a list y_{n_list}

- Go to the next increment step

▪ Plot the list y_{n_list} in the x axis and the list F_{y_list} in the y axis to get the load-displacement curve.

B. Annex: Layup Design

The layup design is based on the methodology in [Lim et al., 2014], assuming a very low contribution to the stiffness by the thin ply materials, and taking into account that the hybrid configurations $[IM7/M55/IM7]$ and $[IM7/M46J/IM7]$ yield gradual failure in tension according to the model of [Jalalvand et al., 2015]. The optimum configuration in bending is computed for a non-symmetric hybrid specimen of the type $[SG_m/IM7_n]$, where the values of m and n are selected in the following way:

- The value of m starts from 18 in a purely S-Glass composite (0 % carbon) and goes to zero in a purely IM7 composite (100 % carbon).

- The value of n starts from zero in a purely S-Glass composite (0 % carbon) and goes up to 22 in a purely IM7 composite (100 % carbon).

- S-Glass is always on the top layers.

- Average layup thickness = 2.8 mm

- Support span/ Load span = 3

- Support spam L = 16/32/40 * layup thickness

- Width = 12.7 mm

The variables to be evaluated are the representative strength and the representative stiffness, computed according to ASTM D6272 - 17, using the methodology in [Lim et al., 2014]; besides, the optimum configuration should yield failure in the tensile side, this way gradual failure can be achieved if a thin-ply material is added. See Figure **B-1** for a more graphical explanation.

The representative strength and representative stiffness plots are shown in Figure **B-2** and **B-3**. The best layup configuration is the one that gives the highest strength and holds at least the average stiffness.
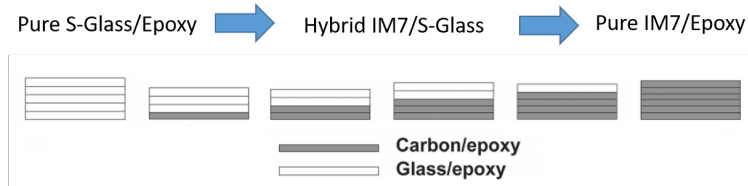
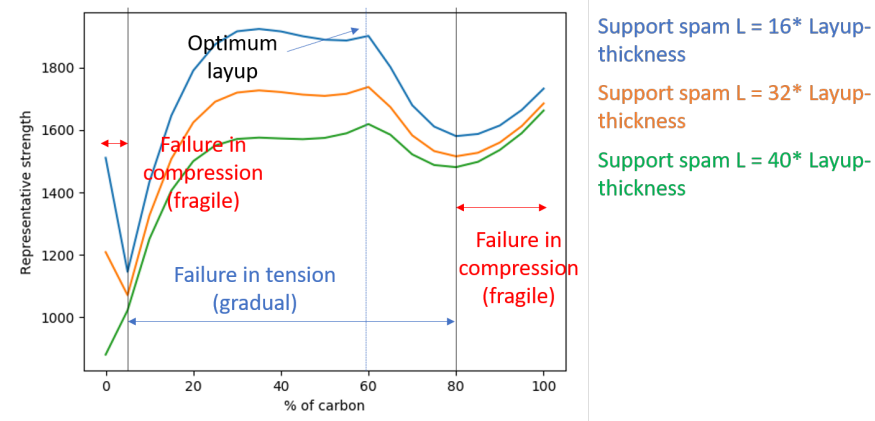**Figure B-1**.: Design methodology [Lim et al., 2014].
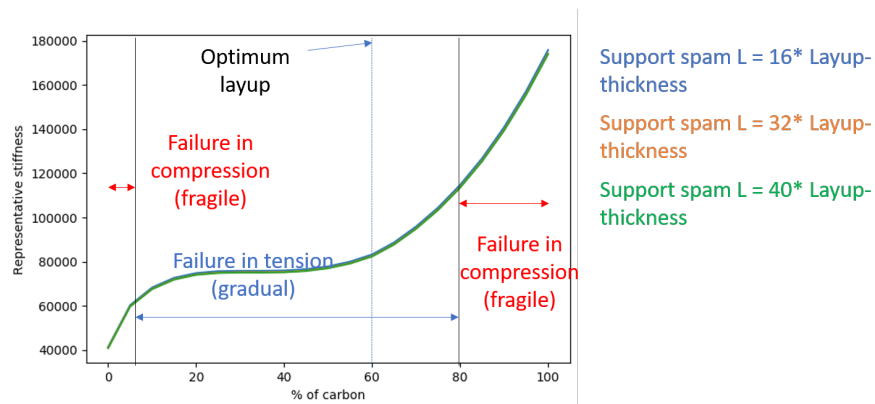

Figure B-2.: Representative strength.

Figure B-3.: Representative stiffness.

Bibliography

[Albaigés, 2013] Albaigés, J. (2013). Stanley e. manahan, environmental chemistry. *International Journal of Environmental Analytical Chemistry*, 93(14):1559–1560.

[Ary Subagia et al., 2014] Ary Subagia, I., Kim, Y., Tijing, L., Pant, H., and Shon, H. K. (2014). Effect of stacking sequence on the flexural properties of hybrid composites reinforced with carbon and basalt fibers. *Composites Part B: Engineering*, 58:251–258.

[Askeland, 2018] Askeland, D. R. (2018). *Ciencia e Ingenieria de los Materiales, Tercera ed.* International Thomson Editores, Mexico.

[ASTM, 2019] ASTM (2019). Standard test methods for flexural properties of unreinforced and reinforced plastics and electrical insulating materials. Technical report, ASTM.

[Barbero, 2008] Barbero, E. (2008). *Finite Element Analysis of Composite Materials.*

[Barbero, 2018] Barbero, E. (2018). *Introduction to Composite Materials Design, Third Edition.* Tailor & Francis Group, New York.

[Cusack, 2018] Cusack, J. (2018). Optimization of hybrid composite layups for bending applications to promote a gradual failure. Master's thesis, University of Strathclyde.

[Czél et al., 2017] Czél, G., Suwarta, P., Jalalvand, M., and Wisnom, M. (2017). Investigation of the compression performance and failure mechanism of pseudo-ductile thin-ply hybrid composites. 21st International Conference on Composite Materials, ICCM 2017 ; Conference date: 20-08-2017 Through 25-08-2017.

[Dong, 2016] Dong, C. (2016). Uncertainties in flexural strength of carbon/glass fibre reinforced hybrid epoxy composites. *Composites Part B: Engineering*, 98.

[Dong and Davies, 2014] Dong, C. and Davies, I. (2014). Flexural and tensile strengths of unidirectional hybrid epoxy composites reinforced by s-2 glass and t700s carbon fibres. *Materials and Design*, 54:955–966.

[Dong and Davies, 2012] Dong, C. and Davies, I. J. (2012). Optimal design for the flexural behaviour of glass and carbon fibre reinforced polymer hybrid composites. *Materials and Design*, 37:450 – 457.

[Dong and Davies, 2013] Dong, C. and Davies, I. J. (2013). Flexural properties of glass and carbon fiber reinforced epoxy hybrid composites. *Proceedings of the Institution of Mechanical Engineers, Part L: Journal of Materials: Design and Applications*, 227(4):308–317.

[Dong and Davies, 2015] Dong, C. and Davies, I. J. (2015). Flexural strength of bidirectional hybrid epoxy composites reinforced by e glass and t700s carbon fibres. *Composites Part B: Engineering*, 72:65 – 71.

[Dong et al., 2012] Dong, C., Ranaweera-Jayawardena, H. A., and Davies, I. J. (2012). Flexural properties of hybrid composites reinforced by s-2 glass and t700s carbon fibres. *Composites Part B: Engineering*, 43(2):573 – 581.

[Fiore et al., 2011] Fiore, V., Bella, G. D., and Valenza, A. (2011). Glass–basalt/epoxy hybrid composites for marine applications. *Materials and Design*, 32(4):2091 – 2099.

[Grupo, 2008] Grupo, F. P. J. C. J. M. A. B. (2008). *Introducción al análisis y diseño con materiales compuestos.*

[Hashin, 1983] Hashin, Z. (1983). Analysis of Composite Materials—A Survey. *Journal of Applied Mechanics*, 50(3):481–505.

[Hexcel, 2018] Hexcel (2018). Hextow im7 carbon fiber.

[Hibbeler, 2001] Hibbeler, R. C. (2001). *Mechanics of materials.* Pearson Prentice Hall, US.

[Hill, 2018] Hill, E. (2018). Achieving gradual failure in composites under bending through fibre hybridisation. Master's thesis, University of Strathclyde.

[Idárraga, 2019] Idárraga, G. (2019). *Failure analysis and optimisation of multi-directional pseudo-ductile hybrid composites.* P.h.d. thesis, National University of Colombia, Medellín.

[Jalalvand et al., 2014] Jalalvand, M., Czél, G., and Wisnom, M. (2014). Numerical modelling of the damage modes in ud thin carbon/glass hybrid laminates. *Composites Science and Technology*, 94:39–47.

[Jalalvand et al., 2015] Jalalvand, M., Czél, G., and Wisnom, M. (2015). Damage analysis of pseudo-ductile thin-ply ud hybrid composites - a new analytical method. *Composites Part A: Applied Science and Manufacturing*, 69:83–93.

[Jesthi et al., 2018] Jesthi, D., Mandal, P., K., A., and Nayak, R. (2018). Effect of carbon/glass fiber symmetric inter-ply sequence on mechanical properties of polymer matrix composites. *Procedia Manufacturing*, 20:530–535.

[Kalantari et al., 2016a] Kalantari, M., Dong, C., and Davies, I. (2016a). Multi-objective analysis for optimal and robust design of unidirectional glass/carbon fibre reinforced hybrid epoxy composites under flexural loading. *Composites Part B: Engineering*, 84:130–139.

[Kalantari et al., 2016b] Kalantari, M., Dong, C., and Davies, I. (2016b). Multi-objective robust optimisation of unidirectional carbon/glass fibre reinforced hybrid composites under flexural loading. *Composite Structures*, 138:264–275.

[Kalantari et al., 2016c] Kalantari, M., Dong, C., and Davies, I. (2016c). Numerical investigation of the hybridisation mechanism in fibre reinforced hybrid composites subjected to flexural load. *Composites Part B: Engineering*, 102:100–111.

[kansu.tripod.com,] kansu.tripod.com. A literature survey study on metal and ceramic matrix composites/ceramic matrix composite materials.

[Lim et al., 2014] Lim, J., Rhee, K., Kim, H., and Jung, D. (2014). Investigation of the compression performance and failure mechanism of pseudo-ductile thin-ply hybrid composites. *Carbon letters*, 15:125–128.

[Mangalgiri, 1999] Mangalgiri, P. D. (1999). Composite materials for aerospace applications. *Bulletin of Materials Science*, 22:657–664.

[Megahed, 2019] Megahed, K. (2019). *Introduction to Nonlinear Finite Element Analysis*.

[Naik and Kumar, 1999] Naik, N. and Kumar, R. S. (1999). Compressive strength of unidirectional composites: evaluation and comparison of prediction models. *Composite Structures*, 46(3):299 – 308.

[Paolinelis and Ogorkiewicz, 1976] Paolinelis, S. and Ogorkiewicz, R. (1976). Large deflections of beams in four-point bending. *The Journal of Strain Analysis for Engineering Design*, 11:144–149.

[Philpot et al., 2002] Philpot, T. A., Oglesby, D. B., Flori, R. E., Yellamraju, V., Hall, R. H., and Hubing, N. (2002). Interactive learning tools: Animating mechanics of materials.

[Recupero et al., 2005] Recupero, A., D'Aveni, A., and Ghersi, A. (2005). Bending moment – shear force interaction domains for prestressed concrete beams. *Journal of Structural Engineering*, 131:1413–1421.

[Reis et al., 2007] Reis, P., Ferreira, J., Antunes, F., and Costa, J. (2007). Flexural behaviour of hybrid laminated composites. *Composites Part A: Applied Science and Manufacturing*, 8:1612–1620.

[Rose et al., 2013] Rose, C., Dávila, C., and Leone, F. (2013). Analysis methods for progressive damage of composite structures.

[Simulia, 2014] Simulia, D. S. (2014). *Abaqus 6.14 User Guide.*

[Sudarisman et al., 2009] Sudarisman, ., Miguel, B., and Davies, I. (2009). The effect of partial substitution of e-glass fibre for carbon fibre on the mechanical properties of cfrp composites.

[Swolfs, 2019] Swolfs, Y. Verpoest, I. G. L. (2019). Recent advances in fibre-hybrid composites: materials selection, opportunities and applications. *International Materials Reviews*, 64:181–215.

[Swolfs et al., 2014] Swolfs, Y., Gorbatikh, L., and Verpoest, I. (2014). Fibre hybridisation in polymer composites: A review. *Composites Part A: Applied Science and Manufacturing*, 67:181 – 200.

[Torayca(R), 2012] Torayca(R) (2012). Torayca(r) m46j carbon fiber product data sheet.

[Turon Travesa, 2007] Turon Travesa, A. (2007). *Simulation of delamination in composites under quasi-static and fatigue loading using cohesive zone models.*

[Vasiliev and Morozov, 2007] Vasiliev, V. V. and Morozov, E. V. (2007). Chapter 1 - introduction. In Vasiliev, V. V. and Morozov, E. V., editors, *Advanced Mechanics of Composite Materials (Second Edition)*, pages 1 – 30. Elsevier Science Ltd, Oxford, second edition edition.

[Velmurugan and Manikandan, 2007] Velmurugan, R. and Manikandan, V. (2007). Mechanical properties of palmyra/glass fiber hybrid composites. *Composites Part A: Applied Science and Manufacturing*, 38(10):2216 – 2226.

[Whitney, 2005] Whitney, J. (2005). On the 'ply discount method' for determining effective thermo-elastic constants of laminates containing transverse cracks. *Composites Part A: Applied Science and Manufacturing*, 36:1347–1354.

[William et al., 2007] William, G., Branko, S., and Max, U. (2007). Composite structures: the first 100 years. *International conference on composite materials*, 16:1–10.

[X. Wu and Wisnom, 2017] X. Wu, J. F. and Wisnom, M. (2017). Combining the nonlinearity of angle-plies and fibre fragmentation in carbon fibre laminates under compressive loading. *21st International Conference on Composite Materials*, 87.

[Zhang et al., 2012] Zhang, J., Chaisombat, K., He, S., and Wang, C. H. (2012). Hybrid composite laminates reinforced with glass/carbon woven fabrics for lightweight load bearing structures. *Materials and Design (1980-2015)*, 36:75 – 80. Sustainable Materials, Design and Applications.